UNIVERSITY OF GHANA
COLLEGE OF BASIC AND APPLIED SCIENCES

PERFORMANCE EVALUATION OF LINAC SYSTEMS: ANALYSIS OF A FIVE-YEAR QUALITY ASSURANCE (QA)/QC DATA

BY

SIMON MENSAH AMOH

(10252483)

THIS THESIS/DISSERTATION IS SUBMITTED TO THE UNIVERSITY OF GHANA, LEGON, IN PARTIAL FULFILMENT OF THE REQUIREMENT FOR THE AWARD OF MASTER OF PHILOSOPHY (MPHIL) MEDICAL PHYSICS DEGREE

DEPARTMENT OF MEDICAL PHYSICS

SCHOOL OF NUCLEAR AND ALLIED SCIENCES

JULY, 2018

DECLARATION

This thesis is the result of research work carried out by Simon Mensah Amoh in the Department of Medical Physics, School of Nuclear and Allied Sciences, University of Ghana, under the Supervision of Prof. J.J. Fletcher, Prof. Signe Denielsen and Mr. George Felix Acquah.

…… Date: ……

SIMON MENSAH AMOH

(STUDENT)

…….. Date: ……

PROF. J.J. FLETCHER

(PRINCIPAL SUPERVISOR)

……... Date: ……

PROF. SIGNE DENIELSEN

(CO- SUPERVISOR)

…… Date: ……

MR. GEORGE FELIX ACQUAH

(CO-SUPERVISOR)

ABSTRACT

The main objective of radiotherapy is to increase therapeutic ratio (ratio of tumor control probability to the normal tissue complication probability) with minimal exposure to the personnel. In order to achieve this, the performance of the LINAC must be optimized to obtain the desired treatment result. The data collected on the equipment must be investigated retrospectively and extensively to assess the actual performance to check if it is functioning within the required standard. Quality Assurance helps to minimize errors and uncertainties in radiation therapy. Also with quality assurance errors can be detected and rectified sooner if they should occur. The objective of the study was to perform an in depth analysis on the quality assurance(QA)/ quality control (QC) data of LINACS(SB2, SB3, SB4 and SB6) over a five year operational period and to verify their performance against their acceptable limits. As part of this study new quality controls were measured to assess the current performance of the equipment and based on the risk assessment of the outcome some QA/QC data were analyzed on four LINACS (SB2, SB3, SB4, and SB6) over a five year operational period at St. Olav's hospital in Norway.

The results showed that all the deviations in the three directions (x, y and z) of the X-ray volumetric imaging (XVI) were within the tolerance limit of ±1 mm of SB2, SB3, and SB4 except for SB6 which recorded a mean deviation in 2015 that exceeded the tolerance limit by -0.01 cm, 0.12 cm and 0.1cm in the lateral(x), longitudinal (y) and vertical (z) directions respectively. In the absolute dose calibration measurements, the mean deviations were 0.149, -0.132, 0.013 and -0.400 % for SB2, SB3, SB4 and SB6 respectively for 6 MV whiles 15 MV produced mean deviations of 0.119, -0.059, -0.062 and -0.232% for SB2,

SB3, SB4 and SB6 respectively. The absolute dose calibration readings of the LINACS (SB2, SB3, SB4 and SB6) were within the tolerance limit of ±0.5%.The mean deviations of Tissue Phantom Ratio (TPR) of SB2 were -0.040% and -0.110% for 6 MV and 15 MV respectively, and SB3 recorded mean deviations of -0.467% for 6 MV and -0.287% for 15 MV that fell within the limit of ±1%.The current deviations were 0.05% for 6 MV, -0.140% for 15 MV of SB2 and -0.560 and -0.01% for 6 and 15 MV respectively of SB3. The mean deviations in R_{50} of the electron energies were 0.200, 0.140, -0.180, -0.160 and -0.100 mm for 6 MeV, 8 MeV, 10 MeV 12 MeV and 15 MeV respectively which were within the tolerance limit of ±0.5 mm. The recent measurements of the electron energies showed deviations of 0.2, -0.3, -0.2, 0.3, and -0.3 for 6 MeV, 8 MeV, 10 MeV 12 MeV and 15 MeV respectively. The mean deviations in flatness, symmetry and fieldwidth of crossplane and inplane profiles of both electrons and photons were found to be in the tolerance limit of ±1%, ±1% and ±1mm (for 10 x 0 cm^2 and 20 x 20 cm^2 field size and ±2 mm for 40 x 40 cm^2 field size) respectively.

DEDICATION

This research is dedicated to my late mother, Theresa Ama Wirekuaa for her love, advice and the sacrifices she made to bring me this far. And to the family of Amoh Mensah for their support, prayers and encouragement, and finally to everyone who contributed to the success of this work.

ACKNOWLEDGEMENT

Glory and honour to the Most High God for His everlasting kindness, grace, peace and love bestowed on me throughout this research.

I would like to express my utmost appreciation and gratitude to my supervisors; Prof. Signe Denielsen, Prof. J.J. Fletcher and Mr. George Felix Acquah for their selfless and immeasurable guidance, suggestions, encouragement and contributions in the conduct of this research and the preparation of this thesis.

My sincere thanks also go to all the medical physicists and the staff at the radiotherapy center (St. Olav's hospital- Norway) for their assistance, suggestions and contributions towards this work.

I am also grateful to the coordinators of NORPART programme: Prof. J.J. Fletcher, Prof. Erik Pal Goa, Dr. Stephen Inkoom, Dr. Francis Hasford and Dr. Mercy Afadzi for the opportunity to undertake part of my research in Norway. And finally my sincere appreciation goes to all my lecturers and my colleagues at the School of Nuclear and Allied Sciences for their contributions in diverse ways.

TABLE OF CONTENTS

LIST OF FIGURES

LIST OF TABLES

LIST OF ABBREVIATIONS

3D-CRT	Three Dimensional Conformal Radiation Therapy
AAPM	American Association of Physicist in Medicine
ANOVA	Analysis of Variance
COIN	Clinical Oncology Information Network
Dmax	Depth of Maximum Dose
ESTRO	European Society for Radiology and Oncology
EFD	Electron Field Diode
FMEA	Failure Mode and Effect Analysis
FTA	Fault Tree Analysis
IAEA	International Atomic Energy Agency
IBA	Ion Beam Application
ICRU	International Commission on Radiation Units and Measurements'
IEC	International Electro Technical Commission
IGRT	Image Guided Radiation Therapy
IMRT	Intensity Modulated Radiotherapy
LINAC	Linear Accelerator
MLC	Multileaf Collimator
MU	Monitor Unit
MV	Mega Voltage
MeV	Mega Electron Volt

NTCP	Normal Tumor Control Probability
ODI	Optical Distance Indicator
PPC	Plane Parallel Chamber
QA	Quality Assurance
QC	Quality Control
RCA	Root Cause Analysis
RPN	Risk Priority Number
RNT	Radionuclide Therapy
SPC	Statistical Process Control
SPSS	Statistical Package for the Social Science
SSD	Source to Surface Distance
SSDL	Secondary Standard Dosimetry Laboratory
TPR	Tissue Phantom Ratio
TCP	Tumor Control Probability
VMAT	Volumetric-Modulated Arc Therapy
WHO	World Health Organization
XVI	X-ray Volumetric Imaging

CHAPTER ONE

INTRODUCTION

1.1 Background

The main purpose of putting a good organizational structure, processes, procedures and the required resources to develop and implement a quality assurance program in the cancer treatment centers is to address the unforeseen or unpredictable events during the course of treatment delivery, and maintaining the output of the equipment used in radiotherapy within their acceptable standard. Some of the important terms related to a good quality assurance program in radiation therapy are quality assurance, quality system, quality control and quality standards and quality system management. In cancer treatment, it is defined as "a set of procedures that ensure a high therapeutic ratio while reducing exposure to the personnel"(WHO et al., 1988). QA is used in radiation therapy to ensure that the treatment outcome matches the outlined objectives of the treatment. This means that to achieve these stated objectives, all equipment involved in the treatment of the tumor must function within the given tolerance recommended by the quality assurance protocols. Assessing how effective quality assurance is has been always difficult, yet it has been shown that quality control which forms part of quality assurance sees to it that errors such as systematic and random errors that could have propagated undetected are identified and rectified to enhance the effectiveness of QA. These errors add up and the cumulative error is influenced by the component with the biggest error. Therefore, effective QA minimizes the dominant error enhancing a better treatment results. There are two key concerns for

quality assurance; to deliver the dose to the volume prescribed by the oncologist and the last one relates with the safety of the patient and prevention of treatment errors.

Quality Control is the "regulatory process through which the actual quality performance is measured, compared with existing standards, and the actions necessary to keep or regain conformance with the standards"(Thwaites et al., 2003). Quality Control deals with the technical aspect of quality assurance, it evaluates the current performance of a machine parameter, compares the parameter with the set standards and works on the deviation to achieve the desired goal. The principal objective for accurate dose delivery for cancer treatment is keeping a narrow deviation in the radiation production of an accelerator (Uddin, 2010). To maintain an accurate delivery of dose in cancer treatment hinges on how stable the accelerator is, high precision of quality control measurements and the ability of quality control procedure to detect true shifts in the beam parameters. Quality controls are performed on the medical accelerators to ensure that the right dose is delivered for the treatment of tumor (Uddin, 2010)**.** Quality controls lay down the procedures for testing and test equipment, the parameters to be tested and the frequency of testing, the responsibilities of different members of staff, the baseline values and tolerances for these values, action levels and documentation guidelines to ensure a good performance of the LINAC system.

Quality standard in radiotherapy is a set of acceptable yardsticks with which the quality of the activity in question can be evaluated (Thwaites et al., 2003). What this definition means is without quality standards, quality cannot be evaluated. We cannot determine the quality of the output from the LINAC machine without quality standards. Different nationals or international organizations such as WHO in 1988, AAPM in 1994, ESTRO in 1995 and

COIN in 1999 have given out recommendations for standards in radiation therapy (Podgorsak, 2008). Quality system is a system which is made up of organizational structure, responsibilities, procedures, processes and resources that are required for carrying out a quality assurance program. The major aim for developing a quality system in radiation therapy centers is to make available a formal written scheme to ensure that all the important aspects of quality assurance in the radiotherapy department are clearly defined, documented, understood and put into use.

Processes of machine QA

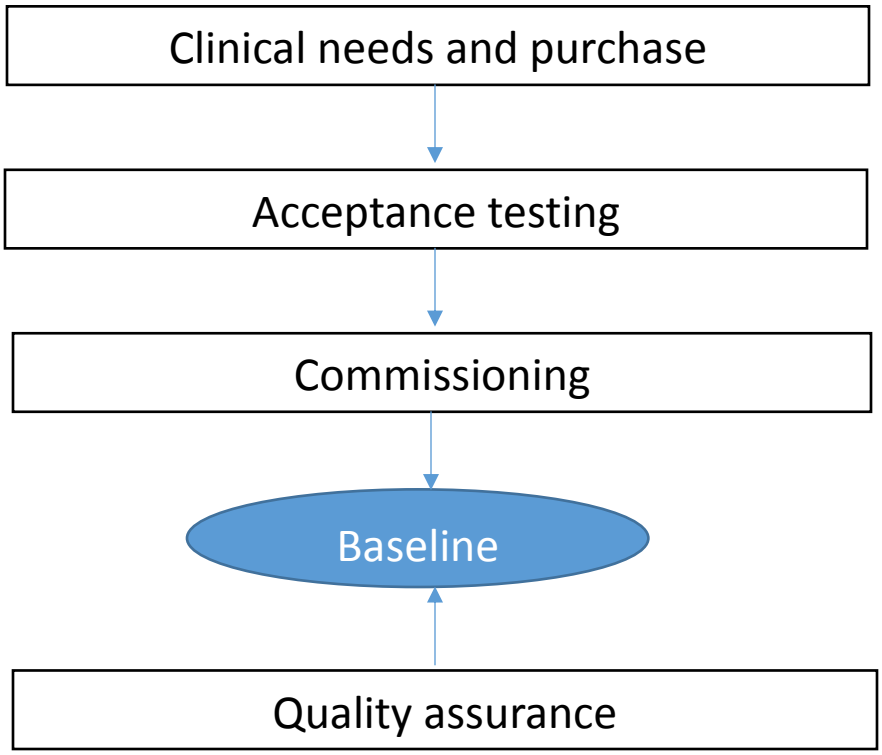

Figure 1. 1: The processes of machine QA by (Laoui, 2015)

The evolution of treatment techniques of cancer have called for an increased demand for new equipment in the radiotherapy department. Modern treatment techniques such as IMRT, IGRT, VMAT require that new equipment with the state of the art functionality are needed to execute these treatment procedures in order to achieve the main purpose of radiotherapy which is high tumor control rates with minimal normal tissues complication. When the purchase is done there is a need for acceptance testing to be performed on the machine to show that its performance is within the specifications and criteria of the manufacturer. The supplier has to demonstrate the output of the equipment to the customer's satisfaction. All the dosimetric and mechanical measurements should satisfy the specification values agreed upon by the supplier and customer in the contract. After acceptance of the equipment follows commissioning which means acquiring all the treatment beam characteristics required to make the equipment useable in a specific clinical setting (Klein et al., 2009). Acceptance testing and commissioning establish the baseline for future dosimetric measurements for beam performance constancy and verifies that the equipment is mechanically functional and operates within certain tolerances from absolute specified values.

The quality assurance program for linear accelerators is set up to make sure that the machine characteristics do not deviate considerably from their baseline values obtained during the process of acceptance testing and commissioning. Deviation from the baseline values could thus lead to suboptimal treatment of patients. Machine parameters can stray from their baseline values due to machine malfunction, mechanical breakdown, physical accidents, or component failure. Major component replacement such as the magnetron, waveguide, bending magnet etc may also alter machine performance from the original

parameters. Also there can be gradual changes as a result of aging of the machine components. These patterns of failure must be taken into consideration when establishing a periodic quality assurance program.

1.2 Problem Statement

The delivery of accurate prescribed dose to patient is a paramount objective of radiotherapy treatment because this can damage healthy organs around the target tumor. Daily, weekly, monthly and annual QA on LINAC systems are performed to ensure that this objective is achieved. Many radiotherapy centers perform QA/QC checks on their LINAC systems and generate a lot of data in the process. However, analysis of the data in a number of these centers is absent, leading to difficulty in tracking the detailed performance of the systems on regular basis (Suvendu et al, 2016).

Sometimes fewer than necessary QA checks are also performed on LINAC systems and this has a potential of affecting the performance and output of the machine (Lee, Jeong, Jo, & Yoon, 2015).

1.3 Objectives

The primary objective of this work is to retrospectively perform an in-depth evaluation of the performance of four linear accelerators over a five-year operational period. This work will thoroughly investigate and analyze the accrued quality assurance data (QA) / quality

control (QC) of the equipment for over a five year operational period to assess its performance.

The specific objectives of this research include:

- Taking QA/QC measurements in 2018 and comparing them with the outcome of the analyzed QA/QC data for the period. The new measurements will also be compared with values acquired at the time of commissioning.
- Assessment of the present-day performance of the linear accelerators and make recommendations for its use.
- Make recommendations for setting up QA programs for LINACS in future in Ghana.

1.4 Justification and Relevance of the Study

To achieve a high therapeutic index, both high accuracy and high precision are required. This means uncertainty and errors must be reduced in each of the steps to meet the intended treatment outcome. Detailed analysis of the QA data over the years would help to measure the stability and the performance of the linear accelerator so that it's characteristics do not drift away considerably from the baseline values obtained at the time of acceptance testing and commissioning, and also to make sure that all the items on the daily, weekly, monthly and annual QA's are performed.

1.5 Scope of study

The goal of this study is to do a thorough analysis of a five year operational quality assurance data of four medical linear accelerators at St. Olav's hospital in Norway. At St. Olav's Hospital the QA program consists of a number of periodic controls, and key parameters from these controls have since 2011 been collected and stored in a database. This study is limited to the quality assurance data of the medical accelerator since it plays a key role in an accurate and precise delivery of the prescribed dose and dose distribution in radiotherapy. Also the analysis of the data will be limited to these software and analytical tools; Microsoft Access Database, Microsoft Excel, SPSS and Statistical Process Control (SPC)

CHAPTER TWO

LITERATURE REVIEW

2.1 Background

Radiotherapy also called radiation therapy is the use of ionizing radiation to control or kill cancer cells. When an energy from radiation is absorbed by a biologic material it results in either excitation or ionization. If the absorbed energy raises an electron from an atom or a molecule from a lower energy level to a higher energy level without removing the electron it is known as excitation. Ionizing radiation on the other hand has enough energy to eject one or more orbital electrons from an atom or molecule and it is called ionization. Ionizing radiation can be grouped into two categories. They are directly and indirectly ionizing radiations. Directly ionizing radiations have sufficient kinetic energy to disrupt the atomic structure of the matter through which they pass directly and produce chemical and biologic changes. Examples of directly ionizing radiations are electrons, protons, alpha-particles etc. Indirectly ionizing radiations transfer their energy in the absorber to produce fast-moving charged particles which cause chemical and biologic damage. Indirectly ionizing radiations do not cause the biologic changes themselves. Electromagnetic radiations (x- and y-rays) are examples of indirectly ionizing radiations. When radiation interact with a medium the amount of energy absorbed is given by:

$$D_{w,Q_0} = M_{Q_0} N_{D,W,Q_0} \quad \ldots\ldots\ldots\ldots (2.1)$$

Where M_{Q_0} is the reading of the dosimeter under the reference conditions used at the SDL, and N_{D,W,Q_0} is the calibration factor in terms of absorbed dose to water of the dosimeter obtained from the SSDL. The center of the ion chamber is placed at the reference depth**.** (Mayles, Nahum, & Rosenwald, 2007)

The principle of cancer treatment is demonstrated by plotting two sigmoid curves for tumor control probability (TCP) and normal tissue complication probability (NTCP) as shown in figure 2.1

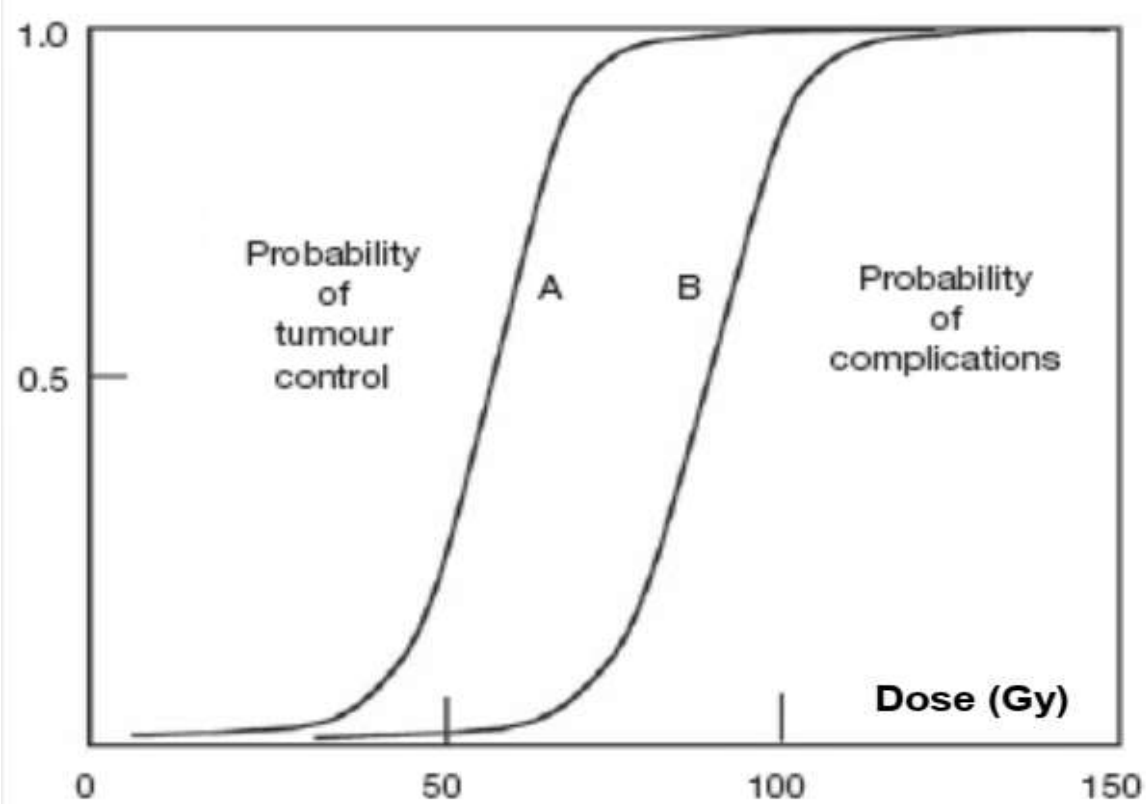

Figure 2. 1: The concept of therapeutic ratio (Thwaites et al., 2003)

The choice of the absorbed dose to be given for treatment should be such that it maximizes the TCP and at the same minimizes the NTCP. The therapeutic ratio is the ratio of the TCP and NTCP at a specified level of response (0.05) for normal tissue. In any good treatment outcome, TCP $\geq$ 0.5 and NTCP $\geq$ 0.05. From figure 2.1**,** the wider the NTCP curve is to the right of TCP curve, the greater the therapeutic ratio and the less likely are the treatment complication.

Radiation therapy can be administered through the following ways:

1.Unsealed source therapy: Unsealed sources therapy which is also called unsealed source radionuclide therapy (RNT) uses radioactive sources in the form of solid, liquid or gas which are administered (orally, by inhalation or intravenously) into tumors or body cavities. For instance capsules containing radioactive iodine are also often administered orally.

2. Brachytherapy: also called sealed source therapy is a short distance treatment of tumor with the radiation emanating from small encapsulated sources. Here the sources are placed directly into the target volume or near the target volume. Examples of brachytherapy sources are Cs-137, Ir-192, I-125, Pd-103 etc.

3. External beam radiotherapy is also known as teletherapy: is where the source of the ionizing radiation is at a distance away from the patient. It is the most commonly used type of radiation therapy. The X- rays and the electron beams are most common radiation sources of ionizing radiations in external beam radiation therapy. These beams are controlled and transmitted through the body to the location of the tumor to damage the tumor cells. The tumor is usually surrounded by normal tissues. The treatment is planned in such way that a greater dose is given to the tumor to achieve a high tumor control probability, while the dose to the healthy tissues is lowered to minimize normal tissue complication. The prescribed dose in external beam radiotherapy is fractionated to allow normal tissues time to recover from radiation effect. The photons used in external beam radiation therapy can be either gamma rays which are generated by Co-60 machine or X rays which are produced by linear accelerator (Akorsah, 2016).

2.2 Linear Accelerator (LINAC)

Linear accelerator in radiation therapy is a machine that can produce either both electron beams (MeV) and high energy X rays (MV) or high energy X rays (MV) only. The electrons are produced from a heated cathode filament through a process called thermionic emission. The magnetron produces radiofrequency pulses (RF) which accelerate the electrons in the accelerating waveguide. As the electrons exit the accelerating waveguide, they are deflected by a series of magnets in the flight tube before they reach the patient for treatment. The electrons can be used to treat patients directly or a heavy metal target can be used to create bremsstrahlung photons for treatment.

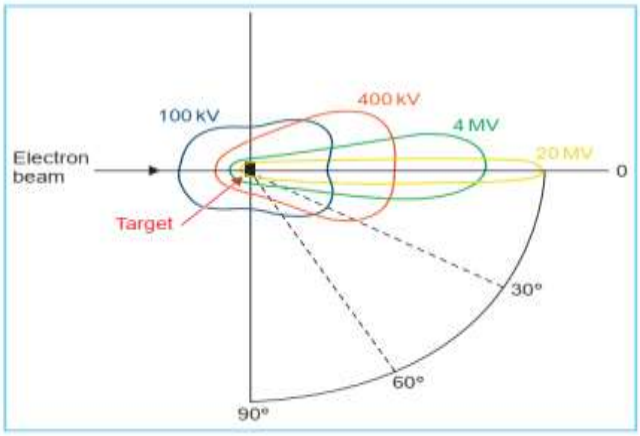

Figure 2. 2: Spatial distribution of bremsstrahlung radiation around the target. (Khan et al, 2014).

2.3 Components of linear accelerator

Linear accelerators are fixed firmly in a position so that all the beams used in the treatment will have a common focal point. The five major and different components of the machine are the gantry, gantry stand or support, modulator cabinet, patient support assembly (couch) and control console form the operational systems of linear accelerators (Podgorsak, 2008).

The gantry rotates on horizontal axis bearings located inside the drive stand, a large rectangular cabinet that is firmly mounted on the floor of the treatment room. The gantry helps in directing the X-ray (photons) or electron beams to the site of the tumor. It rotates 360 degrees around a line/point, called the isocentre. The gantry houses the electron gun, accelerator structure and treatment head. The modulator cabinet is the noisiest of the LINAC system components and is located inside the treatment room. It contains three sub-components which are fan control cooling the power distribution system, the auxiliary power distribution system containing the emergency off button that shuts the power to the LINAC and primary power distribution system. The treatment couch or table is where the patient is positioned still to receive the radiation energy for treatment. It moves in lateral, vertical and longitudinal directions (Tello, 2016). The control console is located outside the treatment room where the LINAC's movement and operation are controlled, while delivering the radiation to the patients.

Figure 2.3 below depicts how the major components of the LINACS are interrelated and function to achieve the treatment results. It gives an overview of the arrangement of the

components of linear accelerator, though there are significant differences from one manufacturer to another.

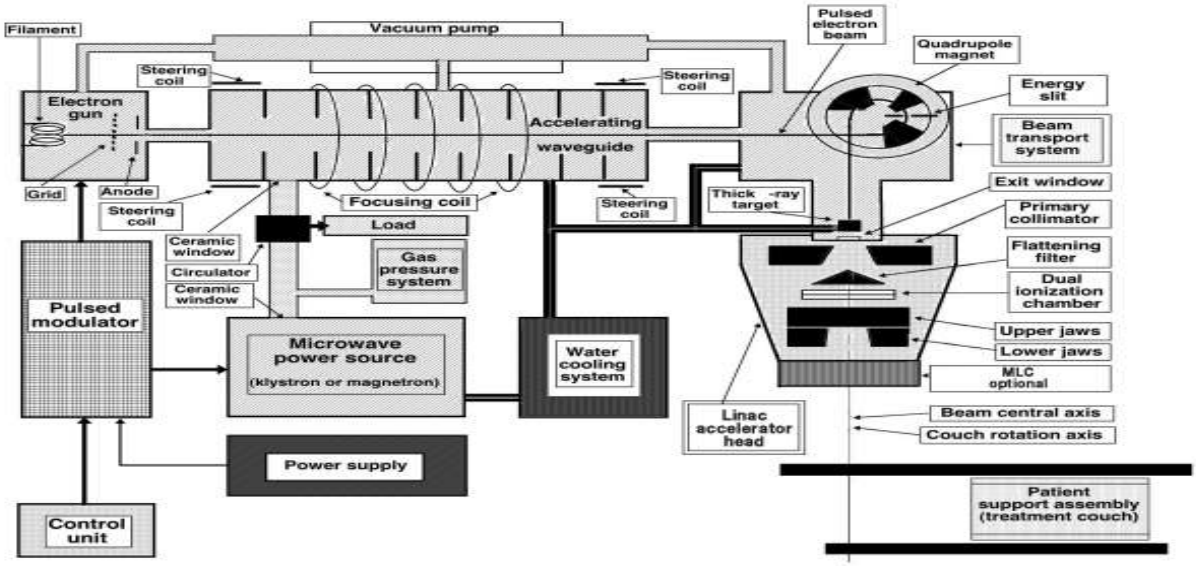

Figure 2. 3: **Schematic diagram of a modern linear accelerator (Podgorsak, 2005)**

The main clinical beam generating components of the linear accelerator are categorized into six groups **(**Podgorsak 2008):

1 Injection system

2 RF power generation

3 Accelerating waveguide

4 Beam transport

5 Beam collimation and monitoring

6 Auxiliary systems (e.g. cooling, vacuum)

2.4 Injection system

The injection system which is also called the electron gun is the main source of electrons for the beam. The diode and the triode are the two types of electron guns which are used as sources of electrons in medical linear accelerators. The electron gun is made up of cathode and anode. Electrons are emitted from the filament of the cathode through a process called thermionic emission (Podgorsak, 2008). A high voltage pulsed produced by the modulator is applied between the cathode and anode generating a strong focusing field and eject electrons from the electron gun. Electrons are guided into the accelerating waveguide by the fields at a velocity of approximately 0.4 C, where C is the speed of light.

Figure 2.4: An electron gun (Almberg, 2017)

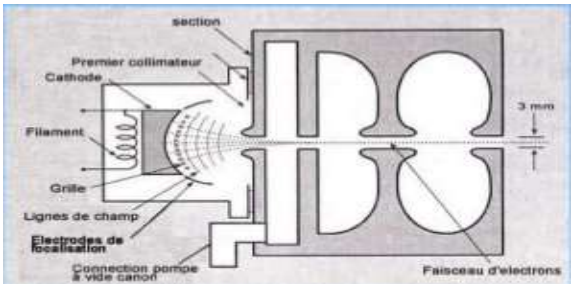

Figure 2.5: Electron from electron gun being injected into the accelerator waveguide (Tello, 2016).

2.5 Radio frequency (RF) power generation

The electrons injected into the accelerator structure are accelerated to the required kinetic energy using microwave radiation which is produced by the radiofrequency power generation system. The RF power generation system is made up of two major components: RF power source and pulsed modulator (Podgorsak, 2008). It also has a circulator which

prevents reverse propagation of RF power from the source to the accelerating waveguide (Tech & Forest, 2014).

The RF power source can be either a magnetron or a klystron. They make use of electron acceleration and deceleration in a vacuum to generate high power RF fields. The process of thermionic emission is applied in both types of the power source. The distinguishing feature in these types of power source is their design principles (Podgorsak, 2008).

2.6 Magnetron

Magnetron is a vacuum tube that generates high- frequency microwave power for accelerating the electrons in the waveguide structure. It operates like a high-power oscillator, producing microwave pulses with each pulse of a microwave frequency which is about 3,000 MHz (Khan & Gibbons, 2014). The principle of operation is based on the interaction between electron and electromagnetic field. The magnetron is suitable for lower electron energies such as 4 MeV to 6 MeV. It is a cylindrically shaped construction consisting of a central cathode surrounded by a resonant cavity anode structure. When a high voltage pulse is applied to the magnetron cathode, the cathode is heated by an inner filament, and the electrons are produced by thermionic emission which are accelerated towards the anode. The influence of the magnetic field from the magnetron magnet allows the electrons to follow a curved path between the cathode and anode. The current around the resonant cavities cause them to radiate electromagnetic energy at a resonant frequency (microwaves/RF). The generated microwave pulses are guided into the accelerator structure through the waveguide.

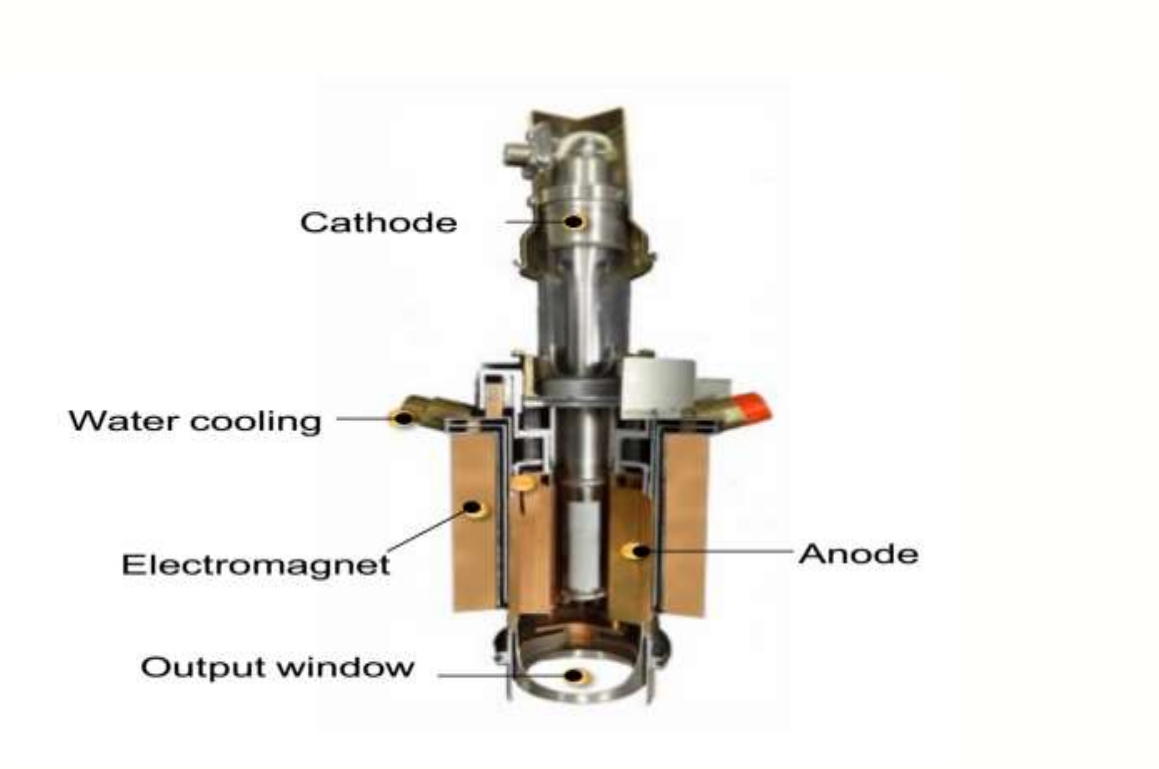

Figure 2. 6: Magnetron: microwave power source (Elekta)

The magnetron produces microwaves which propagate at the speed that is so high that it cannot synchronize with the speed of the electron from the electron gun. Therefore to synchronize the speed of the microwaves with that of the electrons, a structure called an input mode transformer is used to slow down the speed of the microwave by decreasing the width of the rectangular waveguide. Hence the microwave exiting the input mode transformer has its speed lowered to 0.4 C to be at the same speed of the electrons from the electron gun.

2.7 Klystron

A Klystron is a microwave amplifier unlike the magnetron which is a generator of microwave. A klystron is different type of vacuum tube that is used to supply microwave to increase the speed of electrons. It needs to be driven by a low-power microwave oscillator. The klystron is usually used in high energy linear accelerators where the generation of microwaves with peak power is on the order of 7 MW or higher (Tech & Forest, 2014) **.** Klystron can be constructed to function either as an amplifier or as an oscillator, where RF oscillations are sustained by internal feedback mechanisms within the structure. It has an assembly which is almost the same as a linear accelerator in that linear electron beams are accelerated through a series of cavities and controlled by series of focusing coils towards the collector (Gray Cancer Institute, 1996)**.**

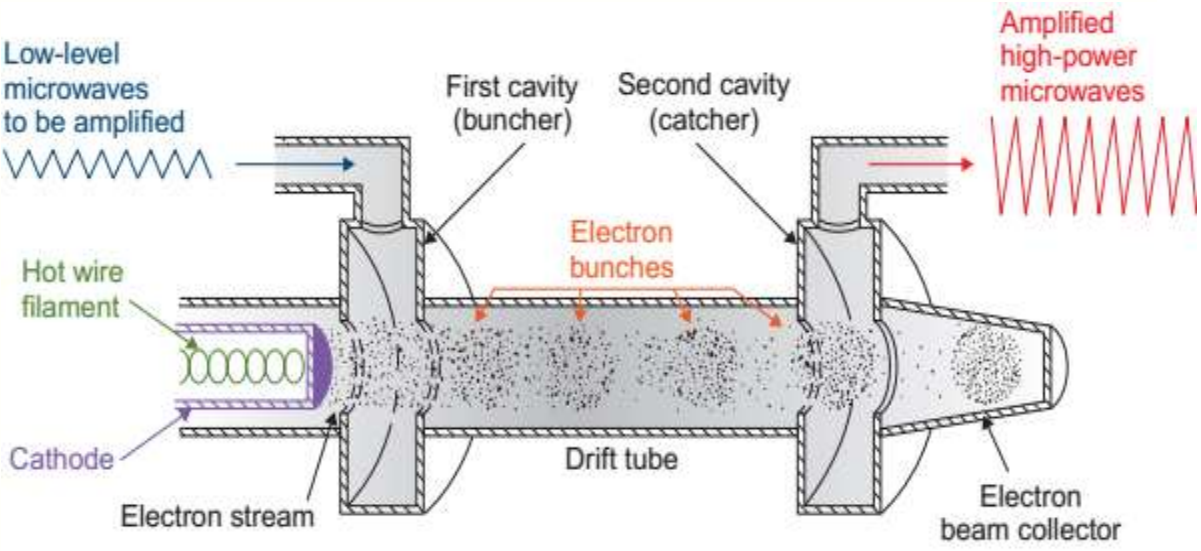

Figure 2. 7: Cross-sectional drawing of a two-cavity klystron (From Karzmark CJ, Morton RJ. A Primer on Theory and Operation of Linear Accelerators in Radiation Therapy.

Rockville, MD: U.S. Department of Health and Human Services, Bureau of radiological Health. (Khan et al., 2014)

2.8 Pulsed modulator

The pulsed modulator generates the high voltage, short duration pulses and high current used by either the magnetron or the klystron and the electron gun. The whole electrical system of the pulsed modulator is accommodated in the modulator cabinet which can be found in the treatment room, in special mechanical room next to the treatment room or in the linear accelerator control room depending on the installation design (Podgorsak, 2008). The modulator cabinet has three major components which are: fan control which automatically turns the fans off and on when there is a need for cooling the entire power supply system. The auxiliary power- distribution system contains the emergency off button that shut off the power to the treatment unit and primary power distribution system.

2.9 Accelerating waveguide

Waveguides are evacuated or gas filled metallic structures of rectangular or circular cross-section used for propagating the microwaves to accelerate the electron beam to relativistic speed (Podgorsak, 2008) . The length of the waveguide ranges from 30cm for 4 MeV to more than 1 m for higher energies. (Tech & Forest, 2014). Linear accelerators use two types of waveguides: RF power transmission waveguide and accelerating waveguides. The RF power transmission waveguide transports the microwaves/RF from the magnetron or klystron into the accelerating waveguide where the electrons are accelerated. The accelerating waveguide uses the energy transmitted from the RF power generators to

accelerate the electrons. The accelerating waveguide is evacuated to enhance free passage of the electrons (Podgorsak, 2008). Travelling wave (figure 2.8) and standing wave (figure 2.9) are the two types of accelerating waveguides used in linear accelerators (Podgorsak, 2008). There are no set rules with which to determine the type of accelerating waveguide to choose for a linear accelerator. However, travelling wave accelerators are usually appropriate when working with particles with relativistic velocity such as electrons and also when dealing with short beam pulses (Pichoff, 2006).

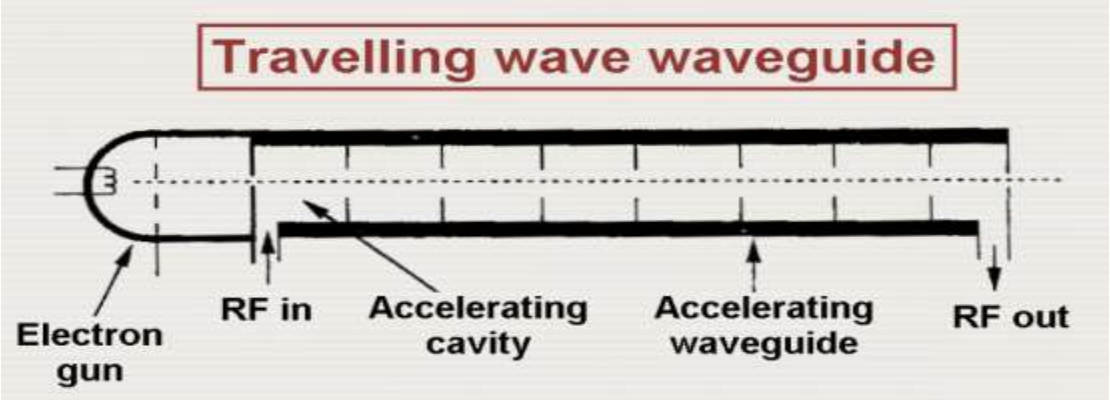

Figure 2. 8: Diagram for travelling wave waveguide (Podgorsak, 2005).

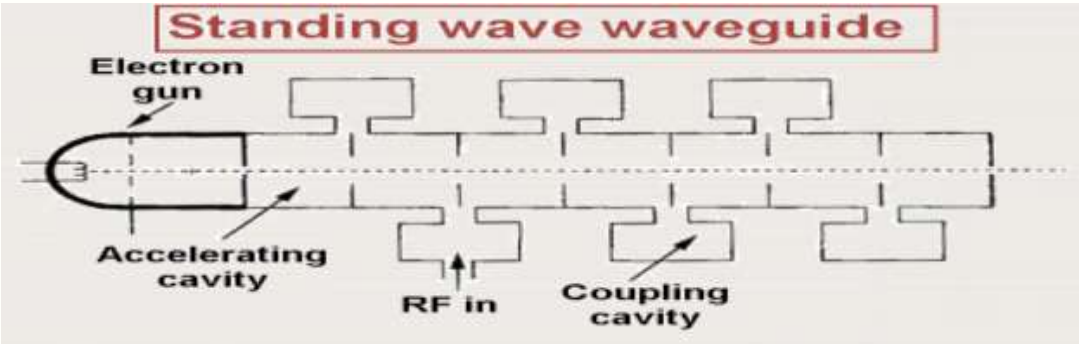

Figure 2. 9: Schematic diagram of standing wave waveguide (Podgorsak, 2005)

2.10 Auxiliary system

The LINAC auxiliary system is made up of the structures that make acceleration feasible and help the LINAC function effectively, but they are not directly involved with acceleration of electrons. The auxiliary system consists a vacuum pumping system, a water cooling system, a gas dielectric system for transmission of microwaves from the RF power source to the accelerating waveguide and shielding against radiation leakage. The major components of the LINAC must work either under vacuum or at a high gas pressure to avoid voltage failure. Also an evacuated vacuum system prevents scattering of the electron beam throughout the beam transport.(Tech & Forest, 2014)

The electrons being accelerated must not change their direction or energy as a result of impact with gas atoms. The vacuum system is maintained at a lower pressure to prevent deflection of the electron beam by gas molecules. This is to say that the mean-free path between collisions needs to be long compared to the overall flight path. This distance is typically between 1 m and 3 m (Mayles, Nahum, & Rosenwald, 2007). The vacuum system consists of transmission waveguide, the electron gun, the accelerating waveguide and the beam transport system. Ion pumps are used to keep the pressure in the vacuum system.(Tech & Forest, 2014). A vacuum pumping system producing a vacuum pressure of ~ 10^{-6} torr in the accelerating guide and the RF generator (Podgorsak, 2008).

The water cooling system is used for lowering the temperature of the accelerating waveguide, RF generator, target and other parts of the linear accelerator such as the beam focusing and steering coils when they are overheated. Most of the electron's energy is absorbed by the target in the form of heat after a small fraction of the energy has been

converted into X- rays. 94% of the electrons energy goes to heat. Efficient target cooling system is necessary for removing the heat (Juntong et al., 2016).

Leakage radiation is the braking or bremsstrahlung radiation transmitted through the treatment head of the lINAC. The common source of the leakage radiation comes from the accelerator target; however, the electron gun, magnetron or klystron, accelerating waveguide, and beam bending magnets may also produce some bremsstrahlung photons in the treatment room. Lead and tungsten shielding are placed around all possible sources of unwanted bremsstrahlung in the linear accelerator (Tech & Forest, 2014)

2.11 Electron beam transport system

The velocity of the electron is increased from 0.4 C in electron gun to approximately 0.998 C in the accelerating waveguide. The frequency of the microwave is constant, but the wavelength increases leading to acceleration of the electrons.

$$V = f \times \lambda \quad \text{..... (2.3)}$$

Electron beam transport system gives a description of how the electron beam is transported from the accelerating waveguide to the x- ray target or to the LINAC exit window for patient treatment. In low energy LINACS the target is fixed in the accelerating waveguide structure hence transporting the electron beam from accelerating waveguide to the target is not needed, this is contrary to medium (10 MV) and high energy (above 15 MV) LINACS which require electron beam transport system. The system consists of evacuated drift tubes, bending magnets, steering and focusing coils (Podgorsak, 2008).

Bending magnets are used in LINACS that operate at energies above 6 MeV. The electron beam must be bent towards the patient else the total height of the LINAC would be unreasonable. As the electron beam exits the accelerating waveguide it has a range of energies, so the beam is made to pass through a series of electromagnets and the current in these bending magnets is set to allow electrons with correct range of energies to hit the target to generate the required energy of X-rays or exit through a thin metallic window for electron therapy. Three systems for electron bending have been developed: 90º bending, 270º bending (achromatic) and 112.5º (slalom) bending (Podgorsak, 2008)

90º bending: Higher energy electrons in the electron beam spectrum are bent less than lower energy electrons; Defocuses and spreads the electron beam.

270º bending (achromatic): Refocuses electron beam spread and directional spread; provides small focal spot on x-ray target.

112.5º (Achromatic): Requires no more vertical space than 90° bending (Tech & Forest, 2014).

Focusing coils provide a static axial magnetic field. They are used to limit beam divergence and cross section. Two sets of focusing coils (focus 1 and 2) shown in figure 8 are used in LINAC configuration. The need for focusing decreases as the electron energy increases.

Two sets of beam steering/centering coils (R: radial, T: transversal) primary steering coils fixed at the gun-end and secondary steering coils which are located midway along the waveguide as shown in figure 8 Steering coils are used to keep the accelerated electron

beam as close as possible to the axis of the cylindrical accelerating waveguide and direct the beam towards the beam transport system.

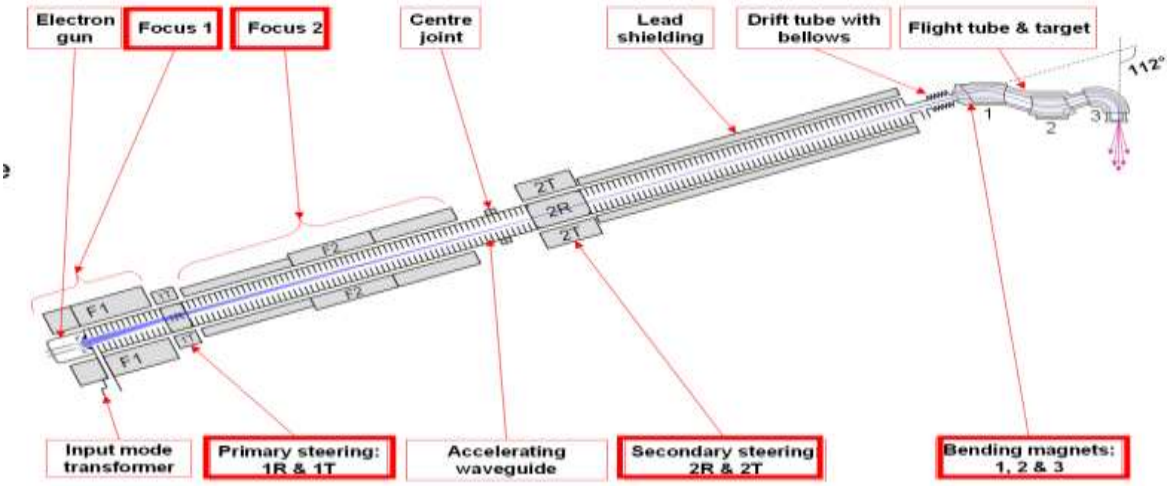

Figure 2. 10: Magnetic focusing and steering of electron beam (Elekta)

2.12 Beam collimation and monitoring

The treatment head of the linear accelerator contains the components responsible for the production, shaping, localizing and monitoring of the clinical photon and electron beams. All the components necessary for beam collimation and monitoring systems are found in the treatment head of the linear accelerator. The important components found in the treatment heads of modern medical linear accelerators are X-ray target, primary scatter filter, primary collimator, secondary filter, flattening filter, dual ion chambers, wedge and shutter, multi-leaf collimator (MLC), diaphragms (secondary collimators/ jaws) and field light (Podgorsak, 2008). These components will be described in more detail in the subsequent sub-chapters.

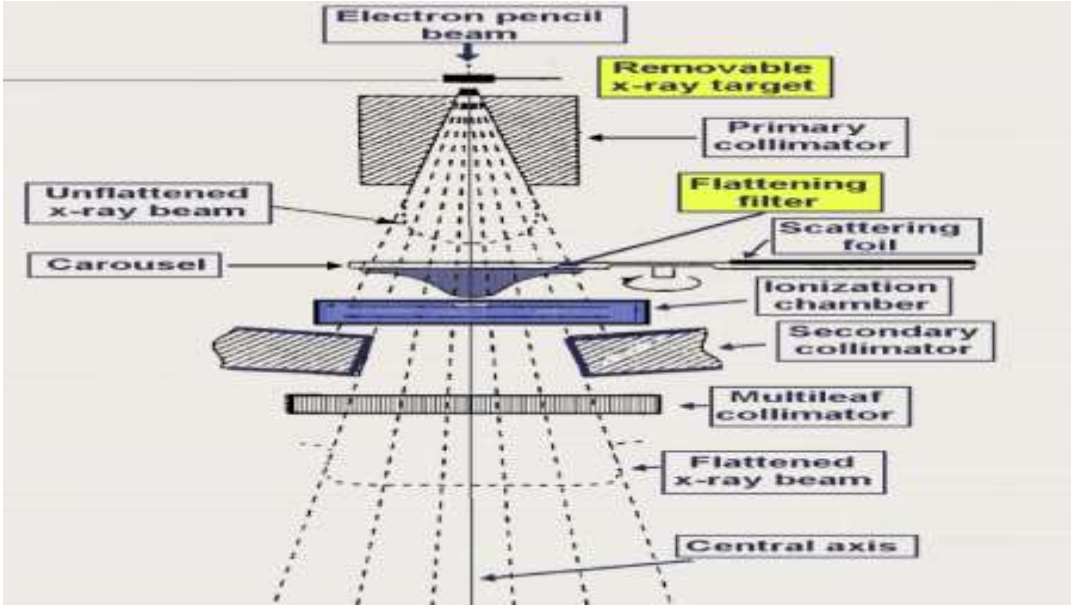

Figure 2. 11: schematic diagram showing components of LINAC treatment head (Podgorsak, 2005).

2.13 X-ray Target

Focusing and bending of the electron beam result in the reduction of the cross-section of the electron beam of diameter around 1- 2 mm. The electron beam is used directly with appropriate scatter foils or it can be converted to bremsstrahlung x-rays when it strikes against a heavy metal target. The dose rate of X- rays is influenced by the target material and its thickness. When electron beam collides with targets, the intensity of the braking radiation is proportional to the square of the atomic number of the target (Z). Materials with high atomic number such as tungsten (W), tantalum (Ta), and gold (Au) are suitably used as x ray targets (Juntong et al., 2016). Work done by Juntong et al. (2016) and Qao et al. (2013) suggest that tungsten is widely used as a target material with high dose rate. In (Juntong et al, 2016) study to find the optimized thickness of tungsten target, their results

proved that the optimized thickness for tungsten target was 2.682 mm. The thickness of the tungsten is 1 mm**.** A thicker target has more electron filtering efficiency than a thinner target. A low atomic number material should be thicker than a high atomic number material in order to achieve the same filtering efficiency (Juntong et al., 2016).

2.14 Primary scatter filter

The primary scatter filter is used to broaden the electron beam to make it useable for patient treatment. The primary scatter filter is located between the target and primary collimator. It is a structure with six port scattering filter that is fixed on a movable carrier. Tantalum foil with a varying thickness is used to fill five of these ports leaving one hole for x ray mode. Tantalum is an element with atomic number of 73 and its dense nature makes it suitable for electron scattering.

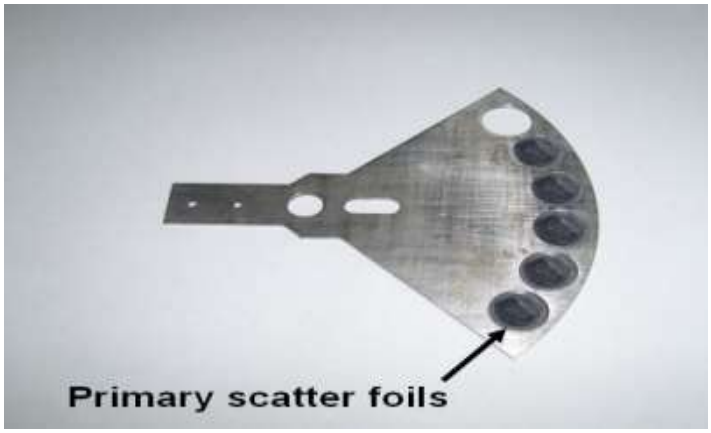

Figure 2. 12: A primary scatter filter (Elekta)

2.15 Primary collimator

The primary collimator outlines the largest available field size and is a conical hole created into a tungsten shielding block, the conical aperture stretches from the edges of the target on one end of the block to the flattening filter on the other end. It can also be made from an alloy of tungsten and lead. It may also be constructed of depleted uranium (DU) as this material is approximately 1.6 times denser than lead. The primary collimator has open aperture and filter aperture. The open aperture is used for low and mid energy x rays as well as electrons, while the filter aperture contains the difference filter for high energy x rays and beam hardening filter for 25 MV**.** The thickness of the shielding block is constructed such that the attenuation of the average primary X ray beam intensity is less than 0.1% of the initial value. The International Electro technical Commission (IEC) recommends that the maximum leakage should not go beyond 0.2% of the open beam value (Podgorsak, 2008)

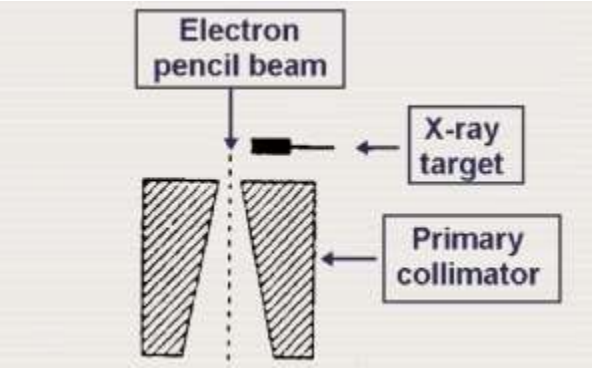

Figure 2. 13: Primary Collimator (Podgorsak, 2008)

2.16 Flattening filter

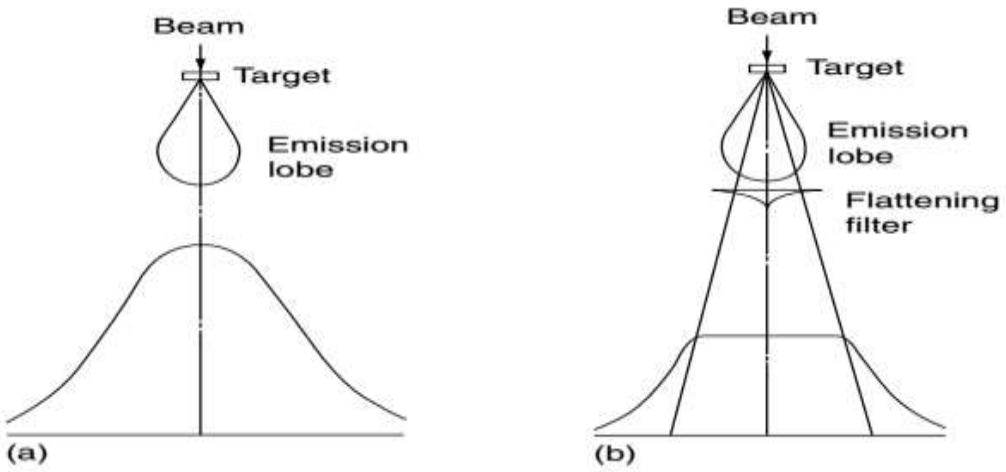

Figure 2. 14: Photon beam (a) without flattening filter and (b) with a flattening filter (Mayles, Nahum, & Rosenwald, 2007)

The filter system consists of a rotating carousel with five positions. One position which has a flattening filter made of stainless steel and aluminum is used for low energy x rays. Another position also made of thin metal plate is used for flattening filter free photons beams. The remaining three scattering/flattening filters are for available electron energies. The bremsstrahlung X ray generated as a result of high energy electron beam striking the target is mainly forward peaked leading to a cone shaped fluence profile as shown in Figure 2.12a. The flattening filter is placed in the beam as indicated in Figure 2.12b to compensate for the lack of scatter at the edge of the field to create a flat photon beam. (Mayles, P., Nahum, A., & Rosenwald, 2007).

2.17 Ion Chamber

Ionization chambers are embedded in the LINAC'S treatment head for the dose monitoring for the safety of the patients Dual transmission ionization chambers are used for monitoring the photon and electron radiation beam output as well as the radial and transverse beam flatness. They are positioned between the flattening filter or scattering foil and the photon beam secondary collimator to continuously monitor the radiation beam output during treatment delivery. To prevent the incidence of patient overdose, two separately sealed ionization chambers are employed so that if the primary ionization chamber fails during dose delivery to the patient, the secondary ionization chamber will terminate the irradiation. The secondary chamber normally stops the irradiation after giving an extra dose of a small percentage above the prescribed dose. As soon as the operator preset number of MUs is reached, the primary ionization chamber electric circuit shuts the LINAC down and terminates the dose delivery to the patient. Before a new irradiation can be started, it is necessary to reset the MU displays to zero. Furthermore, irradiation is not possible until a new selection of MUs has been done (Podgorsak, 2008).

2.18 Wedges

Wedges are filters for compensating for the fields that do not perpendicularly enter the body, or they are used to create homogenous dose delivery when combining multiple fields. They are mostly used for photons only. Physical wedge filters are simply constructed from elements like brass, aluminum, or lead that are placed in front of the collimators. The most commonly used wedge angles in radiation therapy are 15, 30, 45 and 60 degrees.

Wedged fields can be created by the movement of the jaw during dose delivery instead of a physical wedge.

The manufacturer first to introduce the concept of automatic or motorized wedge was Philips (now Elekta). This is located in the treatment head and can be automatically moved in and out of the beam during treatments (Mayles, Nahum, & Rosenwald, 2007).

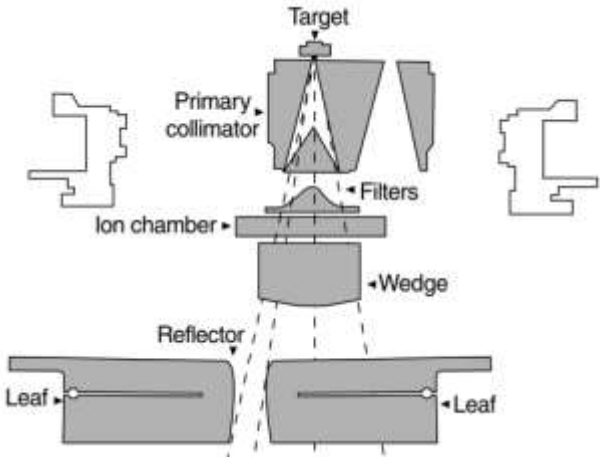

Figure 2. 15: illustration of a motorized wedge in the radiation beam ((Mayles, Nahum, & Rosenwald, 2007)

The idea of dynamic or flying wedges was first developed by Varian, which is now available for other manufacturers. With the dynamic wedge, one of the jaws is static while the other jaw moves during treatment delivery to obtain a wedged beam profile. There is more flexibility in using dynamic wedges than fixed wedges in that it is possible to make any shape of beam profile needed (Mayles, Nahum, & Rosenwald, 2007)

2.19 Shutter (backscatter plate)

The shutter which is 3mm in thickness is embedded in the beam limiting device to minimize backscatter from the wedge and diaphragms into the ion chamber during treatment with photons. It remains permanently in the beam during the treatment with photons. The shutter is retracted when treating with electrons.

2.20 Collimating System

Minimizing radiation beam to the surrounding healthy tissues and critical structures is important in radiation therapy and beam shaping is one of the means of reducing the absorbed dose to these healthy structures. Conventional collimators only provide a rectangular treatment field but the volume to be treated is not rectangular in shape hence additional shaping is required to achieve a good therapeutic result. Modern multileaf collimators were introduced in 80s to allow flexibility in the shape of the radiation beam. The multileaf collimators have up to 80 pairs of leaves each with its separate motor which enhance the independent movement of the leaves to create conformal beam shape. Modern treatment techniques such as 3D- CRT, IMRT, IGRT etc employ multileaf collimators for a successful treatment outcome. Intensity modulated radiation therapy (IMRT) uses hundreds of tiny radiation beam-shaping devices, known as collimators, to deliver a single dose of radiation. The collimators can be stationary or can move during treatment, thereby altering the intensity of the radiation beams during treatment sessions.

In IGRT, the machines used are equipped with imaging technology that allows the physician to image the tumor before and during treatment for accurate radiation dose delivery.

Three-dimensional (3D) conformal radiation therapy is a technique where the beams of radiation used in treatment are shaped to match the tumor. The multileaf collimators can be grouped into three main types.

Type A: with this type the MLC provides all the collimation excluding the primary collimator and completely replaces the standard collimation system. e.g. Siemens

Type B: this MLC type is responsible for field shaping but additional shielding is provided by backup collimators. The MLC together with the backup collimators replaces the standard collimation system. E.g. Elekta.

Type C: this provides field shaping in addition to the standard collimation system. Although it is part of the head assembly, it is externally mounted and complements the standard collimation system. eg Varian.

2.21 Secondary Collimator (Diaphragms)

The secondary collimators also called diaphragms are made of tungsten/nickel/iron alloy

It has a thickness of 7.7 cm with low transmission. It is made of four blocks, two of these blocks making up the upper jaws and the remaining two forming the lower jaws. These jaws together provide a rectangular or square fields at isocentre of the linear accelerator. Modern LINACS incorporate independent (asymmetric) jaws that can provide asymmetric

fields, most commonly one half or three quarter blocked fields in which one or two beam edges, respectively, are coincident with the beam central axis.

2.22 Field light

The radiation field on most megavoltage radiation therapy units are shown by a light field projected through the collimator by a light source mounted inside the collimator. Depending on the manufacturer, this light source may be positioned at the location of the x-rays target by a rotating carousel or a sliding drawer assembly, or it may be positioned to one side of the collimator axis of rotation with the light reflected from a mirror. The light field is traditionally used for patient alignment. Hence it is imperative that the light field is congruent with the radiation field. Because of its significance, recommendations for quality assurance of megavoltage radiation therapy equipment require checks of the degree of congruence of the light and radiation fields.

2.23 Isocentre

The isocentre is a fixed point in space where the beam central axis and the gantry rotation axis intercept. It can also be defined as the point in space about which the gantry, the treatment head and the couch rotate. Generally, the centre of rotation is not a single point, but the locus of the centre of rotation will be confined within a sphere whose diameter defines the size of the isocentre. Accurate treatment requires a very small isocentre

deviations. Radiation isocentre and mechanical isocentre are the two known isocentres in radiation therapy.

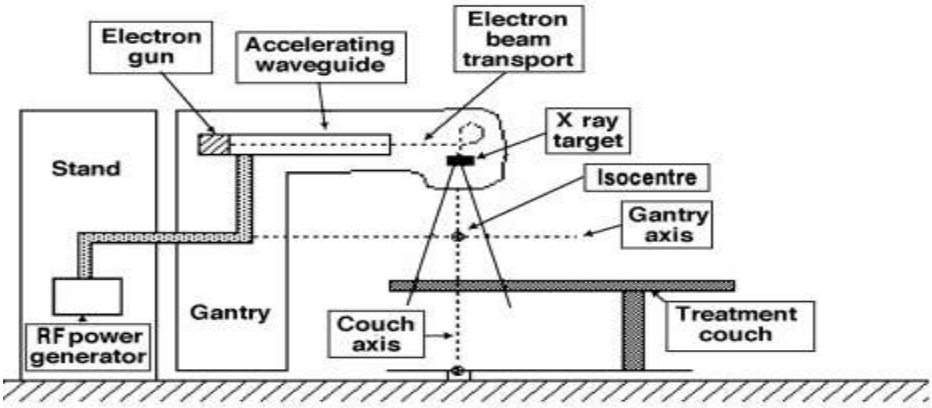

Figure 2. 16: Illustration of an isocentre (Podgorsak, 2008)

Mechanical isocentre is the intersection point of the axis of rotation of the collimator and the axis of rotation of the gantry. Due to its heavy weight, the gantry frame may flex during rotation. This may cause the axis of the gantry rotation to miss the axis of the collimator rotation, thereby creating an uncertainty in the position of the isocentre. The radiation isocentre is the point where the radiation beams intersect if the gantry, collimator or couch is rotated. Current manufacturers of linear accelerators use 100 cm for their isocentre distance (i.e. the distance from the isocentre to the x-ray target). The isocentre clearance is the actual space available for the patient (i.e. the distance between the isocentre and the treatment head covers or accessory tray position). The isocentre height is the height of the isocentre above the floor.

2.24 Quality Assurance

It is an undeniable fact that radiotherapy is a complex process due to the fact that cancerous cells are treated with something (radiation) that cannot be seen. (Mackie, 2015.). From diagnosis to the delivery of treatment, radiation therapy encompasses different groups of professionals from numerous fields of study who are involved in the different stages of cancer treatment as represented in the Figure 2.17. A dedicated teamwork is therefore critical for cancer treatment in radiotherapy. For a QA program to be effective, all the staff involved with the radiation oncology service must be well coordinated and committed to QA (Khan et al, 2014). There must be cooperation among administrators, radiation oncologists, nurses, medical physicists, and therapy technologists to achieve quality in radiotherapy.

The uncertainty in the dose delivered to control tumor cells is as a result of errors that may occur at different stages in the treatment process such as determination of patient anatomy (errors in obtaining outline, patient positioning, defining organs at risk, estimating tissue inhomogeneities, etc.), definition of target volume(s) (shapes and location, failure to take into account movements of organs or tissues due to circulation and respiration and or of the whole patient, etc.), treatment planning (errors in beam data, beam models, computer software and hardware, etc.), treatment delivery (errors in machine calibration, patient set-up, improper machine settings, etc.), patient data (identification, diagnosis, treatment prescription, records of previous treatment given, portals of entry, etc**.)** These sources of errors show the complexity of radiotherapy process and emphasizes the need to follow and

adhere to a comprehensive quality assurance programme, if the best possible therapeutic outcomes are to be obtained (WHO et al., 1988).

2.24.1 Need for QA

The accelerated rate of development and inception of new technologies during the past ten years have enhanced the delivery of highly conformal, individually-shaped dose distribution with high accuracy (Nordström, 2012). On the other hand, the increased complexity of some of the stages of cancer treatment such as treatment planning and treatment delivery may also create a room for a higher chance of incidents (WHO, 2008). Riverside OH, Tyler TX, Indiana PA, Cleveland (Plain Dealer), Epinol, Panama, Glasgow, Zarragosa, New York (Times),etc. are names synonymous with radiotherapy events for which patients were either injured or killed because QA procedures were not followed or QA procedures were outdated (Orton & Hendee, 2012).These technologies introduced with the aim of obtaining enhanced accuracy of treatments could turn out be a new source of error if they are not used correctly . In order to get a high accuracy and high precision that would result in increased tumor control rates and at the same time keep normal tissues complication within the recommended limits, a comprehensive quality assurance program is needed to minimize uncertainties and errors. (Khan & Gibbons, 2014). Again if high accuracy and precision are achieved through quality assurance it will help to exploit improved technology and more complex treatments in modern radiotherapy. Also quality assurance increases the chances of detecting errors and rectifying them sooner if they occur hence minimizing the negative effect on patient treatment. Quality assurance sometimes helps in the comparison of results among different radiotherapy centres, ensuring a more

uniform and accurate dosimetry and treatment delivery. This is necessary for clinical trials and also for sharing clinical radiotherapy experience and transferring it between centres.

2.25 Quality Management

The growing complexity of modern cancer treatment procedures challenges the traditional quality management approaches like quality assurance, quality control, quality audit, etc. These approaches lay more emphasis on the output of the performance of the equipment in radiation therapy procedure. It has been realized that many errors that happened in radiotherapy are not attributed to the failures in the equipment and the software employed in the course of the treatment process, but these errors are due to failures in the workflow and the process. With the systematic understanding of the likelihood of occurrence and the clinical effects of potential failures in radiotherapy process, quality management resources can be allocated to the needed areas to produce optimum safety and quality of patient care. Quality management therefore involves all the activities which are designed to achieve the required quality goals in radiotherapy. Quality management acts as a barrier that protects the patient from the consequences of failures caused by factors such as equipment (e.g. linear accelerator, treatment planning software), process, human and organizational factors and external environment. The components of quality management include quality planning, quality control, quality assurance and quality improvement (Ford et al., 2014). Risk management forms part of the complete quality management program. Quality management has the goal of focusing on the risk assessment for the system and the entire

process involved in the treatment of cancer patient and adopt actions which will suppress failures and prevent degradation of treatment quality if failure occurs (Huq et al., 2016).

2.26 Risk Management

Risk used in this context means radiation risk which means risk of all the various ways in which a patient could be harmed in using ionizing radiation for treatment (European Commission, 2015). Some of the terms linked with accidents in radiation therapy are event, adverse error - event and near miss event. An event is anything that occurs or is associated with patient during cancer treatment. An adverse error-event is an event that leads to unintended harm either minor or serious to the patient by an act of omission or commission. Near miss is an event that could have led to unintended harm to the patient but which did not get to the patient.

Risk management can be described as all the institutional arrangements and processes that are devised to optimize safety, and avoid or minimize the occurrence of risks or limit its effect. It can also be defined as identifying, assessing, analyzing, understanding and acting on the risks issues in order to reach optimal balance of risk, benefit and cost. Risk management is related to significant traditional tools of quality management like quality assurance, quality control and quality audit. A new structure should not be created for risk management but rather it should be integrated with quality management to attain its objectives. There are two main approaches to safety in risk management which are the

proactive risk assessment and reactive analysis of event. These tools are usually used together to provide optimum outcome of risk management.

2.27 Reactive analysis of event

Reactive analysis of event concentrates on a specific event and involves the investigation of causes, identification of barriers that failed and corrective action required. It is usually employed when a failure is spotted whether or not the consequences of the failure propagated through the treatment process to affect the patient. The underlying objective of the reactive analysis approach is to help improve systems and processes to reduce risk of harm to patient in the future because of repetition of a specific failure mode. This objective can be achieved by locating the causes of the failure mode and with the help of these identified causes appropriate actions are taken to make changes in the procedures or quality management program. The process of identifying the causes of events is what is termed as "Root Cause Analysis" (RCA). A root-cause-analysis tree begins with an event and works backward in time, considering the actions and conditions that immediately led to that event to assist in understanding the causes of an event (Thomadsen, 2013).

The root cause analysis is a reactive tool that determines the causes of failures in radiotherapy process, and with the knowledge of the root causes of these failures the process can be improved through quality management program hence reducing the probability of the failure from recurring. Adverse error event can be prevented be applying the concept of "Swiss cheese" model in the defense system used in the treatment centers. James Reason compared defense systems to a series of slices of Swiss cheese that are

placed perpendicularly to each other with spaces between them in his "Swiss Cheese" model as shown in Figure 2.19 and Figure 2.20. According to his model the presence of errors (holes) in a single layer do not lead to bad treatment outcome, rather undesired result occurs when the errors in various layers of the defense system are lined up to allow propagation of an adverse error event to cause harm to patient. Active failures and latent conditions give rise to the holes in the layers. Active failures are unsafe acts or omissions committed by people who are in direct contact with the patient or system. They are the result of an interaction between an individual and a larger part of the system (such as a linear accelerator or a patient). Latent conditions are bugs within the system. They arise from decisions made by designers, builders, procedure writers, and top level management. They can be related to the equipment (hardware or software) or the procedures (European Commission, 2015).

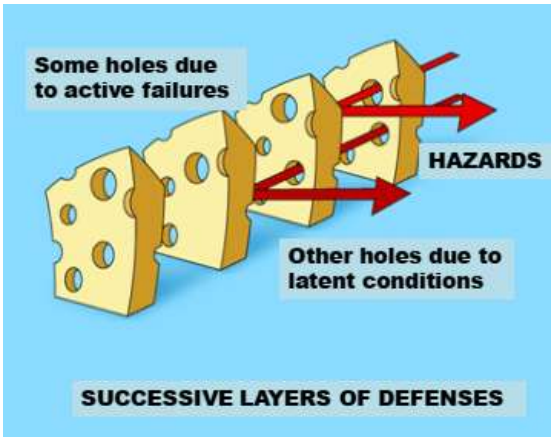

Figure 2.29: holes in the individual layers are not lined up hence errors do not propagate to cause harm to patients. (European Commission, 2015)

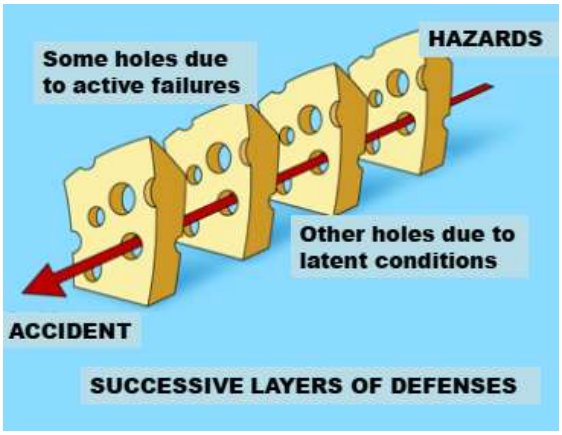

Figure 2.20: The holes are lined up in the defense layers allowing propagation of errors to cause accident. (European Commission, 2015)

2.28 Proactive Risk Assessment

Risk assessment is an analysis of a process to identify the components or areas which are prone to errors or hazards. Risk assessment helps to locate the weakest or riskiest process steps before a failure occurs. A new process is designed or the existing system is modified to reduce the probability of occurrence of a potential failure or increase the chance of

detecting the failures before the intended result is compromised. The steps involve in risk assessment are:

1. Identification of failures
2. Analysis of the severity of the failures
3. Evaluation of the likelihood of the failures
4. Evaluation of the risk on the basis of likelihood and severity
5. Using risk criteria for making decision
6. Measures to minimize the risk

Among the many tools used for risk assessment, AAPM TG 100 has recommended process mapping, failure mode effect analysis (FMEA) and Fault Tree Analysis (FTA) for risk analysis in radiotherapy.

2.29 Process Mapping

Process mapping shows a visual representation of the steps involved in a process. It forms the basis of other quality and safety tools such as FMEA and FTA. It allows one to see where incidents are happening along the workflow. When process are mapped out visually weakness in the workflow can be easily observed and addressed. It the first step in risk assessment. Developing and understanding the process map are crucial to performing FMEA and providing the medical physicists and the rest of the risk assessment team an overview of the entire process.

Process map of the radiotherapy procedure

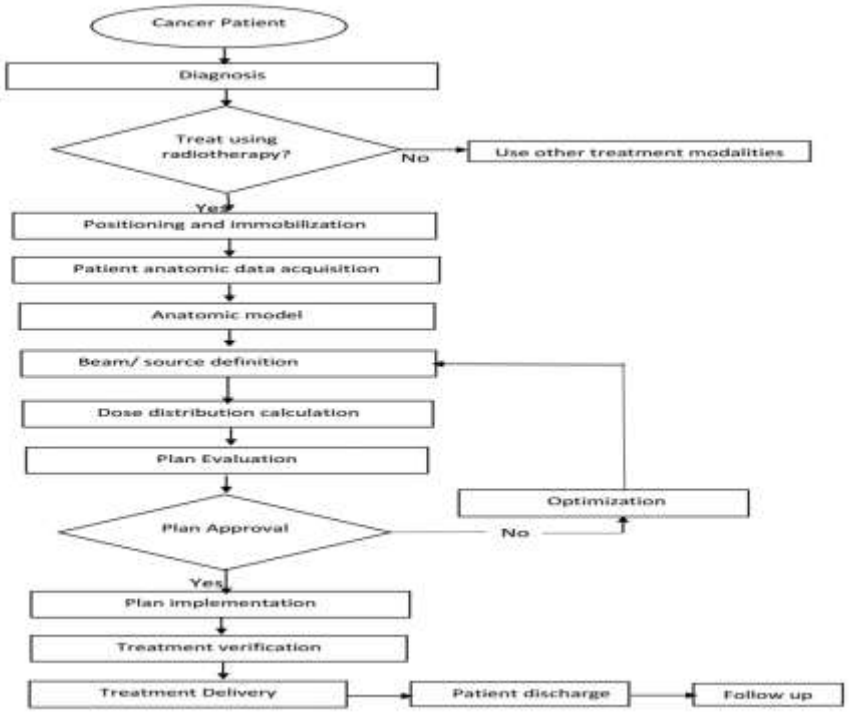

Figure 2. 17: Diagram of process mapping in radiotherapy (Khan et al., 2011)

2.30 Failure Mode and Effect Analysis

A failure mode is the way in which a failure occurs or is observed or the way in which a sub process step fail to meet its intended purpose. Example of failure modes are Incorrect isocentre, dose delivered to incorrect volume, wrong dose (too high or too low), total power loss of the LINAC system, incorrect beam adjustment etc. failure modes are caused by; inadequate training, lack of good procedures, stressful environment, insufficient time to

perform work properly, improper calibration of equipment, lack of machine maintenance, malfunctioning equipment or devices etc (Huq et al., 2016).

After mapping out the entire process with a process map, then follows the assessment of the potential risks involved in the process. Failure mode effect analysis defines, locates and removes or intercept known or potential failures before reaching the patient. Failures in each step of the process can be evaluated using FMEA to determine the likelihood that they will not be detected, assess the severity of these failure modes and their consequence on the patient. Numerical values are assigned to three components of failure which are likelihood of occurrence (O), severity of the effect of the failure (S) and likelihood that the failure would go undetected (D). The numbers range from 1 to 10 for each of these components, with 1 assigned to no appreciable danger and 10 to the most severe. The risk priority number (RPN) of each identified failure mode is then calculated to help prioritize these failures (Huq et al., 2016).

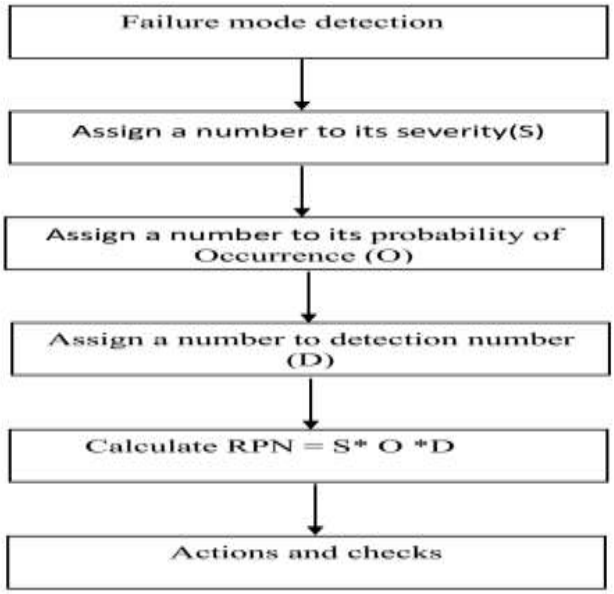

Figure 2. 18: Indicates steps of quantitative FMEA analysis (Huq et al., 2016).

2.31 Fault Tree Analysis (FTA)

Fault tree analysis is used to evaluate the propagation of failures in a process. A fault tree augments a process tree and provides an overview in the form of a diagram indicating how failures are propagated through a procedure, and it aids in developing intervention strategies and measures to eliminate or reduce the risks that have been identified. Fault tree analysis allows one to visualize potential locations in the process for effective and efficient quality management (QM) measures (Huq et al., 2016).

It is not advisable for a radiotherapy center to be dependent on a single quality management step to handle failures occurring in the process. Although a quality assurance step may have the tendency of blocking the propagation of errors from the many steps involved, but failure of the quality assurance step would result in vulnerability of the entire procedure. When relying on only QA, step failure could only be detected after several incorrect steps have happened and it sometimes becomes difficult to identify the step contributing to the failure as this information is needed in order to correct the failure. Thus integrating multiple quality management steps enhance efficiency of the entire process.

CHAPTER 3

Materials and methodology

This chapter gives a description of the materials and the clinical procedures for carrying out some of the quality controls of the LINACS at St. Olav's hospital. It will also describe how the research was done to achieve its objectives. The QA data for over a five year operational period were collected and stored in a database. Elekta linear accelerator (Elekta, Stocholm, Sweden), QUASAR pentaguide phantom, and equipment such as IBA blue phantom, cylindrical ionization chamber (CC 13, IC 15), plane parallel chamber (PPC 594) and diodes (EFD,CC13) all from IBA Dosimetry, Schwarzenbruck, Germany were employed.

Figure 3. 1: An ELEKTA LINAC at St. Olav's Hospital

The radiotherapy department of the hospital has five LINACS (SB2, SB3, SB4, SB5 and SB6) machines from Elekta Company for treatment. Some of them use both electrons and photons for treatment whiles others use photons only. The photon energies of the LINACS are 6 MV and 15 MV while the electron produces 6, 8, 10, 12 and 15 MeV energies for treatment. The MLCs of the machines have two banks with each bank containing 80 leaves (field size 40×40 cm). Each of the leaves is driven by its individual motor allowing different shapes of radiation beams to be formed. The maximum field size that can be treated with the LINACS is 40×40 cm^2. The LINACS employ treatment techniques such as 3DRT, IMRT, VMAT, and SRS. They are also integrated with XVI which forms a vital tool for positioning of patients and verification in IGRT.

Table 3. 1: Description of the LINACS at St Olav's hospital

Name of LINAC	Model	Photon Energy	Electron Energy	MLC	Year installed	Treatment delivery	KVI Imaging for IGRT	Treatment couch
SB2	Elekta synergy MC1020	6 and 15 MV	6,8,10, 12 and 15 MeV	80 MLC (field size 40×40cm, leaf thickness - 10mm)	2011 (new head in 2014)	3D, IMRT, VMAT, SRS,	XVI	Hexapod
SB3	Elekta Versa HD 153245	6 and 15 MV	N/A	160 MLC(field size 40×40cm, leaf thickness - 5mm)	2014	3D, IMRT, VMAT, SRS,	XVI	Hexapod
SB4	Elekta synergy MC5928	6 and 15 MV	6,8,10, 12 and 15 MeV	80 MLC(field size 40×40cm, leaf thickness - 10mm)	2011 (new head in 2014	3D, IMRT, VMAT, SRS,	XVI	Hexapod
SB6	Elekta Versa HD	6 and 15 MV	N/A	160 MLC(field size 40×40cm, leaf thickness - 5mm)	2015	3D, IMRT, VMAT, SRS,	XVI	Hexapod

3.1 Water phantom

The annual controls are performed to check the beam quality of the photon and electron energies, fieldwidth, flatness and symmetry of the beam.

The annual controls are measured using the blue water phantom manufactured by IBA. The blue phantom is used for measuring and analyzing the radiation field of medical linear accelerators. It consists of perspex water tank of dimensions 48 cm x 48 cm x 48 cm and 1 cm on sides and 1.5 cm base thickness. It has a high precise control mechanism for the movement of the ionization chamber. The weight of the phantom without water is 45 Kg and it has a pumping rate of 20litres/min. It has a movement range of 50 cm in the vertical direction with filling and draining time of 8 and 10 minute respectively. The phantom consists of three-dimensional servo tank, a control unit with integrated two channel electrometer (CCU) and two single detectors (ionization chamber), one for measurement and the other used for reference. Other accessories of the blue phantom are the water reservoir, temperature and pressure sensor and a lift table. The temperature and pressure sensor is set up inside the water tank for the measurement of water temperature within ± 0.30 degree Celsius. The water temperature measurement is used in combination with the pressure measurement (build-in pressure sensor provided in the CCU) to allow automatic temperature and pressure correction (KTP) for output factor determination or absolute dosimetry (IBA. 2014).

Figure 3. 2: IBA blue phantom being filled with water from the reservoir for annual QA (St. Olav's hospital).

3.2 Methods

In this research the current performance of the LINACS was assessed by investigating the current measurements of the daily, monthly and annual controls. Based on the deviation of these measured controls, the Risk Priority Number (RPN) was calculated for the failure modes such as dose delivered to incorrect volume, wrong dose (too high or too low dose) and incorrect isocentre. Numerical values between 1 and 10 were assigned to the three components of FMEA; Occurrence (O), Detection (D) and Severity(S). The products of these components gives the RPN value. The higher the RPN, the more likely the failure mode is to occur, the less likely the failure mode will be detected and the more severe the result of the failure mode.

Table 3. 2: FMEA ranking scales for occurrence, detection and severity (Huq et al., 2016)

Rank	Occurrence	Detection	Severity
1	Remote probability	Always	No effect
2	Low probability	High likelihood	Minor effect
3			
4	Moderate probability	Moderate likelihood	Moderate effect
5			
6			
7	High probability	Low likelihood	Serious effect
8			
9	Very high probability	Very low probability	Injury
10	100 percent probable	Never	Death

RPN calculation for dose delivered to incorrect volume

Deviations in the XVI measurements can contribute to this failure mode.

S = 6, D = 7, and O = 4
RPN = S × D × O
RPN = 6 × 7 × 4
RPN = 168

RPN calculation for wrong dose (too high or too low)

Beam quality and beam profiles are controls that have effect on this failure mode.

S = 8, D = 7, and O = 3

RPN = S × D × O

RPN = 8 × 7 × 4

RPN = 224

RPN calculation for incorrect isocentre

The controls that can influence this failure mode are laser alignment, couch movement, gantry rotation isocentre, couch rotation and collimator rotation.

S = 7, D = 7 and O = 4

RPN = S × D × O

RPN = 7 × 7 × 4

RPN = 196

The data of the controls which contribute to these potential failure modes are extracted from the database and analyzed thoroughly using statistical process control (SPC), SPSS and Excel.

3.3 Statistical process control (SPC)

Statistical process control is an analytical tool that uses quantitative data for measuring normal and abnormal variation of a process. SPC employs process behavior charts such as control which can detect the stability of a process. The control chart is graphical tool used to study how a process changes over time. It has central line for the mean, an upper line which is three standard deviations away from the mean ($+3\sigma$) is the upper control limit (UCL) and the lower line which is also three standard deviations (-3σ) away from the mean is the lower control limit (LCL). Data points can be plotted using Xbar/R chart, Xbar/S chart or I/MR chart depending on the number of sample size of the data. If the sample size is equal 1, individual moving range (I/MR) is used. Xbar/R is used if the sample size is

small usually from 3 to 8. Xbar/S for a large sample size greater than 8. Data points falling within these control limits is an indication that the process is performing as expected. Any variation within the limits is likely due to common cause variation that is natural variation that is expected as part of the process. Points outside the control limits mean that an assignable (special) cause is likely the source of the variation and something within the process needs to be done to fix the problem before the failure occurs (Tech & Forest, 2014).

Figure 3.3: Picture of CC13 (IC 15) ionization chamber (St. Olav's hospital)

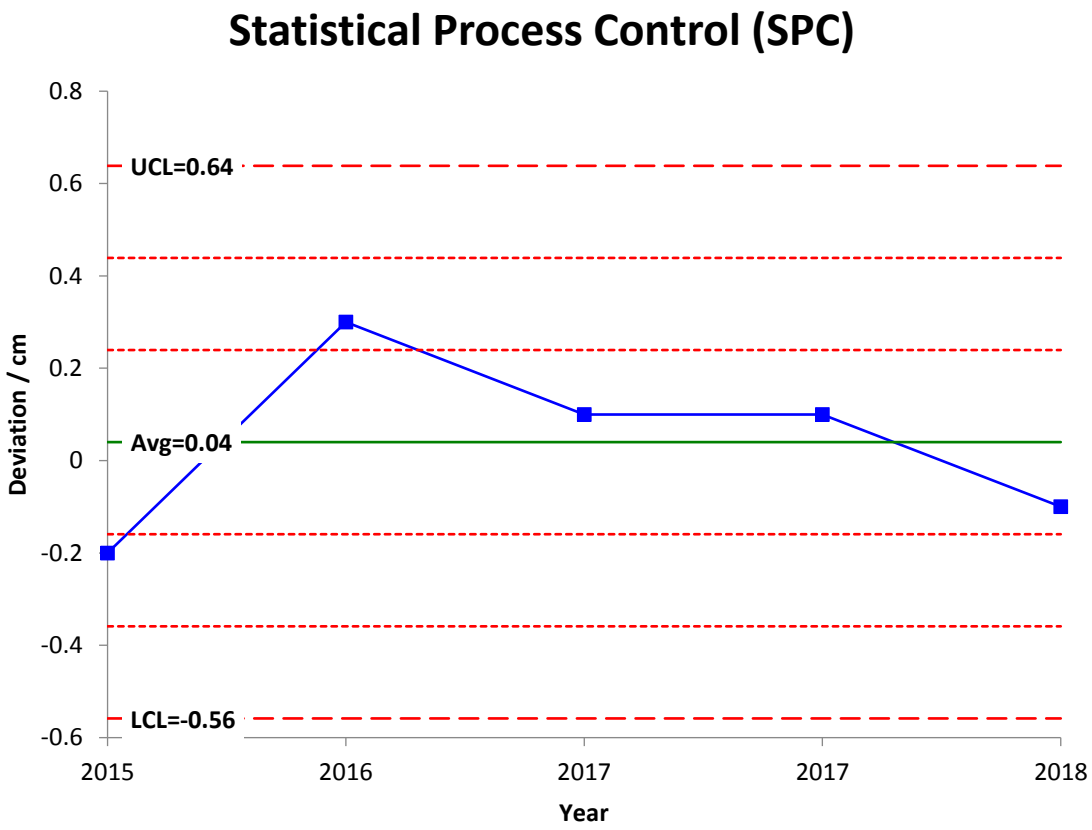

Figure 3. 3: Illustrates an output from SPC, the UCL and LCL are three standard deviations away from the mean (Avg).

Table 3. 3: Some of the controls that are performed during quality assurance procedure (St Olav's hospital)

Procedure	**Frequency**	**Tolerance**
Dosimetry		
Depth doses for photon energies (water phantom)	Annual	±1.0%
Depth Doses for Electron energies (water phantom)	Annual	±0.5 mm
Absolute dose (calibration) in water, photons and electrons	Annual	±0.5%
Absolute dose (calibration) in SW-phantom, photons and electrons	3rd Month	±0.5%
Beam profile (symmetry and flatness) for photons	Annual	±1%
Beam profiles (symmetry and flatness) for electrons	Annual	±1 %
Constancy control beam profile (symmetry and flatness) for photons and electrons	weekly	
Constancy control relative dose, photons and electrons	weekly	
Mechanical		
Collimator rotation	monthly	
Distance Indicator	monthly	±2 mm
Gantry rotation	monthly	
Couch rotation	monthly	
Couch (Table) movement	Daily	
Light field coincidence	Monthly	±2 mm
Localizing lasers	Monthly	
Cross hair centering	monthly	±4 mm
X-ray volumetric imaging	weekly	±1 mm
Laser Alignment	Daily	
Safety		
Door interlocks	monthly	functional
Touch guards (LINAC head, detector panels, table, controller)	monthly	functional

3.4 Controls of LINACS

The output of the linear accelerator is monitored continuously through measurements of controls such as the beam quality, beam profiles (symmetry and flatness), collimator rotation isocentre, gantry rotation isocentre, couch rotation isocentre, coincidence of radiation and mechanical isocentre etc. to ensure that the machine is still performing within the acceptable levels attained at the time of acceptance testing and commissioning.

3.5 Annual Controls

In radiotherapy the primary interest is penetration of the beam into the patient, beam quality is an indication of the penetrating ability of the photons and electrons through a material. Beam quality and beam profiles of the energies are checked during the annual controls to verify that the penetrability and uniformity of radiation energy delivered to the patient are within the acceptable standard. The most commonly approved measure of beam quality for photon energies is the use of quality index (QI), which is also referred to as ionization ratio. It is defined as the ratio (Tissue Phantom Ratio) of doses at different depths (20 cm and 10 cm). The 10 cm is taken as the reference depth and if the reference depth is at d_{max}, TPR gives rise to Tissue Maximum Ratio. The beam quality of the electrons on the other hand is defined by reference to 50% depth dose **R_{50}, i.e**. the depth at which the dose is half the maximum dose is measured.

Table 3. 4: Procedures for checking the controls of quality assurance of LINAC system.

Checking the beam profiles of photons					measurement
Field size	**Energy**	**Depth (cm)**	**Detector**	**SSD(cm)**	**Profiles**
10×10 cm^2	**6 mv**	**1.5**	**Diode**	**90**	**IP/CP**
	“	**10**	**“**	**“**	**“**
40×40 cm^2	**6 MV**	**1.5**	**“**	**“**	**“**
	“	**10**			**“**
10×10 cm^2	**15 MV**	**3**	**“**	**“**	**“**
	“	**10**	**“**	**“**	**“**
40×40 cm^2	**15 MV**	**3**	**“**	**“**	**“**
	“	**10**	**“**	**“**	**“**
Depth doses	**6 mv**	**10**	**Ion chamber**	**100**	**D_{10}**
	“	**20**	**“**	**“**	**D_{20}**
	15 mv	**10**	**“**	**“**	**D_{10}**
	“	**20**	**“**	**“**	**D_{20}**
Checking the beam profile of electrons					
20×20 cm^2	**6 MeV**	**1**	**diode**	**100**	**IP/CP**
“	**8 MeV**	**2**	**“**	**“**	**“**
“	**10 MeV**	**“**	**“**	**“**	**“**
“	**12 MeV**	**“**	**“**	**“**	**“**
“	**15 MeV**	**“**	**“**	**“**	**“**
Depth doses of electrons					
20×20 cm^2	**6 MeV**		**PPC**	**100**	**R_{50}**
“	**8 MeV**		**“**	**“**	**R_{50}**
“	**10 MeV**		**“**	**“**	**“**
“	**12 MeV**		**“**	**“**	**“**
“	**15 MeV**		**“**	**“**	**“**

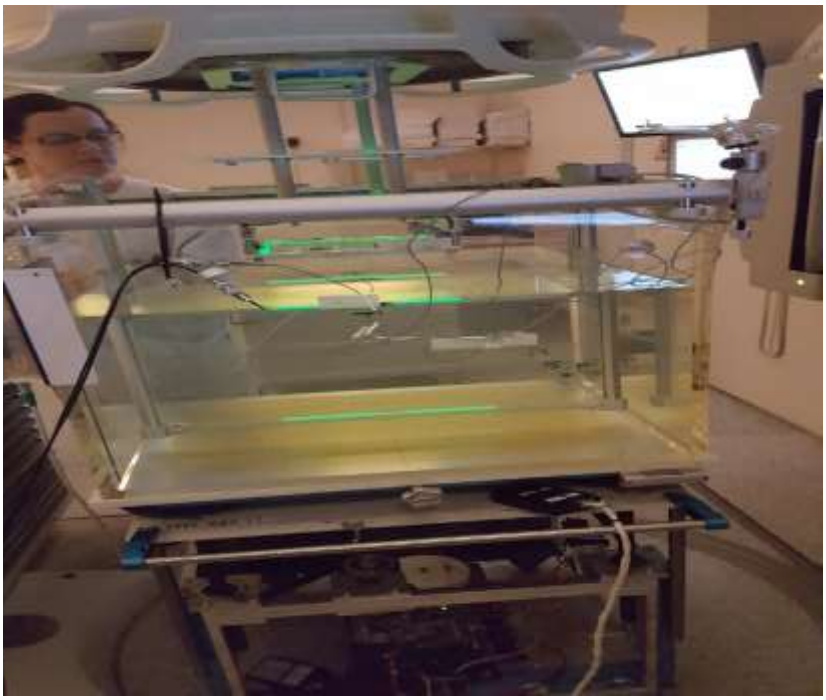

Figure 3. 4: Setup for checking the beam quality and beam profiles of electrons and photons (St. Olav's hospital)

3.6 Procedure for depth dose measurement of photons

Two ionization chambers (one for field measurement and the other as reference for accounting for possible variation in the dose rate) are placed in the water phantom set up, with SSD at 100 cm, 10 cm × 10 cm field size, a photon beam of 6 MV energy was delivered to the water phantom and the doses at the depth of 10 cm and 20 cm were measured and recorded. The TPR was calculated using the doses at a depth of 20 cm and 10 cm. and compared with reference values.

$$\text{TPR} = \frac{D_{20}}{D_{10}} \ldots\ldots\ldots (3.1)$$

The photon energy was changed to 15 MV and with same set up the doses at the depths of 20 cm and 10 cm were measured respectively. Again the TPR of the doses at the depths of 20 cm and 10 cm was calculated and compared with reference values.

3.7 Measuring beam quality of electrons

The water phantom was set up with the two plane parallel chambers one for field measurement and the other as reference at their appropriate positions, SSD at 100cm, field size of 20 cm x 20 cm and the applicator fixed in position, the energies (6, 8, 10, 12 and 15 MeV) of the electrons were checked. For each of the energies the depth of R50 was measured, which is the depth at which the dose is half the maximum dose. The measured depth is compared with reference depth.

3.8 Beam Profiles

Flatness and symmetry are the main parameters for determining the pattern of a photon and electron beam produced by linear accelerators (An, 2009). Flatness and symmetry form part of the significant parameters that need to be kept within the tolerance levels because they can have a huge influence on the accuracy with which the treatment is delivered.

Flatness of radiation beam is defined as;

$$\text{Flatness} = \frac{D_{max} - D_{min}}{D_{min} + D_{min}} \times 100\% \quad \ldots\ldots\ldots \quad (3.2) \quad \text{(Hossain \& Rhoades, 2016)}$$

where D_{max} and D_{min} denote the maximum and the minimum absorbed dose values within the central 80% of a dose profile in a plane transverse to the beam axis. On the other hand electron beam flatness is defined as the ratio of the maximum dose in the field at the depth of dose maximum to the dose on the central axis rather than to the minimum dose.

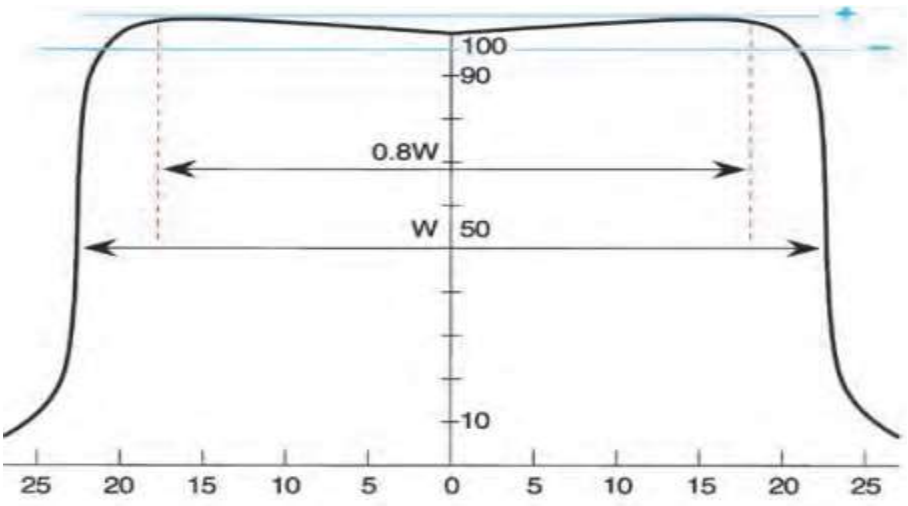

Figure 3. 5: The photon field flatness is measured within a region bounded by 80% of the field width (W). (Khan et al., 2011)

The flatness check was done together with symmetry check, symmetry is also defined as the maximum value of the ratio of the higher to the lower absorbed dose at any two positions symmetrical to the radiation beam axis inside the flattened area. Diodes were used for measurement of the beam profiles, due to high density of atoms in silicon diodes compared to air, a diode detector can be constructed very small and still have a good response. Hence in high gradient field such as penumbra, a diode detector will be more precise. Also in small fields the low energy scatter contribution is low hence diode

shielding is not needed and it also has the highest response per volume, the sensitive volume is usually small to avoid dose volume effect.

3.9 Measurement of electron's beam profile

The plane parallel chambers were removed from the water phantom and replaced with two diode detectors, one for measurement and the other as reference. With an SSD at 100cm and field size of 20 × 20 cm^2 an electron beam of 6 MeV was delivered to the water phantom with the detector at a depth of 1.0 cm, the field width, symmetry and flatness of the beam were measured for both inplane and crossplane profiles and compared to reference values.. The same procedure was repeated for 8, 10, 12 and 15 MeV but this time the depth of the detector was at 2.0 cm as illustrated earlier in Table 3.3.

3.10 Measurement of photon's beam profiles

Beam profiles for the two photon energies (6 MV and 15 MV) were checked. Two diode detectors were used in the setup, one for field measurement and other was used as reference instrument. The SSD was set at 90 cm. the reference detector should always be in the field of the beam during measurement.

With a field size of 10 × 10 cm^2, a 6 MV photon energy was delivered to the water phantom at a depth of 1.5 cm **(d_{max})** and 10 cm. The reading of the field width, flatness and symmetry for inplane and cross profiles were measured and recorded. With the same photon energy of 6 MV and the same setup but with the field size changed to 40 × 40 cm^2,

the field width, flatness and symmetry of both inplane and cross profiles were measured and recorded.

The photon energy was changed to 15 MV for the same setup, for field sizes of 10 × 10 cm^2 and 40 × 40 cm^2, the water phantom was irradiated at a depth of 3 cm (d_{max}) and 10 cm for both field sizes. The field width, the flatness and symmetry of for inplane and cross profiles were measured and compared with reference values.

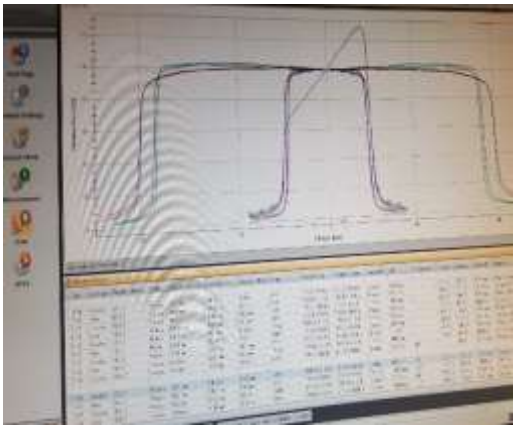

Figure 3. 6: Beam profiles of the photon energies for 10 × 10 cm^2 and 40 × 40 cm^2 field sizes with 60° wedge in the beam. (St Olav's hospital)

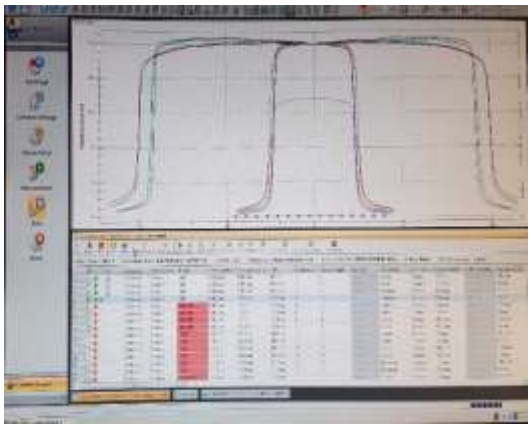

Figure 3. 7: Beam profiles of the photon energies for 10 × 10 cm^2 and 40 × 40 cm^2 field sizes without wedge in the beam. (St Olav's hospital)

3.11 Monthly controls

The monthly controls focus on the geometrical checks such as the lasers, optical distance indicator (ODI), couch movement, lightfield, gantry rotation, collimator rotation and touchguard. A locally manufactured block with markings of 10 cm × 10 cm field, corner indicators for 15 cm × 15cm and calibrated marks for detecting errors was used for performing the monthly checks. The QA block comes with a spirit level to check that the

surface is perfectly level. It also has the letters “G” and “T” inscribed on the surface indicating directions for gantry and target respectively.

Figure 3. 8: A home built monthly QA Phantom (St Olav’s hospital)

Figure 3. 9 The setup of monthly QA phantom for geometrical checks (St Olav’s hospital)

3.12 X-ray volumetric imaging (XVI)

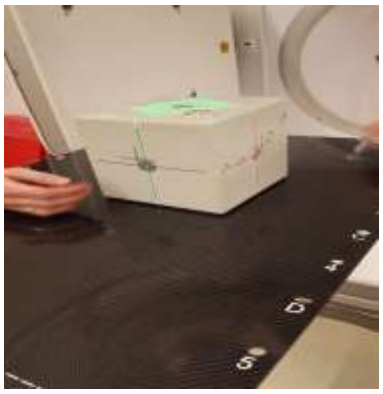

Figure 3. 11: The phantom is repositioned to the center of the XVI (St Olav’s hospital)

Figure 3. 11: A picture of Penta Guide phantom for XVI QC (St Olav’s hospital)

The Penta Guide phantom was positioned at the off-center position using lasers. Perform XVI volumetric uptake and register with reference images. The software calculates a set of values in the lateral, longitudinal and vertical directions that will be used for repositioning of the phantom to the center position. Based on the values calculated in the three directions, an automatic repositioning was performed. Confirm that the phantom is in the center position according to the lasers as shown in Figure 3.11.

CHAPTER FOUR

4.1 Introduction

The controls selected for this research include x-ray volumetric Imaging (XVI), absolute dose calibration of photon energies, depth doses and beam profiles of the photon and electron energies. This section discusses into details the findings of the research. The XVI and the absolute dose calibration were analyzed for four LINACS (SB2, SB3, SB4 and SB6) in the hospital. Depth doses and beam profiles of the energies were also covered for SB2 and SB3 LINACS.

4.2 Yearly performance of SB2 LINAC

All the three directions of the XVI of SB2 LINAC have performed within the tolerance limit throughout the year as shown in the Appendix (Table 5.15), however in 2012, the x (lateral) direction exceeded the limit by -0.16 cm. In 2013, 2014,2015 and 2016 the mean deviation in the first dose calibration readings of 6 MV drifted beyond the limit with values of -0.78%,0.58%,1.04% and 1.26% respectively, after adjustments were made and the machine was recalibrated the second measurements of the absolute dose calibration were within the limit as shown in the Appendix (Table 5.15). The 15 MV recorded mean deviations of 0.71%, 1.10% and 1.35% in 2013, 2014 and 2016 respectively. After the recalibration the mean deviations were found to be in the limit. The beam quality of 6 MV and 15 MV were checked using $TPR_{20/10}$ quality index. All the mean deviations were found in the tolerance limit. The quality of the electron energies were investigated using half

value depth in water (R_{50}), 6 MeV and 8 MeV recorded mean deviations that exceeded the limit in 2016 with values of 1.10 and 0.9 mm respectively. The maximum mean deviation in 12 MeV occurred in 2017 which was greater than the limit by (-0.15 mm). Most of the deviations in the symmetry, fieldwidth and flatness were outside the limit as indicated in the Appendix (Table 5.15).

4.3 Yearly performance of SB3 LINAC

The three coordinates of SB3 LINAC have performed within the tolerance limit since its installation in 2014. The peak mean deviation in the longitudinal (y) and vertical (z) directions were 0.08 cm and 0.07 cm which occurred in 2016. The maximum mean deviation in the x- coordinate was 0.03 cm in 2014 as shown in the Appendix (Table 5.16)

The mean deviations in the first measurement of absolute dose calibration of 6 MV were off the tolerance limit in 2014 and 2017, but in the second calibration after the machine was adjusted the readings fell within the tolerance limit. For the 15 MV the mean deviation in the dose in the first calibration measurement occurred in 2014, 2016 and 2017, the mean deviation dropped within the limit after adjustment was made on the machine. TPR ratios of 6 MV and 15 MV have performed within the tolerance limit. The flatness, symmetry and the fieldwidth of both photon energies were within the tolerance limit.

4.4 Yearly performance of SB4 LINAC

The mean deviations of the three coordinates of the XVI of SB4 LINAC were found to be in the tolerance limit. The mean deviations in the first readings of the absolute dose calibration of 6 MV were within the limit except in 2016 which fell beyond the limit by -0.12%.the second measurements were within the limit as shown in Table 4.1.

In the 15 MV, the mean deviations in 2012, 2013, 2015 and 2016 were outside the tolerance limit, after the machine was recalibrated the mean deviations were found in the tolerance limit in Table 4.1

Table 4. 1: Yearly Performance of SB4 LINAC

Procedure	**Tolerance**	**Average Deviation**							
		2011	**2012**	**2013**	**2014**	**2015**	**2016**	**2017**	**2018**
XVI(X-ray volumetric Imaging)	cm	cm	cm	cm	cm	cm	cm	cm	cm
x(lateral) direction	±0.1	-0.05	-0.02	-0.05	-0.06	-0.05	-0.05	-0.02	-0.01
y (longitudinal) direction	±0.1	0.00	0.01	0.04	0.06	0.05	0.06	0.03	0.04
z (vertical) direction	±0.1	0.03	0.03	0.03	0.05	0.02	0.03	0.02	-0.02
Dose Calibration									
6 MV		%	%	%	%	%	%	%	
1st Absolute dose calibration measurement	±0.5%	0.21	-0.40	-0.04	0.38	0.38	-0.62	0.13	-
2nd Absolute dose calibration measurement	±0.5%	-0.10	0.01	0.08	0.02	0.11	0.01	0.00	-
15 MV									
1st Absolute dose calibration measurement	±0.5%	0.13	-0.85	-0.59	0.33	1.13	-1.03	-0.04	-
2nd Absolute dose calibration measurement	±0.5%	0.04	-0.03	0.06	-0.03	-0.01	0.00	0.02	-

4.5 Yearly performance of SB6 LINAC

The XVI of SB6 LINAC recorded maximum mean deviations of -0.11, 0.22 and 0.20 cm in the lateral, longitudinal and vertical directions respectively in the year 2015. These maximum values exceeded the tolerance limit. In the subsequent years all the mean deviations were found in the acceptable limit. The measurements of the first absolute dose calibration of 6 MV produced mean deviations that fell beyond the tolerance limit in 2015, 2016 and 2018, after recalibration the mean deviation dropped within the acceptable limit as indicated in table 4.2. In 2015 and 2018 the mean deviations in the first absolute dose calibration of 15 MV fell outside the tolerance limit as shown in table 4.2, after adjustments were made on the machine and recalibrated the mean deviations were found to be within the tolerance limit in the second measurements.

Table 4. 2: Yearly Performance of SB6 LINAC

Procedure	**Tolerance**	**Average Deviation**			
		2015	**2016**	**2017**	**2018**
XVI(X-ray volumetric Imaging)		**cm**	**cm**	**cm**	**cm**
x(lateral) direction	±0.1 cm	-0.11	0.00	-0.05	-0.06
y (longitudinal) direction	±0.1 cm	0.22	0.06	0.05	0.04
z (vertical) direction	±0.1 cm	0.20	0.03	0.02	-0.02
Dose Calibration					
6 MV		%	%	%	%
1st Absolute dose calibration measurement	±0.5%	-1.56	-1.04	0.40	-1.19
2nd Absolute dose calibration measurement	±0.5%	0.06	-0.01	0.04	0.10
15 MV					
1st Absolute dose calibration measurement	±0.5%	-0.72	-0.26	0.28	-1.23
2nd Absolute dose calibration measurement	±0.5%	0.00	0.01	0.07	-0.01

4.6 Comparing the X-ray Volumetric Imaging (XVI) of the LINACS

From figure 4.1 all the coordinates of the XVI have performed within the tolerance deviation (±0.10 cm) for SB2, SB3 and SB4 over the operational period, the same cannot be said about SB6 which recorded a significant drift in all the three coordinates of the XVI with the deviations occurring in the same year (2015) as shown from Figure 4.2-4.4. According to Figure 4.2, the x-coordinate of SB6 (XVI) has gone beyond the tolerance deviation by a mean deviation of 0.01cm in 2015.There was a rapid improvement afterwards in 2016 recording a deviation of -0.004 cm and then increased to -0.05 cm and -0.06 cm in 2017 and 2018 respectively. After 2015, the repositioning in the lateral (x) direction of the XVI had mean deviations falling within the tolerance value of ±0.10 cm as demonstrated in the plot of figure 4.2. The y-coordinate recorded a much significant deviation of 0.22 cm exceeding the tolerance limit in 2015 and reduced drastically in 2016 with a mean value of 0.06 cm. The subsequent years maintained a deviation within the acceptable limit of ±0.10 cm with the mean deviation falling further to 0.05 cm and 0.04 cm in 2017 and 2018 respectively in figure 4.3. In 2015, the deviation in z-coordinate of the XVI had a deviation value of 0.20 cm which is twice the tolerance deviation (±0.10 cm), the deviation dropped within the acceptable limit with a value of 0.04 cm in 2016. It again fell slightly in 2017 with a drift of 0.03 cm and -0.01cm in 2018 from figure 4.4.

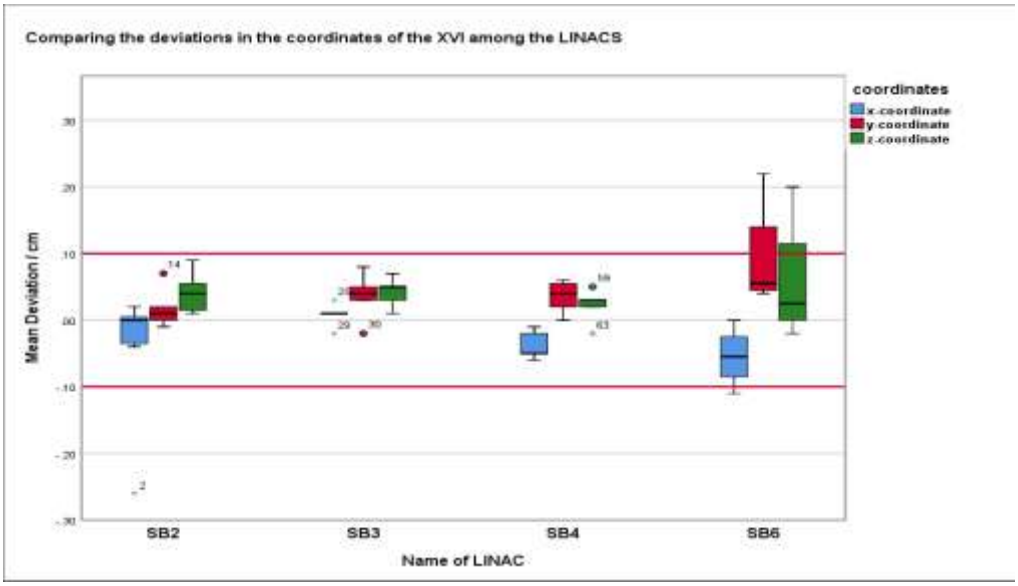

Figure 4. 1: Comparison of the deviations in the three coordinates of XVI among the LINACS

One way ANOVA test was performed on the three components of the XVI of all the LINACS as shown in the Appendix (Tables 5.10- 5.12). The P-value of the x- coordinates of the LINACS was 0.060 (≥ 0.05), which indicates that the difference between the means of the XVI's was not significant. The y-coordinates also recorded a P-value of 0.098 (≥0.05) which was also insignificant. The P- value of the z- coordinates was found to be 0.021 (≤0.05) that is an indication that the difference between the means was significant that is something other chance occurred.

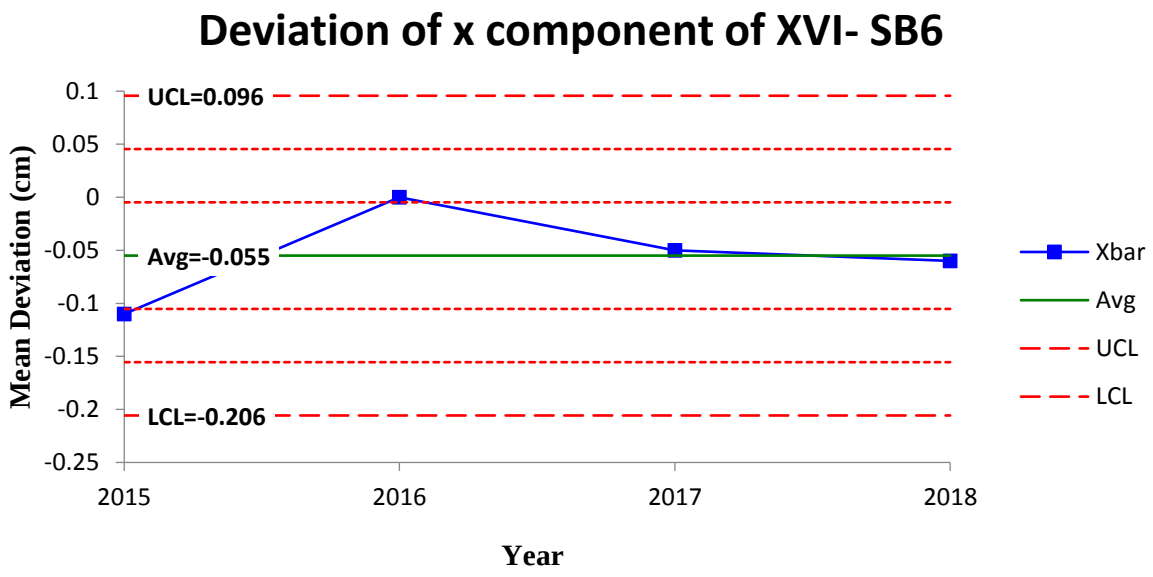

Figure 4. 2: The deviation in the x-coordinate of SB6-XVI

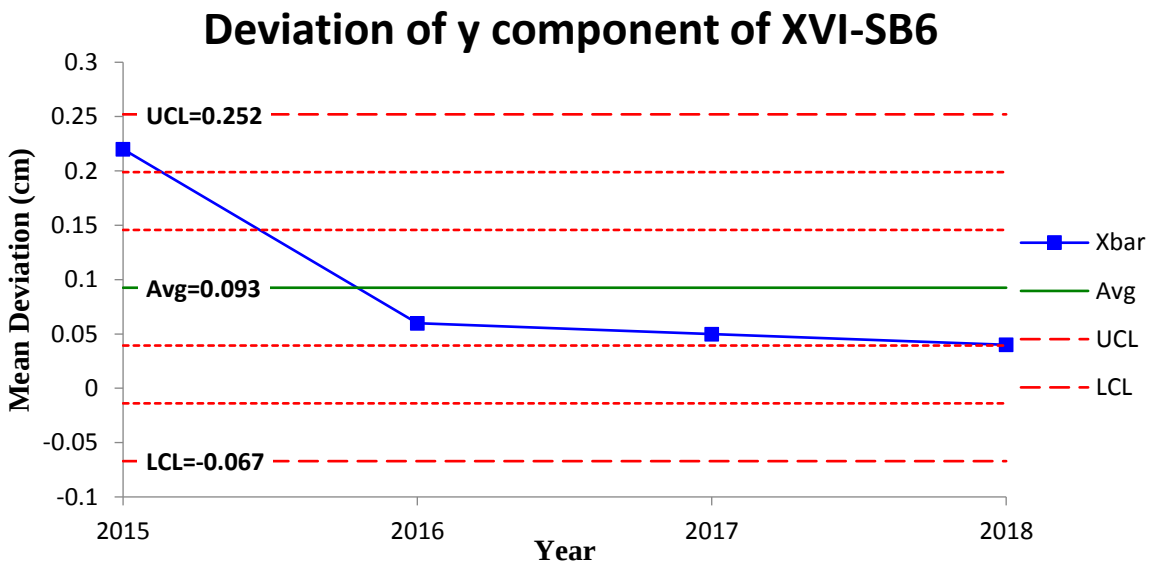

Figure 4. 3: The deviation in the y-coordinates of SB6-XVI

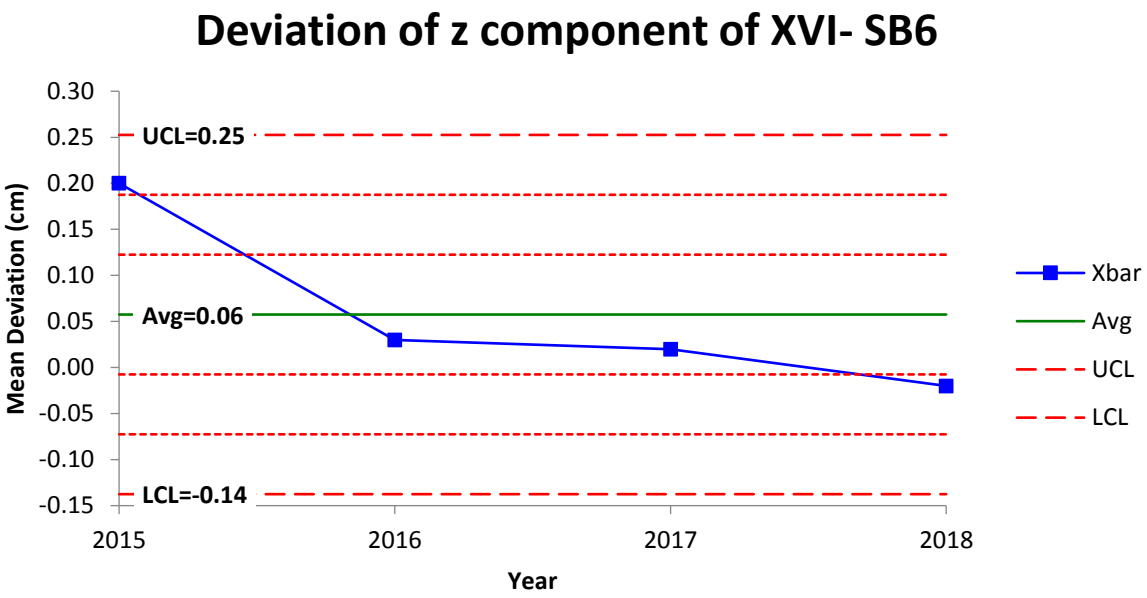

Figure 4. 4: Deviation in the z-coordinate of SB6-XVI

4.7 Dose Calibration

The deviations in the first dose calibration measurements were compared among the LINACS, the mean deviation was found to be significantly high in 15 MV of SB3 LINAC with a value of -2.30% and 1.50% for 6 MV of SB2 LINAC as illustrated in figure 4.5, most of the mean deviations fell outside the tolerance deviation of ±0.5% for all the other LINACS.

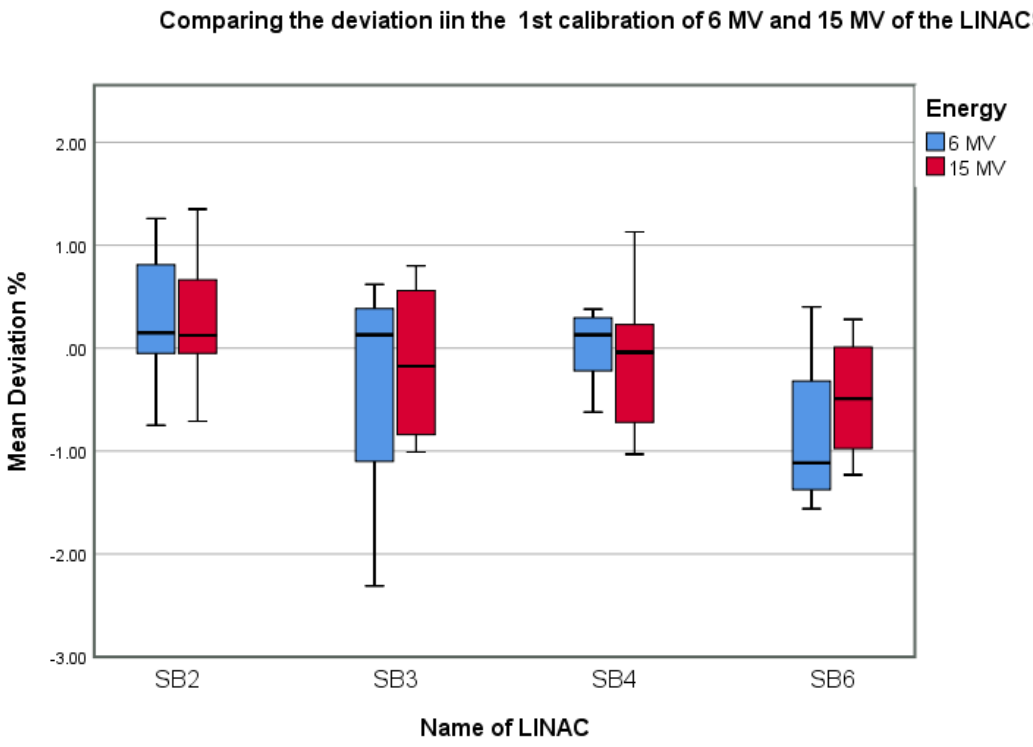

Figure 4. 5: Comparison of deviation in the first dose calibration measurement among the LINACS

After adjustments were made on the LINACS, the deviations in the dose measurement in the second calibration were more stable in all the four LINACS with 15 MV being more stable than 6 MV although the mean deviation of 15 MV was higher than 6 MV of the SB2 LINAC as depicted in figure 4.6. From figure 4.6, 15 MV showed a maximum mean deviation of 0.02% and a minimum mean deviation of -0.01% for SB3 and SB2 respectively, whiles SB4 and SB6 maintained a constant mean deviation of 0.01% over the operational period for the 15 MV energy. On the other hand, the maximum mean deviation was 0.1% and the minimum was 0.01% for SB3 and SB2 respectively, SB4 recorded a mean deviation of 0.03% and 0.04% for SB6 for the 6 MV energy as shown in figure 4.7 confirming that the 15 MV energy was more stable in all the LINACS than 6 MV energy.

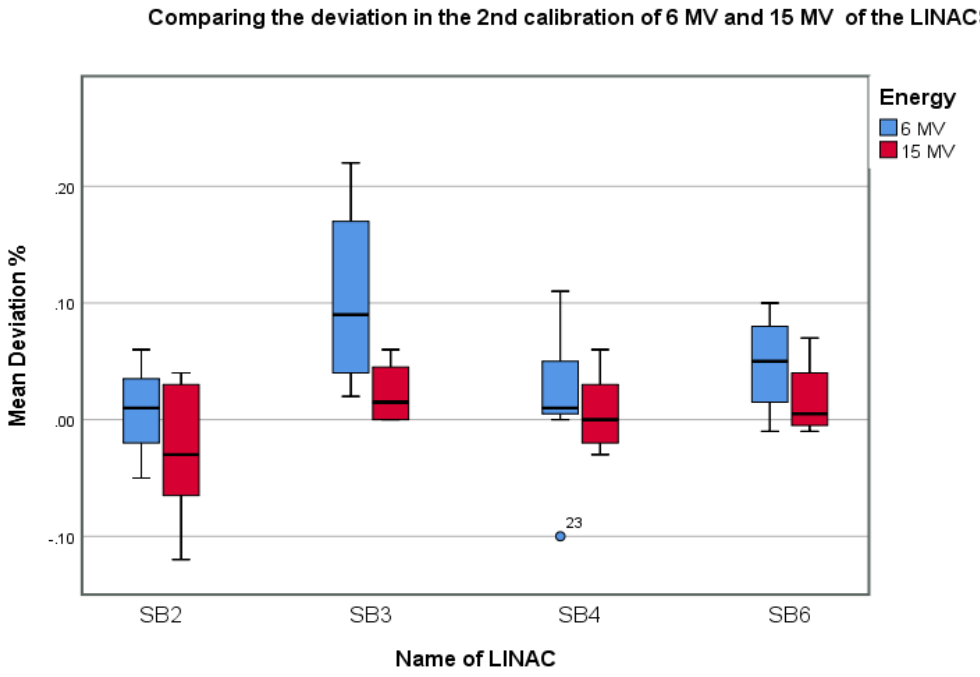

Figure 4. 6: Comparison of deviation in the second dose calibration measurements among the LINACS

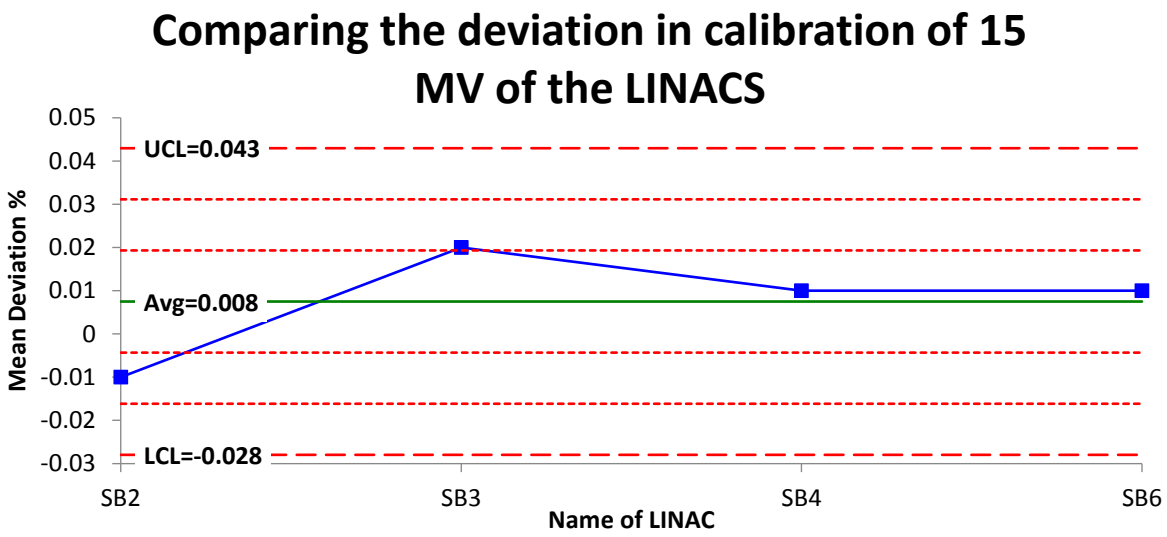

Figure 4. 7: Comparison of deviation in the second dose calibration measurements among the LINACS

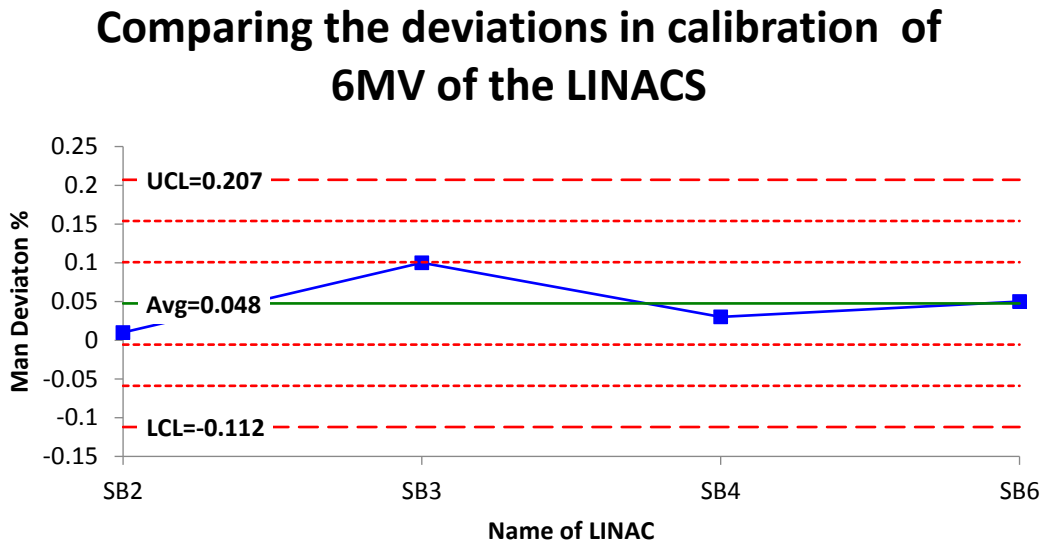

Figure 4. 8: Comparison of deviation in the second dose calibration measurements among the LINACS

4.8 Evaluation of Beam Profiles (Photon Energies)

The symmetry, flatness and fieldwidth of crossplane profiles at different depths and field sizes were compared with the inplane profiles within the individual LINACS and between the LINACS.

4.9 SB2 LINAC

At D_{max} (1.5cm) and the reference depth (10cm), the symmetry of the beam was compared in both inplane and crossplane profiles for the 6 MV photon energy with field size of 10 x 10 cm^2 as shown in figure 4.9. At D_{max} the deviation in the inplane profile exceeded the tolerance limit of ±1% by a value of 0.1%, whiles the crossplane was within the maximum deviation of 1%. The mean deviations of the crossplane and inplane profiles were the same with a value of 0.720% as shown in table 4.3.

Table 4. 3: Deviations in beam profile at Dmax and reference depth in the inplane and crossplane profiles of 6 MV with field size of 10 x 10 cm2 of SB2 LINAC

Year	**Crossplane**				Field width	**Inplane**				Field width
	Flatness		**Symmetry**			**Flatness**		**Symmetry**		
	1.5cm depth	10cm depth	1.5cm depth	10cm depth		1.5cm depth	10cm depth	1.5cm depth	10cm depth	
2015	0.5	0.4	0.6	0.6	0.5	0.2	0.1	0.7	0.6	-0.1
2016	1.1	1.7	0.3	0.4	1.1	0.6	1.4	0.8	0.7	1.0
2017	0.7	0.7	0.8	0.5	0.7	0.1	0.1	0.4	0.4	0.3
2017	0.9	0.8	1.0	0.7	0.8	0.4	0.3	0.6	0.7	0.3
2018	1.1	0.6	0.9	0.8	1.0	0.7	0.4	1.1	1.0	0.5
Mean	0.9	0.8	0.7	0.6	0.8	0.4	0.5	0.7	0.7	0.4
Std dev	0.3	0.5	0.3	0.2	0.2	0.3	0.5	0.3	0.2	0.4
Variance	0.1	0.3	0.1	0.0	0.0	0.1	0.3	0.1	0.0	0.2
Skewness	-0.5	1.7	-0.9	0.0	-0.2	0.0	1.9	0.5	0.4	0.6

At the reference depth (10cm), the deviations in the symmetry was less in the crossplane profile than inplane profile, the inplane profile had outliers which fell exactly on the tolerance limit in the positive direction in figure 4.9. The mean deviation of the inplane profile was greater than the crossplane profile by 0.080% from table 4.3.

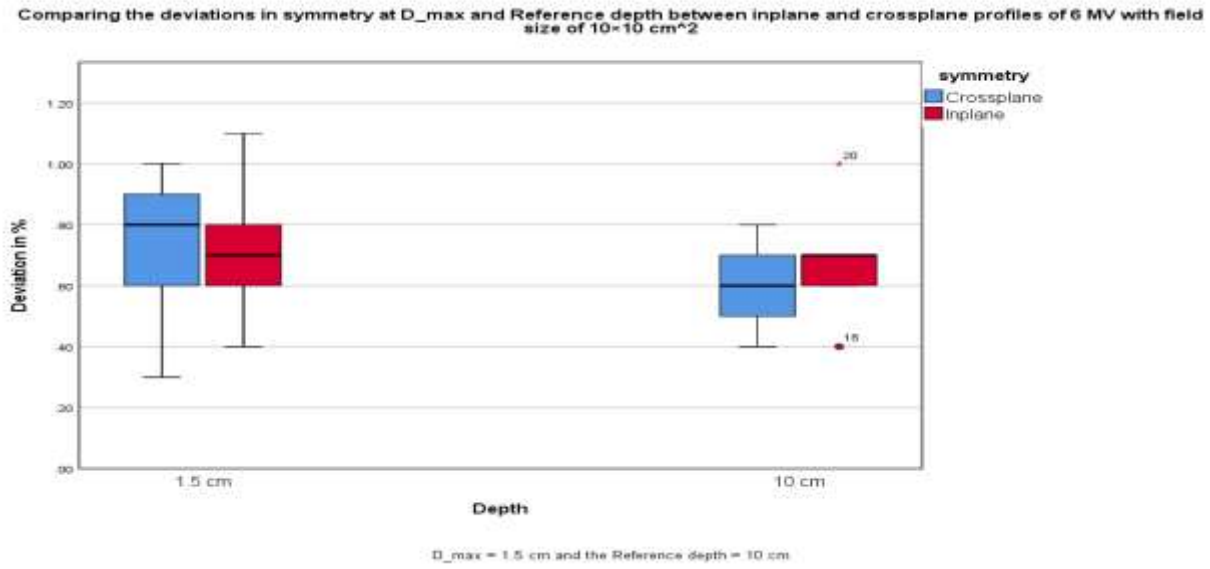

Figure 4. 9: Comparison of deviation in the symmetry at Dmax and reference depth between inplane and crossplane profiles of 6 MV with field size of 10 x 10 cm^2

The flatness was also compared at a depth of D_{max} and reference depth between inplane and crossplane profiles for 6 MV and field size of 10 x10 cm^2 as shown in figure 4.10. At D_{max} the crossplane profile showed a higher deviation in the flatness of the beam than the inplane profile. The mean deviation in the crossplane profile was 0.860% which was twice the mean deviation in the inplane profile from table 4.3.

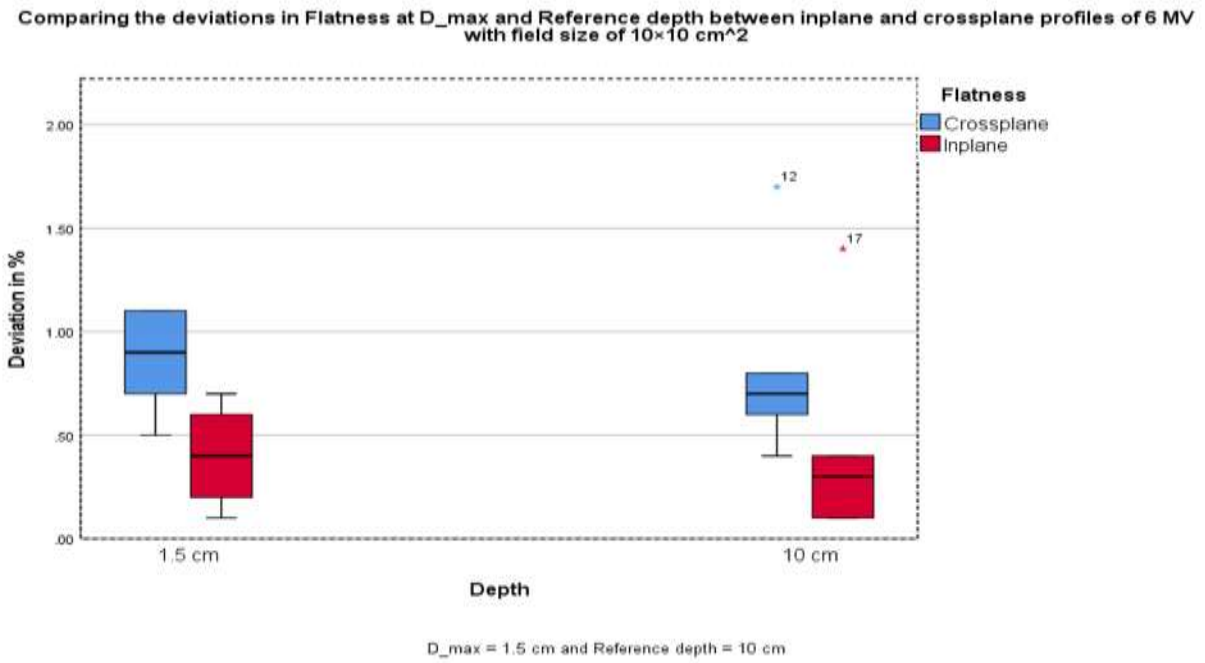

Figure 4. 10: Comparison of deviation in the flatness at Dmax and reference depth between inplane and crossplane profiles of 6 MV with field size of 10 x 10 cm2

At the reference depth, both crossplane inplane profiles had outliers exceeding the tolerance limit of ±1 % in figure 4.10 in the positive direction. The deviation in flatness of 6 MV was higher in crossplane profile with mean deviation of 0.840% than the inplane profile which had a % mean deviation of 0.460% from table 4.3.

The symmetry of 6 MV was compared between inplane and crossplane profiles at D_{max} and the reference depth for 40 x 40 cm^2 field size in figure 4.11, at D_{max}, the deviation was higher in inplane profile with a mean deviation of 0.780% than crossplane profile which had a mean deviation of 0.640% table 4.4. At the reference depth, the inplane was again found to be greater than the crossplane profile by a factor of 0.060 as shown in table 4.4.

The peak deviations at both depths for the inplane profile drifted farther beyond the tolerance deviation of ±1% by 0.1 in figure 4.11.

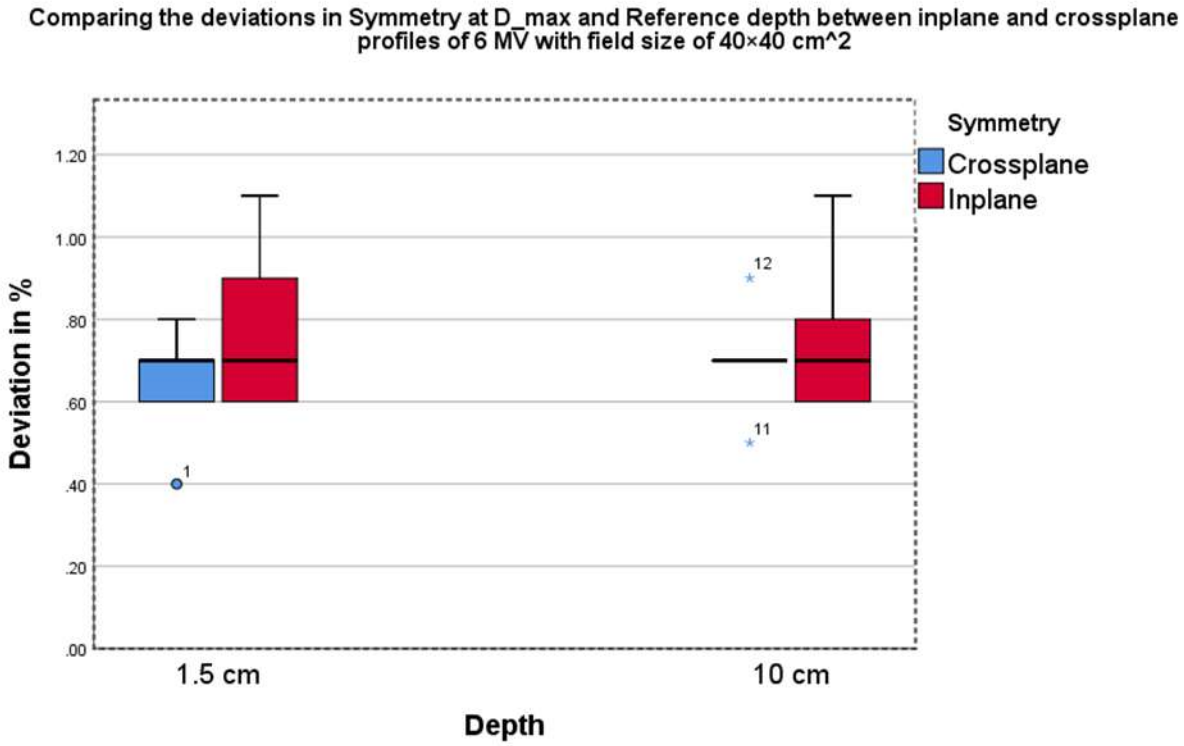

Figure 4. 11: Comparison of the deviation in the symmetry of 40 x 40 cm^2 field size

The flatness of 6 MV was also compared between the inplane and crossplane profiles at D_{max} and at the reference depth for 40x40 cm^2 field size in figure 4.12. At D_{max}, the deviation in the flatness of photon energy of 6 MV was greater in the crossplane than inplane profile with a mean deviation of 0.540% and 0.100% respectively as shown in Table 4.4.

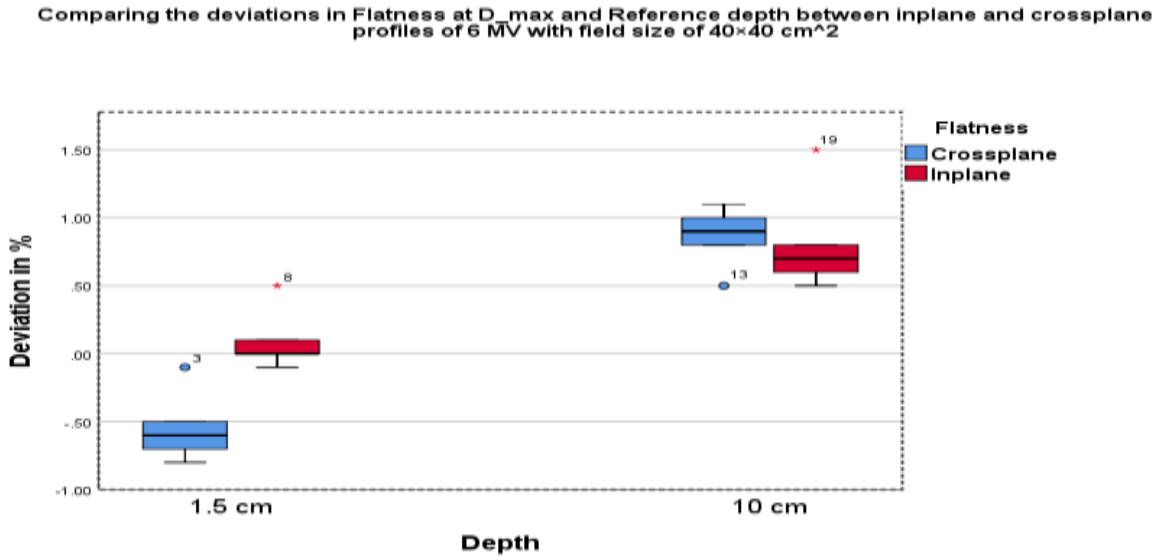

Figure 4. 12: Comparison of the deviation in the flatness of 40 x 40 cm^2 field size

Table 4. 4: shows deviations in beam profile at Dmax and reference depth in the inplane and crossplane profiles of 6 MV with field size of 40 x 40 cm2 of SB2 LINAC

Year	Crossplane					Inplane				
	Flatness		Symmetry		Field width	Flatness		Symmetry		Field width
	1.5m depth	10cm depth	1.5cm depth	10cm depth		1.5m depth	10cm depth	1.5m depth	10cm depth	
2015	-0.8	0.9	0.4	0.5	0.6	0.1	0.8	0.9	0.8	-1.2
2016	-0.7	1.0	0.7	0.9	2.4	-0.1	0.6	0.6	0.6	1.5
2017	-0.1	0.5	0.8	0.7	1.3	0.5	0.7	0.7	0.7	0.1
2017	-0.6	1.1	0.6	0.7	1.1	0.0	1.5	1.1	1.1	0.1
2018	-0.5	0.8	0.7	0.7	1.7	0.0	0.5	0.6	0.6	-0.2
Mean	-0.5	0.9	0.6	0.7	1.4	0.1	0.8	0.8	0.8	0.1
STD	0.3	0.2	0.1	0.1	0.7	0.2	0.3	0.2	0.2	1.0
Variance	0.1	0.1	0.0	0.0	0.5	0.1	0.2	0.0	0.0	0.9
Skewness	1.3	-1.0	-1.1	0.0	0.5	1.7	1.8	0.9	1.4	0.4

At the reference depth, the deviation in the crossplane had a peak value that went beyond the tolerance limit by 0.1%. The deviation was also higher in crossplane profile than the inplane profile by a difference of 0.040%.

The fieldwidth was also compared between crossplane and inplane profiles for 6 MV with field size of 40x40 cm^2. The mean deviation in the fieldwidth was far greater in the crossplane with a value of 1.420% than in the inplane profile which recorded a mean deviation of 0.060%. The maximum deviation was 2.4 mm in crossplane profile exceeding the tolerance limit of ± 2.0 mm by 0.4 mm as shown in Figure 4.13.

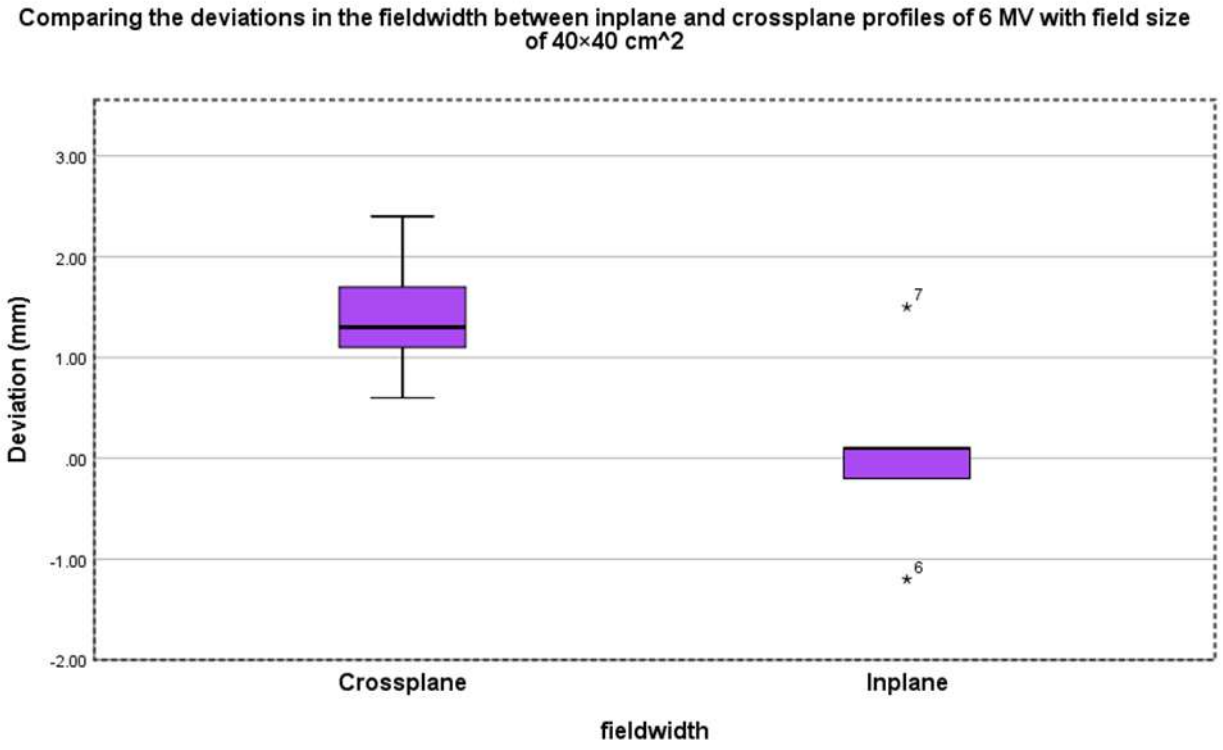

Figure 4. 13: Comparison of the deviation in the fieldwidth of 40 x 40 cm^2 field size

Table 4. 5: Deviations in beam profile at Dmax and reference depth in the inplane and crossplane profiles of 15 MV with field size of 10 x 10 cm2 of SB2

Year	Crossplane					Inplane				
	Flatness		Symmetry		Field width	Flatness		Symmetry		Field width
	3.0cm depth	10cm depth	3.0cm depth	10cm depth		3.0cm depth	10cm depth	3.0cm depth	10cm depth	
2015	0.7	0.5	0.4	0.4	0.6	0.8	0.5	1.1	1.0	-0.1
2016	2.7	2.9	0.8	1.3	1.3	2.2	2.2	0.9	1.0	1.1
2017	1.2	1.1	0.8	1.0	0.8	0.3	0.3	1.0	0.6	0.3
2017	0.9	1.0	0.4	0.5	0.6	0.4	0.4	0.6	0.8	0.3
2018	0.5	0.8	0.5	0.5	0.9	0.5	0.5	0.6	0.7	0.6
Mean	1.2	1.3	0.6	0.7	0.8	0.8	0.8	0.8	0.8	0.4
Std dev	0.9	0.9	0.2	0.4	0.3	0.8	0.8	0.2	0.2	0.4
Variance	0.5	0.9	0.4	0.2	0.1	0.6	0.6	0.1	0.0	0.2
Skewness	1.8	1.9	0.0	0.9	1.2	1.9	2.2	-2.0	-0.1	0.6

At a D_{max} and reference depth the deviation in the symmetry and flatness in both crossplane and

Inplane profiles for 15 MV with field size 10x10 cm^2 were compared as shown in figure 4.14.

At D_{max} (3 cm) the deviation in the symmetry was high in the inplane profile with mean deviation of 0.840% than the deviation in the crossplane which recorded a mean deviation of 0.580% from table 4.5. The maximum deviation in the inplane exceeded the tolerance deviation of $\pm 1\%$ by 0.1% as shown in the Figure 4.14. At the reference depth the mean deviation in the symmetry was found to be greater in inplane than in crossplane by a difference of 0.08%, although the crossplane profile produced a deviation that went beyond the tolerance limit of $\pm 1\%$ as shown in figure 4.14.

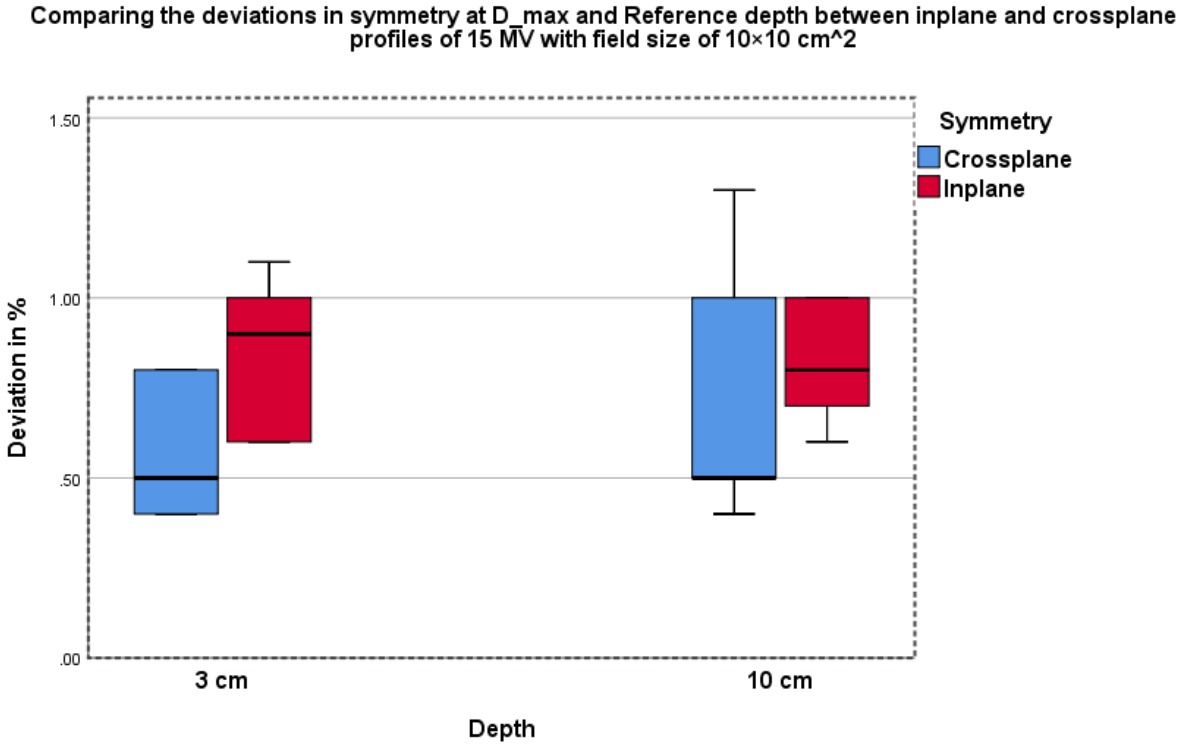

Figure 4. 14: Comparison of deviation in the symmetry at Dmax and reference depth between inplane and crossplane profiles of 15 MV with field size of 10 x 10 cm^2

.

At D_{max} the deviation in both crossplane and inplane profiles had outliers exceeding the tolerance deviation of $\pm 1\%$ as illustrated in figure 4.15 for flatness of the 15 MV with field size of 10 x 10 cm^2. The mean deviation was higher in the crossplane profile than the inplane with values of 1.200% and 0.840% respectively in Table 4.5.

At the reference depth, both crossplane and inplane profiles had outliers of 2.9% and 2.2% respectively, which fell beyond the acceptable limit of $\pm 1\%$ as shown in Figure 4.15. The mean deviation in inplane profile was less than the mean deviation of the crossplane profile by 0.780%.

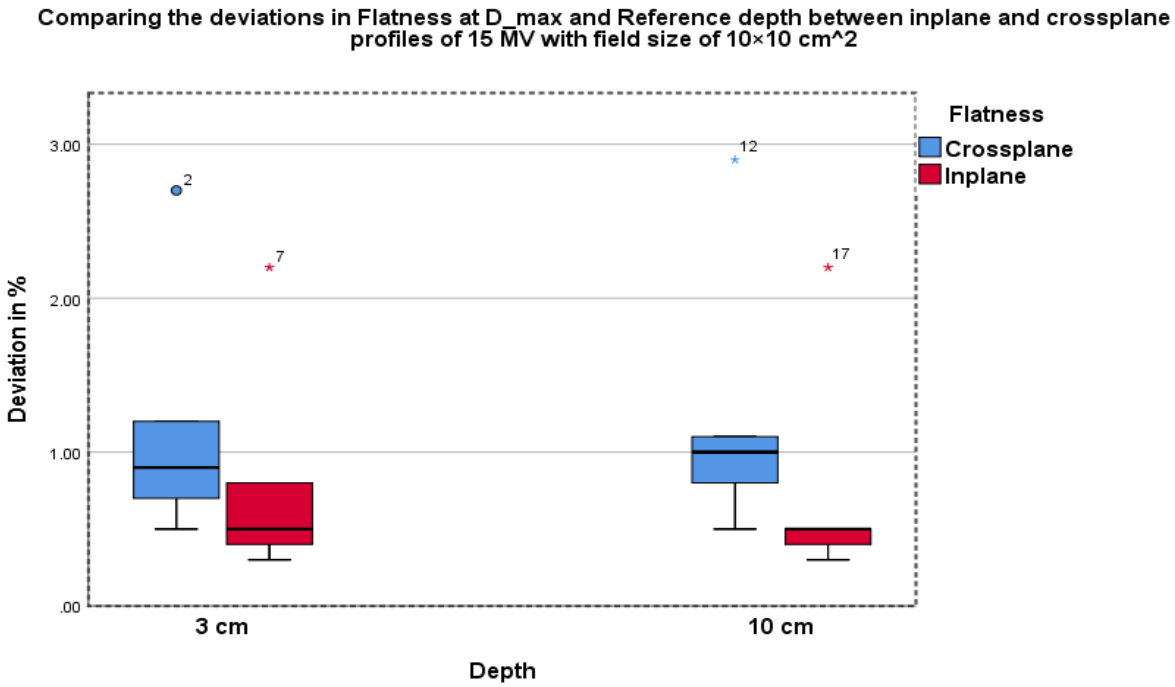

Figure 4. 15: Comparison of deviation in the flatness at Dmax and reference depth between inplane and crossplane profiles of 15 MV with field size of 10 x 10 cm^2

The deviations in the fieldwidth of 15 MV was also compared between crossplane and inplane profile of 10x10 cm^2 field size as depicted in figure 4.16, the deviation in the fieldwidth was greater in the crossplane than in the inplane with mean deviation of 0.840% and 0.440% respectively.

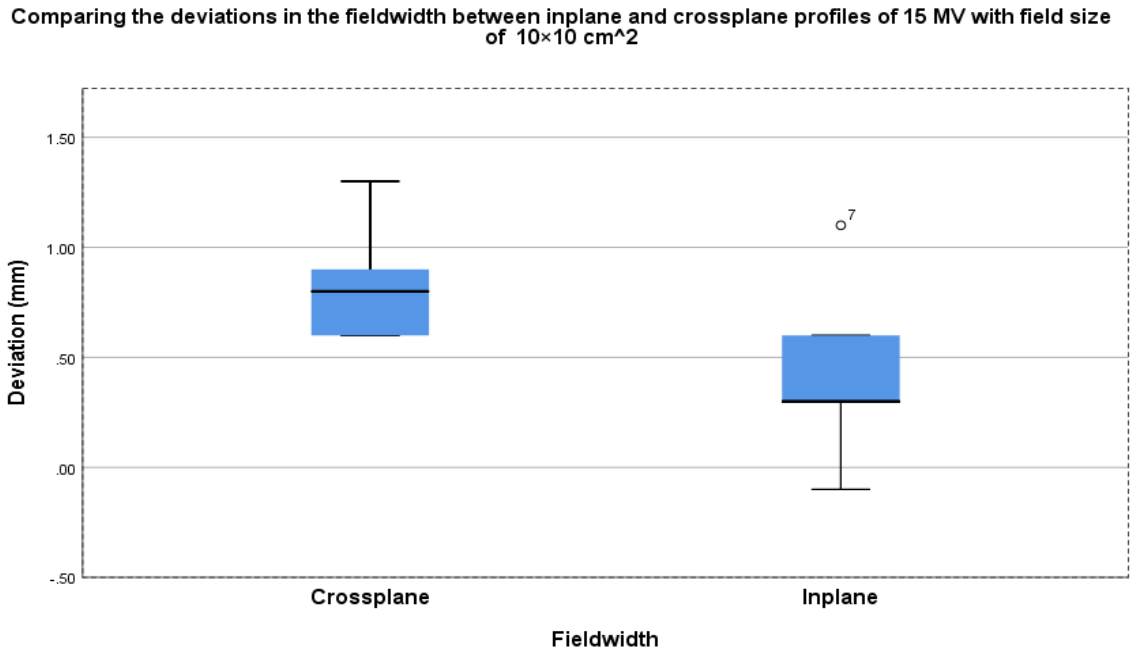

Figure 4. 16: Comparison of the deviation in the fieldwidth of 10 x 10 cm^2 field size

Comparing the deviations in symmetry at D_{max} and reference depth between inplane and crossplane profiles for 15 MV with the field size of 40x40 cm^2 as shown in figure 4.17. At D_{max}, the mean deviation in the symmetry was higher in inplane profile than the crossplane profile. The maximum deviation value in the inplane was 1.4% that fell beyond the tolerance limit of $\pm 1\%$. The difference between the mean deviations was 0.02%.

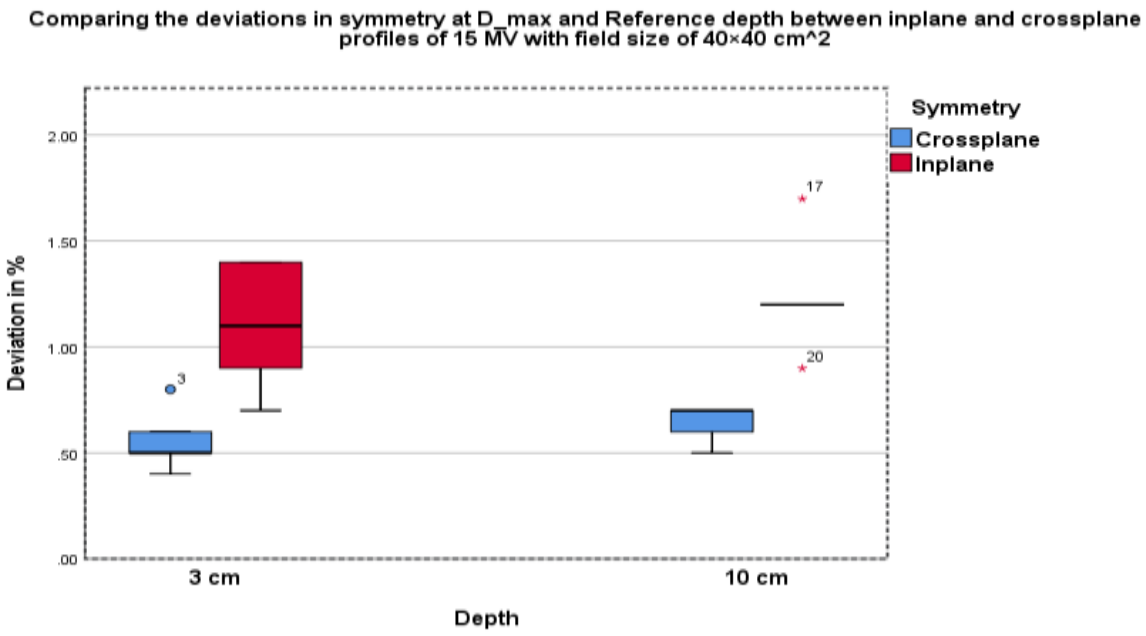

Figure 4. 17: Comparison of deviation in the symmetry at Dmax and reference depth between inplane and crossplane profiles of 15 MV with field size of 40 x 40 cm^2

At the reference depth, the deviation was also greater in inplane profile than in crossplane profile. The deviation in the inplane had outliers exceeding the deviation limit by a value of 0.7%. The mean deviation in the inplane was larger than the crossplane by a factor of 0.600% in figure 4.17.

Comparison of deviation in the flatness between the inplane and crossplane for 15 mv of 40x40 cm^2 as shown in figure 4.18 yields a higher deviation in the crossplane profile than the inplane profile at D_{max} . The mean deviation in the crossplane profile was 0.860%, which was twice the mean deviation in the inplane profile from table 4.6.

At the reference depth (10 cm) most of the deviation in the flatness were significantly high, exceeding the tolerance limit of $\pm 1\%$ in both crossplane and inplane profiles. The

minimum deviation in the inplane was equal to the tolerance limit in the positive direction and median mark falling exactly on the tolerance limit of 1% as shown in figure 4.18. The mean deviation was 1.200% in the inplane profile higher than 0.940% for crossplane profile.

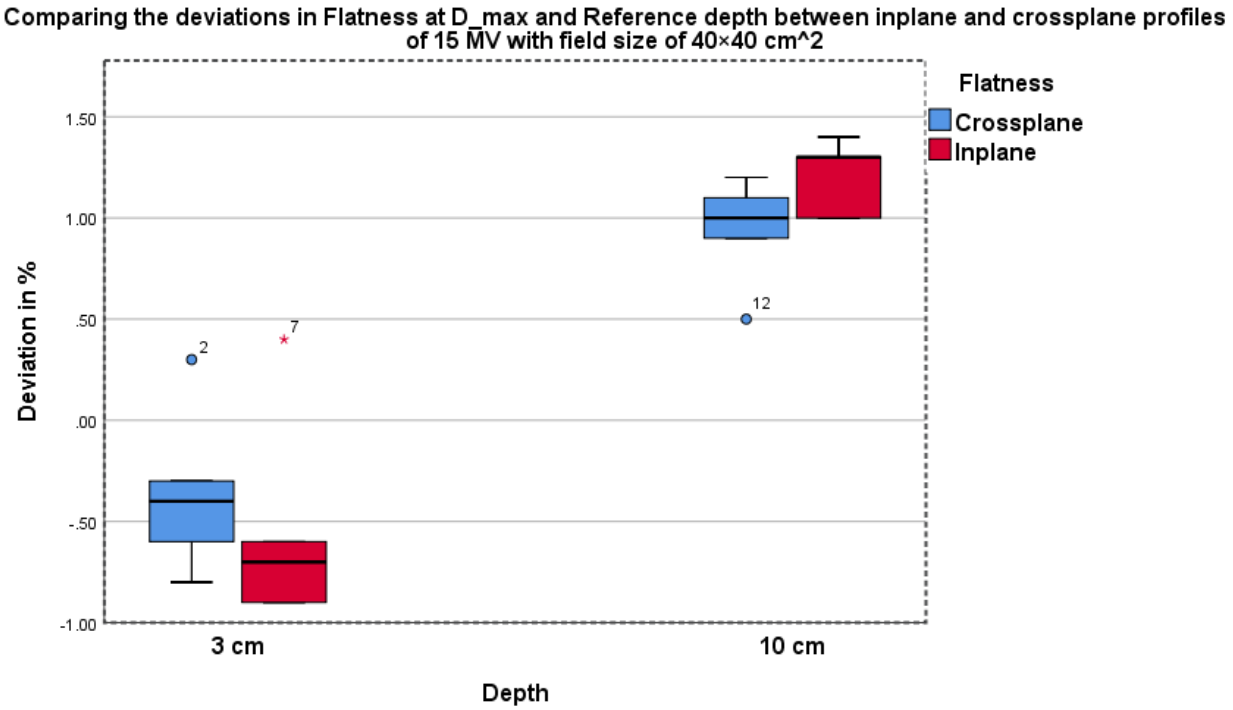

Figure 4. 18: Comparison of deviation in the flatness at Dmax and reference depth between inplane and crossplane profiles of 15 MV with field size of 40 x 40 cm^2.

Comparing the fieldwidth between the crossplane and the inplane profiles of 15 MV with a field size of 40x40 cm^2 as depicted in figure 4.19, the deviation in the fieldwidth in the crossplane was significantly high with a maximum deviation exceeding the tolerance deviation of ± 2 mm by 0.5 mm. The difference in mean deviation was 1 mm.

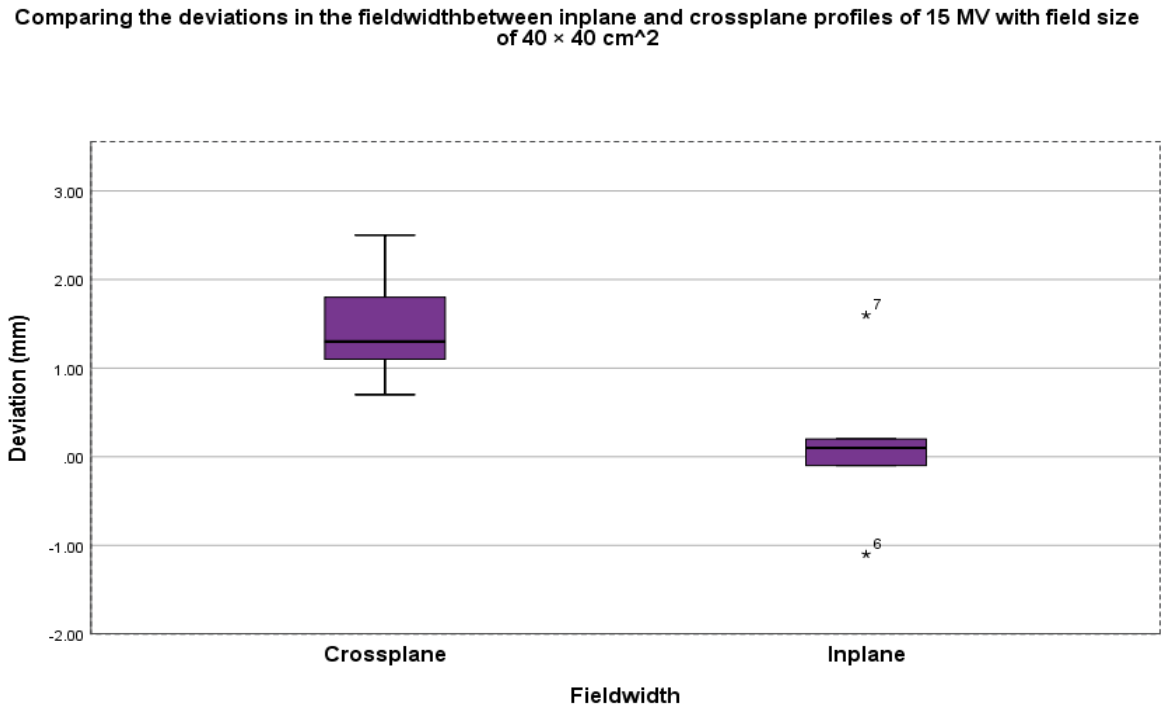

Figure 4. 19: Comparison of the deviation in the fieldwidth of 40 x 40 cm^2 field size

Table 4. 6: Deviations in beam profile at Dmax and reference depth in the inplane and crossplane profiles of 15 MV with field size of 40 x 40 cm2 of SB2 LINAC.

Year	Crossplane				Field width	Inplane				Field width
	Flatness		symmetry			Flatness		symmetry		
	3.0cm depth	10cm depth	3.0cm depth	10cm depth		3.0cm depth	10cm depth	3.0cm depth	10cm depth	
2015	-0.4	1.0	0.5	0.7	0.7	-0.6	1.0	1.4	1.2	-1.1
2016	0.3	0.5	0.6	0.7	2.5	0.4	1.3	1.4	1.7	1.6
2017	-0.3	1.2	0.8	0.7	1.3	-0.9	1.3	0.9	1.2	0.2
2017	-0.8	0.9	0.5	0.6	1.1	-0.9	1.4	1.1	1.2	0.1
2018	-0.6	1.1	0.4	0.5	1.8	-0.7	1.0	0.7	0.9	-0.1
Mean	-0.4	0.9	0.6	0.6	1.5	-0.5	1.2	1.1	1.2	0.1
Std dev	0.4	0.3	0.2	0.1	0.7	0.5	0.2	0.3	0.3	1.0
Variance	0.2	0.1	0.0	0.0	0.5	0.3	0.0	0.1	0.0	0.9
Skewness	1.1	-1.3	1.1	-1.3	0.7	1.9	-0.4	-0.3	1.0	0.6

4.10 Performance of beam profiles of SB3 (Photon Energies)

Deviation in the flatness at D_{max} and at reference depth between inplane and crossplane profiles of 6 MV with field size of 10 x 10 cm^2 as shown in figure 4.20, at D_{max}, both inplane and the crossplane profiles had a maximum deviation of 0.2%, but the mean deviation in the crossplane was higher than the in the inplane profile by a difference of 0.033% from table 4.7. All the deviations were within the tolerance limit of ±1.0%. At the reference depth the deviation in the flatness in the crossplane was greater than the in the inplane profiles with the maximum deviations of 0.60 % and 0.3% respectively also falling within the tolerance deviation of ±1 %. The mean deviation in the crossplane profile was 0.467% and 0.200% for the inplane profile.

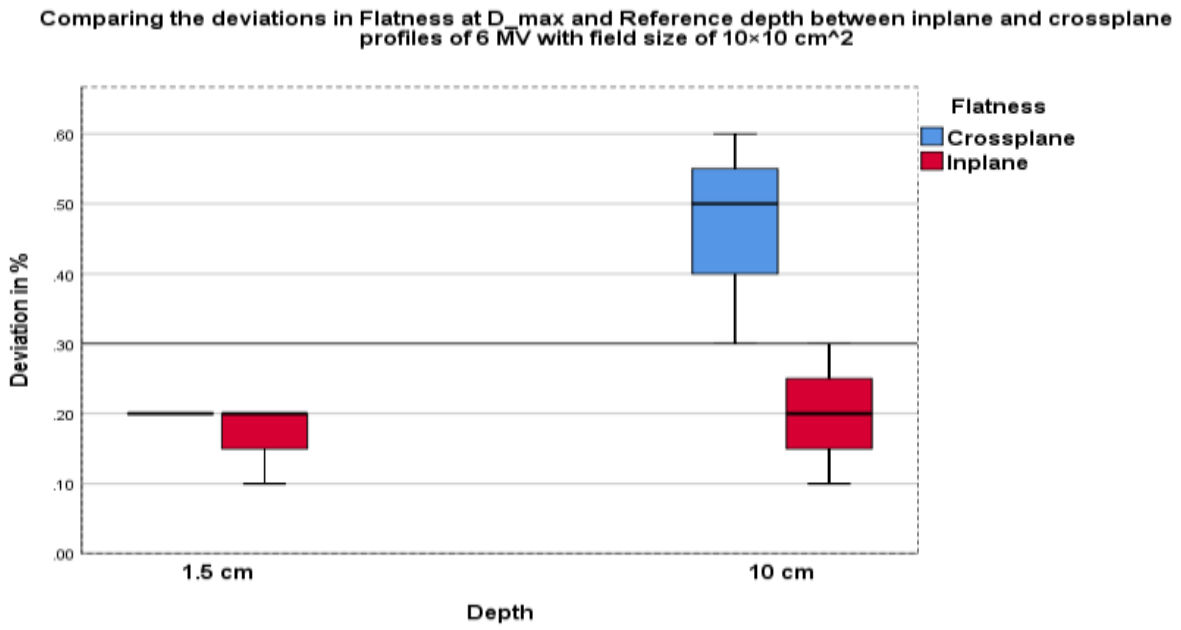

Figure 4. 20: Comparison of deviation in the flatness at Dmax and reference depth between inplane and crossplane profiles of 6 MV with field size of 10 x 10 cm^2

Table 4. 7: Deviations in beam profile at Dmax and reference depth in the inplane and crossplane profiles of 6 MV with field size of 10 x 10 cm2 of SB3 LINAC.

Year	Crossplane					Inplane				
	Flatness		Symmetry		Field width	Flatness		Symmetry		Field width
	1.5cm depth	10cm depth	1.5cm depth	10cm depth		1.5cm depth	10cm depth	1.5cm depth	10cm depth	
2015	0.2	0.6	0.3	0.5	0.8	0.1	0.1	0.6	0.7	0.2
2017	0.2	0.3	0.4	0.5	0.6	0.2	0.2	0.4	0.4	0.1
2018	0.2	0.5	0.3	0.6	0.6	0.2	0.2	0.5	0.9	0.1
Mean	0.2	0.5	0.3	0.5	0.7	0.1	0.2	0.5	0.7	0.1
Std dev	0.0	0.2	0.1	0.1	0.1	0.1	0.1	0.1	0.3	0.1
Variance	0.0	0.0	0.0	0.0	0.0	0.0	0.0	0.0	0.0	0.0
Skewness	--	-1.0	1.7	1.7	1.7	-1.7	0.0	0.0	-0.6	1.7

Comparing the deviation in the symmetry at D_{max} and reference depth between inplane and crossplane profiles of 6 MV with field size of 10 x 10 cm^2 as illustrated in figure 4.21. The deviation in the inplane was larger than the crossplane in the symmetry of the 6 MV energy at D_{max} . The highest deviations were 0.60% and 0.40% for inplane and crossplane profiles respectively which were within the acceptable limit of ±1 %. The mean deviation in inplane profile was greater than crossplane profile by 0.167%. At the reference depth the inplane profile also recorded a higher deviation than the crossplane profile. The maximum deviation was 0.80% for the inplane and 0.60% for the crossplane profiles. The mean deviation in the crossplane was 0.134% less than mean deviation in the inplane profile. All the deviations were within the tolerance limit of ±1%.

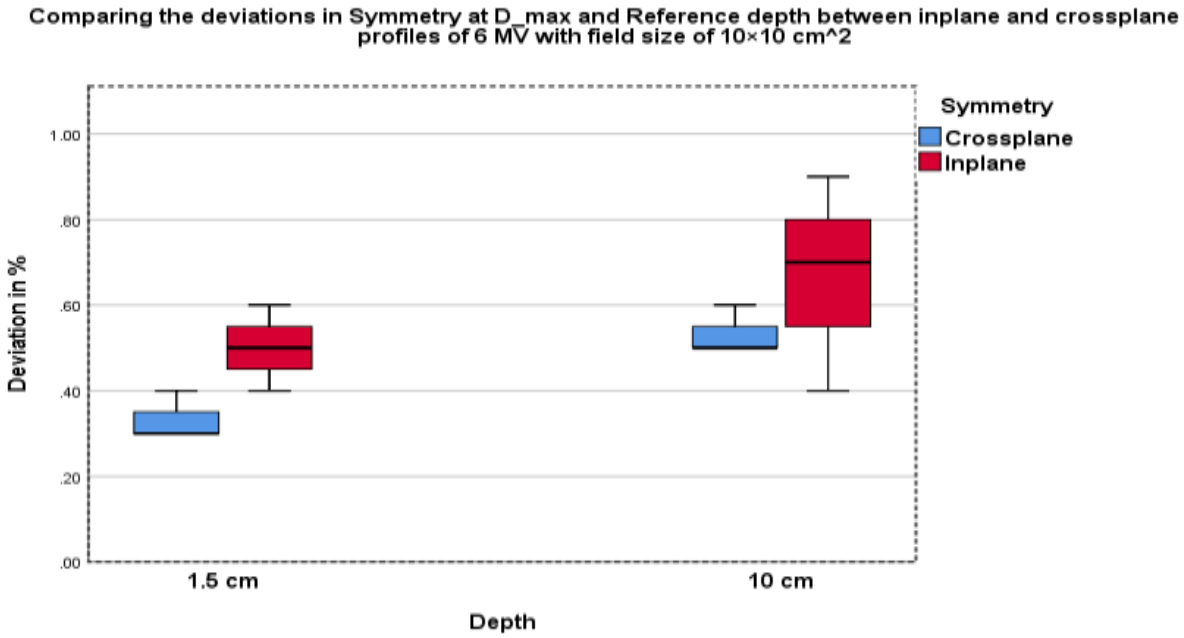

Figure 4. 21: Comparison of deviation in the symmetry at Dmax and reference depth between inplane and crossplane profiles of 6 MV with field size of 10 x 10 cm^2

The deviations in flatness at D_{max} and reference depth between inplane and crossplane profiles of 6 MV with field size of 40 × 40 cm^2 were also analyzed as shown in figure 4.22. At D_{max} the deviation in flatness in the inplane profile was greater than the deviation in the crossplane. The maximum deviation in the inplane exceeded the highest deviation in the crossplane by 0.1% as shown in figure 4.22. The mean deviation in the inplane was larger than the crossplane by 0.167%. At the reference depth, the highest deviation in the crossplane was 0.50% as compared to 0.03% for the inplane profile and hence contributed to a greater mean deviation in the crossplane than the inplane profiles from table 4.8. All the deviations were within the tolerance limit (±1%).

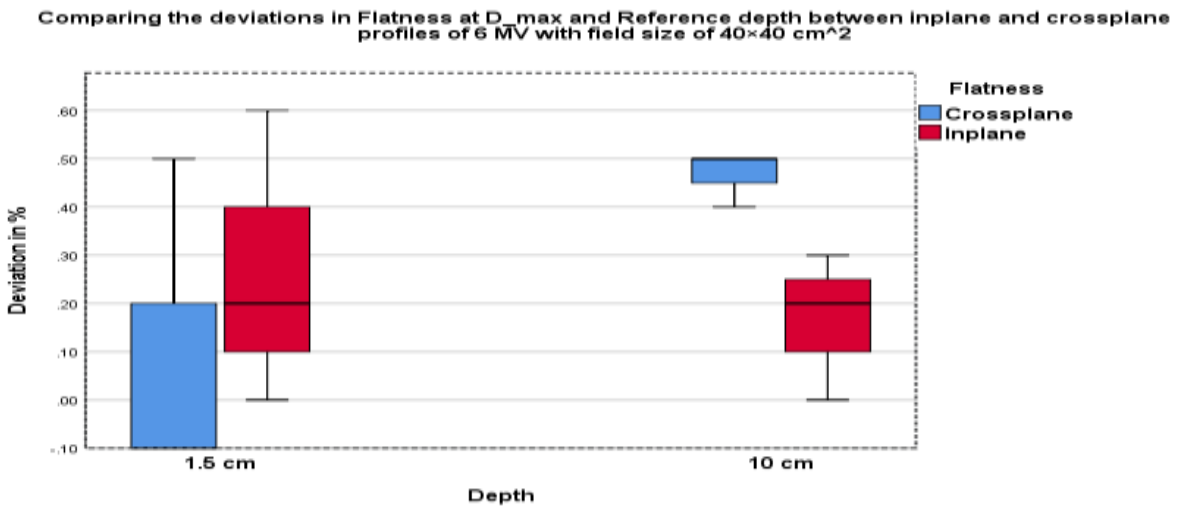

Figure 4. 22: Comparison of deviation in the flatness at Dmax and reference depth between inplane and crossplane profiles of 6 MV with field size of 40 x 40 cm^2

The deviations in the symmetry had a maximum deviation at D_{max} in the inplane profile for 6 MV 40 × 40 cm^2 which equaled the tolerance deviation of ±1%. The difference in mean deviation between the crossplane and inplane profiles was 0.034% at the D_{max}. At the reference depth as shown in figure 4.23, the deviation in the crossplane was found to be

higher than in the inplane by a factor of 0.034, all the deviations were within the tolerance of ±1%.

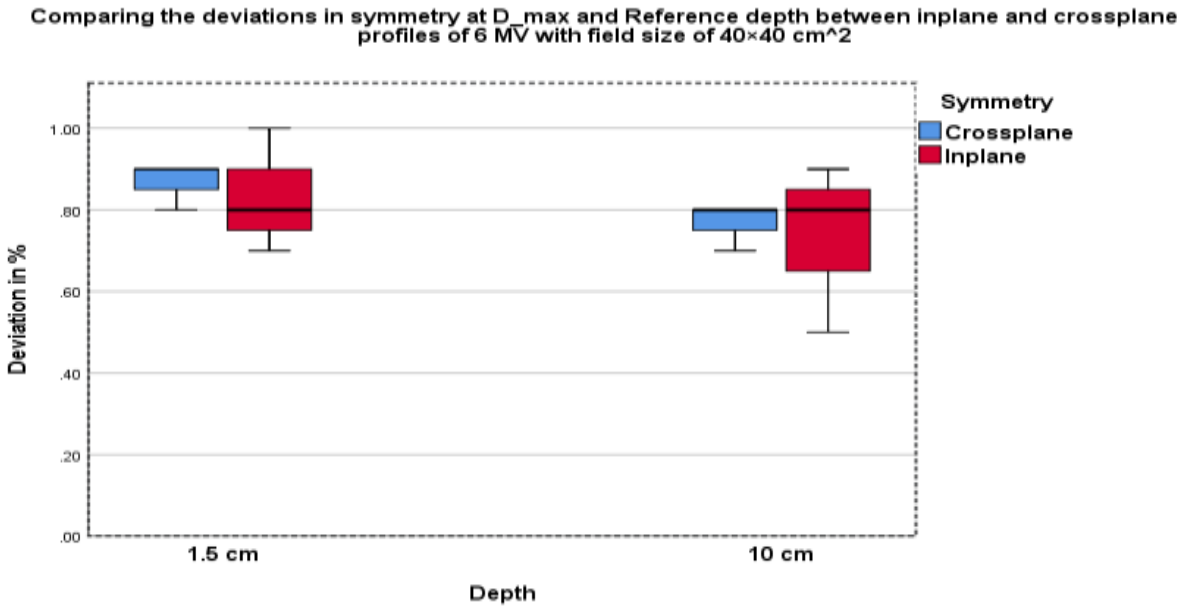

Figure 4. 23: Comparison of deviation in the flatness at Dmax and reference depth between inplane and crossplane profiles of 6 MV with field size of 40 x 40 cm^2

The deviations in the fieldwidth were also compared between the crossplane and the inplane profiles for the 40 x 40 cm^2 field size in figure 4.24, the result showed that there was a greater deviation in the crossplane than in the inplane profile with all the deviations falling within the tolerance limit of ±2 mm.

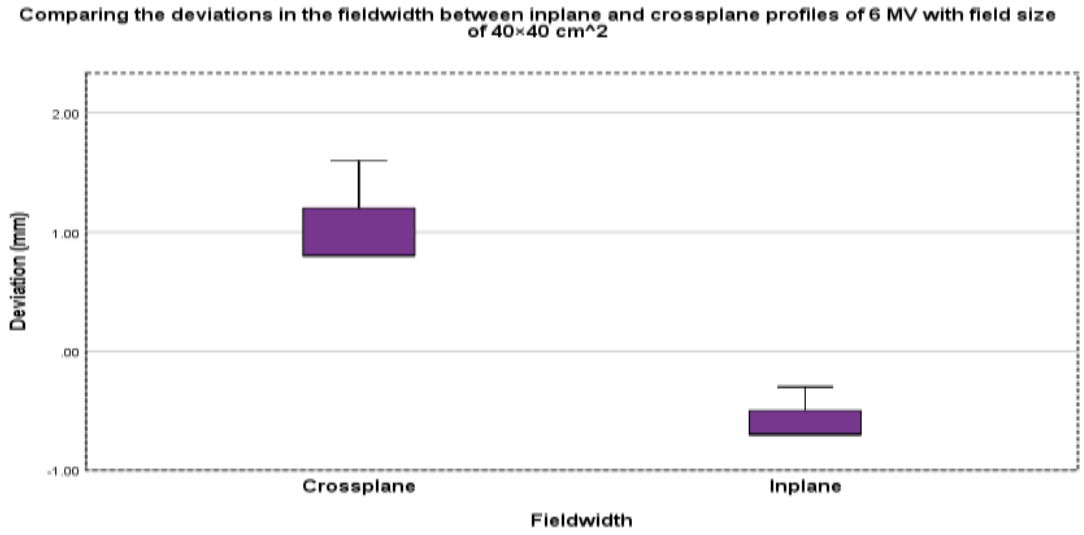

Figure 4. 24: Comparison of the deviation in the fieldwidth of 40 x 40 cm^2 field size

Table 4. 8: Deviations in beam profile at Dmax and reference depth in the inplane and crossplane profiles of 6 MV with field size of 40 x 40 cm^2 of SB3 LINAC.

Year	Crossplane				Field width	Inplane				Field width
	Flatness		Symmetry			Flatness		Symmetry		
	1.5cm depth	10cm depth	1.5cm depth	10cm depth		1.5cm depth	10cm depth	1.5cm depth	10cm depth	
2015	0.5	0.4	0.8	0.7	1.6	0.6	0.3	0.8	0.9	-0.3
2017	-0.1	0.5	0.9	0.8	0.8	0.0	0.2	0.7	0.5	-0.7
2018	-0.1	0.5	0.9	0.8	0.8	0.2	0.0	1.0	0.8	-0.7
Mean	0.1	0.5	0.9	0.8	1.1	0.3	0.2	0.8	0.7	-0.6
Std dev	0.3	0.1	0.1	0.1	0.5	0.3	0.2	0.2	0.2	0.2
Variance	0.1	0.0	0.0	0.0	0.2	0.1	0.0	0.0	0.0	0.1
Skewness	1.7	-1.7	-1.7	-1.7	1.7	0.9	-0.9	0.9	-1.3	1.7

Deviation in the symmetry at D_{max} and at reference depth between inplane and crossplane profiles of 15 MV with field size of 10 x 10 cm^2 were analyzed as shown in figure 4.25, at

D_{max}, deviations in both inplane and the crossplane profiles were within the acceptable deviation of ±1% with the same maximum deviation of 0.7%. The mean deviation in the crossplane was higher than the in the inplane with values of 0.600% and 0.567% respectively table 4.9. At the reference depth the deviation in the symmetry in the crossplane was greater than the in the inplane profiles with the maximum deviations of 0.90 % and 0.80% respectively also falling within the acceptable deviation of ±1 %. The mean deviation in the crossplane profile was greater than the inplane by 0.200% from Table 4.9

Table 4. 9: Deviations in beam profile at Dmax and reference depth in the inplane and crossplane profiles of 15 MV with field size of 10 x 10 cm^2 of SB3 LINAC.

Year	**Crossplane**					**Inplane**				
	Flatness		**Symmetry**		Field width	**Flatness**		**Symmetry**		Field width
	3.0cm depth	10cm depth	3.0cm depth	10cm depth		3.0cm depth	10cm depth	3.0cm depth	10cm depth	
2015	0.3	0.4	0.7	0.9	0.9	-0.1	-0.2	0.3	0.5	0.1
2017	0.9	1.2	0.6	0.8	0.6	0.4	0.4	0.7	0.8	0.1
2018	0.4	0.1	0.5	0.6	0.0	-0.1	-0.5	0.7	0.4	0.0
Mean	0.5	0.6	0.6	0.8	0.5	0.1	-0.1	0.6	0.6	0.1
Std dev	0.3	0.6	0.1	0.2	0.5	0.3	0.5	0.2	0.2	0.1
Variance	0.1	0.3	0.0	0.0	0.2	0.1	0.2	0.6	0.0	0.0
Skewness	1.5	1.2	0.0	-0.9	-0.9	1.7	0.9	-1.7	1.3	-1.7

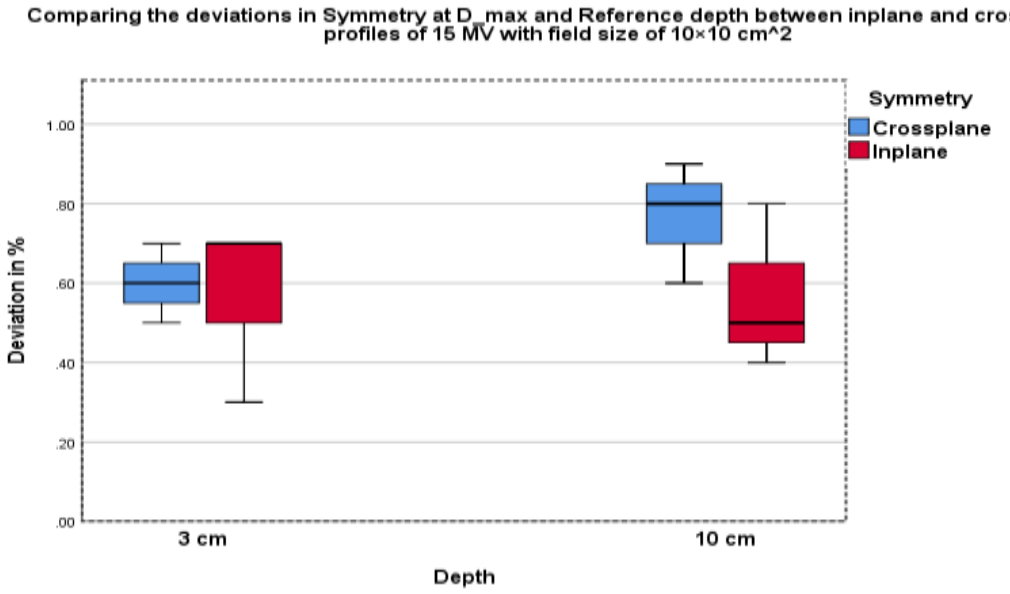

Figure 4. 25: Comparison of deviation in the symmetry at Dmax and reference depth between inplane and crossplane profiles of 15 MV with field size of 10 x 10 cm^2.

At the D_{max} the deviation in the flatness was larger in the crossplane than in the inplane profile in figure 4.26 by a mean deviation of 0.466%. The maximum deviations were 0.90% and 0.40% for crossplane and inplane respectively. All the deviations were within the tolerance limit of ±1%. At the reference depth, the deviation in the crossplane was again greater than in the inplane profile for the flatness of 15 MV with field size 10 x 10 cm^2. The maximum deviation in the crossplane had a value of 1.2% which exceeded the tolerance limit by 0.20% which contributed to a higher mean deviation in the crossplane than in the inplane profiles with values of 0.567% and -0.100% respectively.

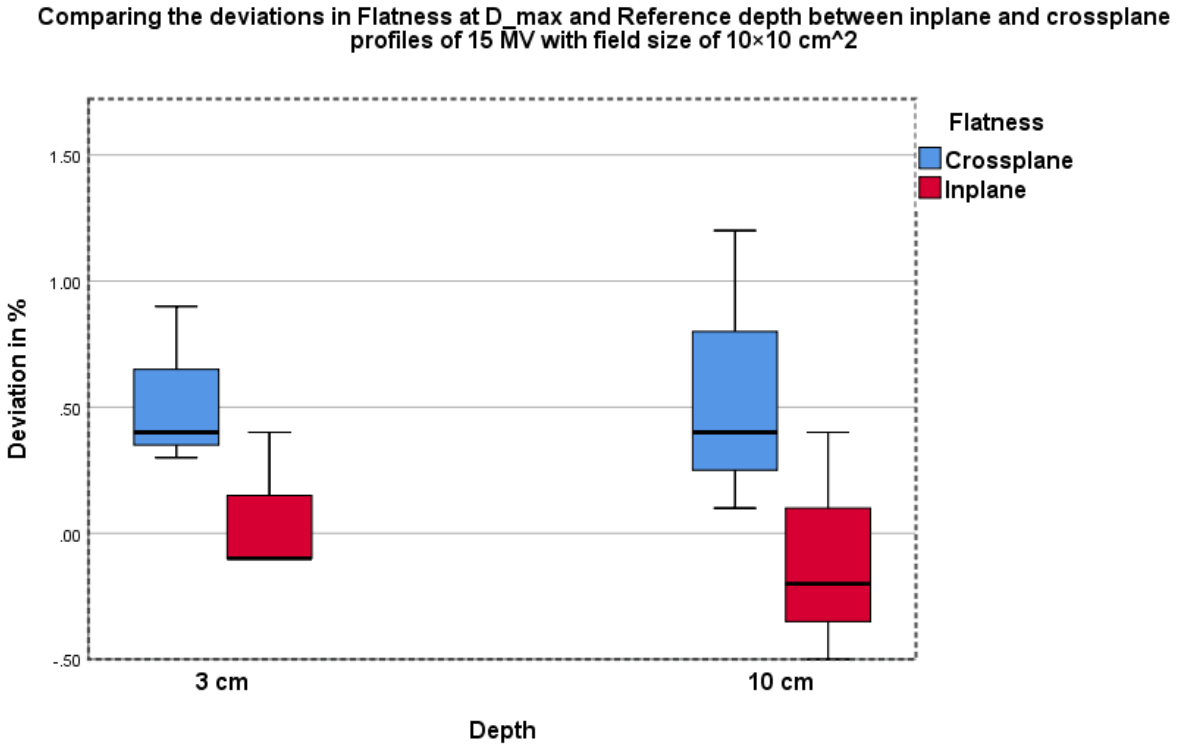

Figure 4. 26: Comparison of deviation in the flatness at Dmax and reference depth between inplane and crossplane profiles of 15 MV with field size of 10 x 10 cm^2

The performance in the symmetry of 15 MV with field size of 40 x 40 cm^2 was analyzed by comparing the deviations at D_{max} and reference depth between inplane and crossplane profiles as indicated in figure 4.27. The result showed that the deviations in the symmetry was higher in the crossplane than in the inplane profiles at D_{max} with mean deviation of 0.567 % and 0.500% respectively. All the deviations were within the acceptable limit of ±1%. At the reference depth, the crossplane produced a greater deviation with a maximum deviation less than 0.1% of the tolerance limit (±1%) than the inplane profile in figure 4.62**.** The mean deviation of the crossplane was higher than inplane profile by 0.034%.

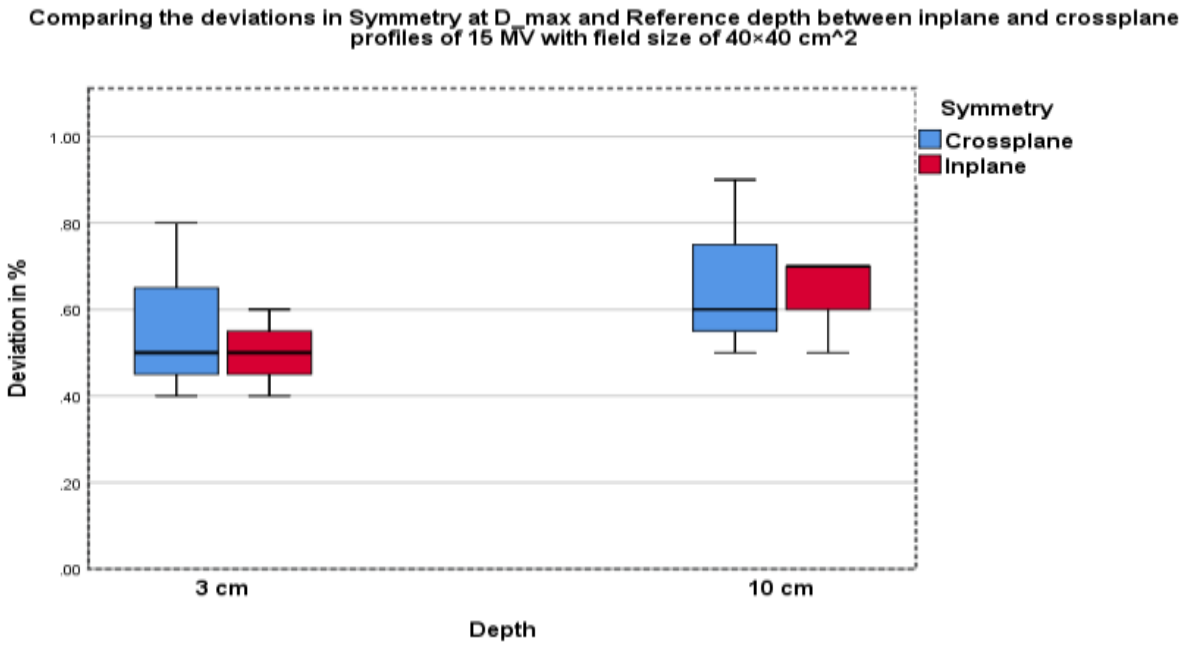

Figure 4. 27: Comparison of deviation in the symmetry at Dmax and reference depth between inplane and crossplane profiles of 15 MV with field size of 40 x 40 cm2

The performance in the flatness of 15 MV with field size 40 x 40 cm^2 was also evaluated in figure 4.28. At Dmax the deviations in the flatness of 15 MV recorded a peak deviation of 1% in the crossplane which was equal to the tolerance limit (±1%) in the positive direction whiles the peak deviation in the inplane was 0.50% which resulted in a greater mean deviation in the crossplane than inplane profiles with values of 0.133% and 0.100% respectively. At the reference depth, the mean deviation in the crossplane was larger than the inplane by 0.167% from table 4.10.

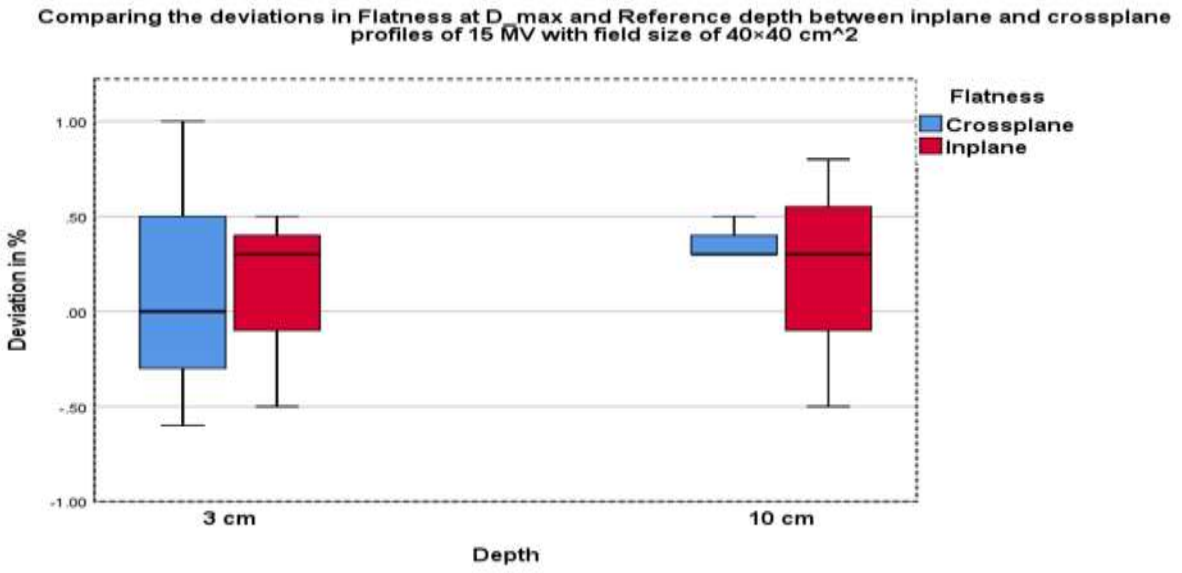

Figure 4. 28: Comparison of deviation in the flatness at Dmax and reference depth between inplane and crossplane profiles of 15 MV with field size of 40 x 40 cm^2

Table 4. 10: Deviations in beam profile at Dmax and reference depth in the inplane and crossplane profiles of 15 MV with field size of 40 x 40 cm^2 of SB3 LINAC

Year	Crossplane					Inplane				
	Flatness		Symmetry		Field width	Flatness		Symmetry		Field width
	3.0cm depth	10cm depth	3.0cm depth	10cm depth		3.0cm depth	10cm depth	3.0cm depth	10cm depth	
2015	1.0	0.5	0.8	0.9	1.6	0.5	-0.5	0.4	0.5	-0.2
2017	-0.6	0.3	0.5	0.6	0.7	-0.5	0.8	0.5	0.7	-0.6
2018	0.0	0.3	0.4	0.5	0.0	0.3	0.3	0.6	0.7	0.0
Mean	0.1	0.4	0.6	0.7	0.8	0.1	0.2	0.5	0.6	-0.3
STD	0.8	0.1	0.2	0.2	0.8	0.5	0.7	0.1	0.1	0.3
Variance	0.7	0.0	0.0	0.0	0.6	0.3	0.4	0.0	0.0	0.1
Skewness	0.7	1.7	1.3	1.3	0.4	-1.5	-0.7	0.0	-1.7	-0.9

The deviations in the flatness between SB2 and SB3 at D_{max} and reference depth of 6 MV with 10×10 cm^2 field size were compared in the crossplane as indicated in figure 4.29, the

results showed that at D_{max} the deviation in the flatness was larger in SB2 than in SB3, SB2 and SB3 had mean deviation of 0.860% and 0.200% respectively. The SB2 had a peak deviation of 1.1% which fell outside the tolerance limit of ±1%. At the reference depth SB2 again recorded a deviation greater than SB3 in the crossplane. The mean deviation of SB2 was larger than SB3 by 0.373%. The SB2 recorded an outlier which exceeded the tolerance limit of ±1% in figure 4.29.

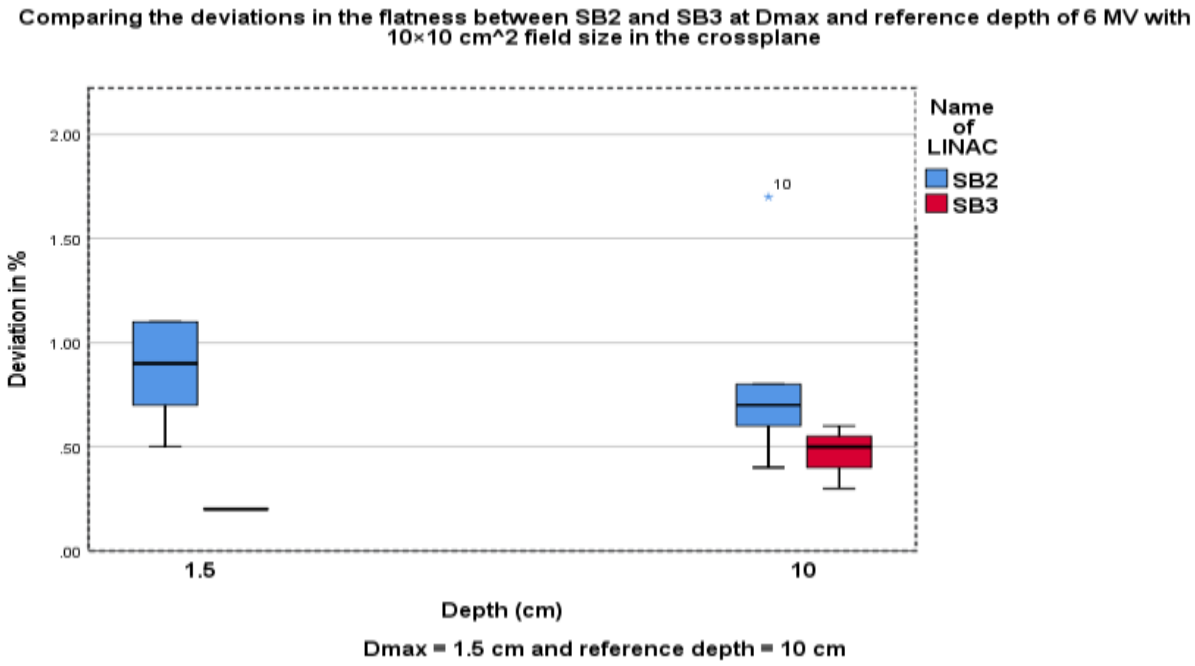

Figure 4. 29: The result of comparing the performance between SB2 and SB3 in terms of flatness (crossplane) at Dmax and reference depth of 6 MV

Comparing the deviations in flatness between SB2 and SB3 at D_{max} and reference depth of 6 MV with 10×10 cm^2 field size in the inplane as shown in the figure 4.30, at D_{max} the deviation in the flatness was found to be greater in SB2 than in SB3 in the inplane profile with a mean deviation of 0.400% and 0.167% respectively. All the deviations were within

the tolerance limit of ±1% at D_{max}. At the reference depth the deviation in the flatness was higher in SB2 than SB3. The SB2 had an outlier which fell beyond the tolerance limit of ±1% contributing to the greater mean deviation in SB2 than SB3. The mean deviations were 0.400% and 0.167% respectively.

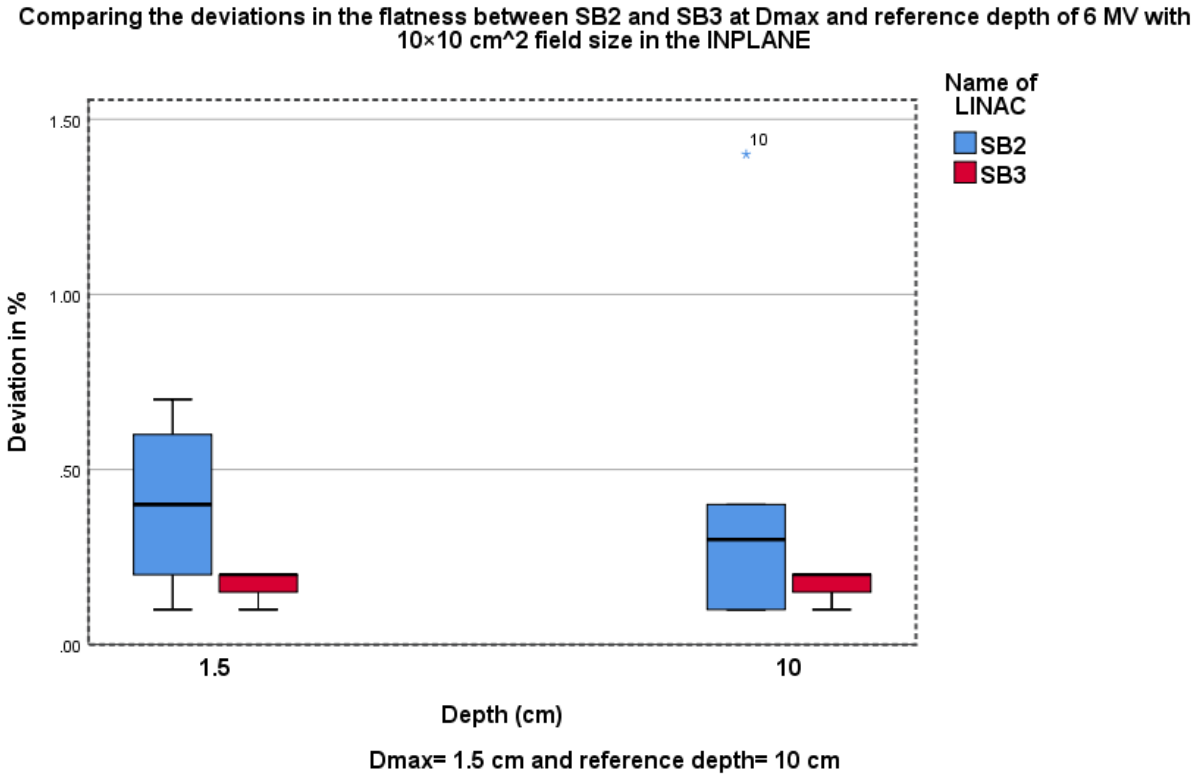

Figure 4. 30: The result of comparing the performance between SB2 and SB3 in terms of flatness (inplane) at Dmax and reference depth of 6 MV

The deviations in the symmetry between SB2 and SB3 at D_{max} and reference depth were also compared for 6 MV for 10×10 cm^2 field size in the crossplane as shown in figure 4.31, at D_{max} the peak deviation in SB2 was 1.00% and 0.40% for SB3. The mean deviation in SB2 was larger than SB3 by a difference of 0.387%. The deviation in SB2 and SB3 had a maximum value of 0.80% and 0.60% respectively at the reference depth. The mean

deviation in SB2 exceeded the mean deviation in SB3 by 0.187% at the reference depth. All the deviations fell within the tolerance limit of 1%.

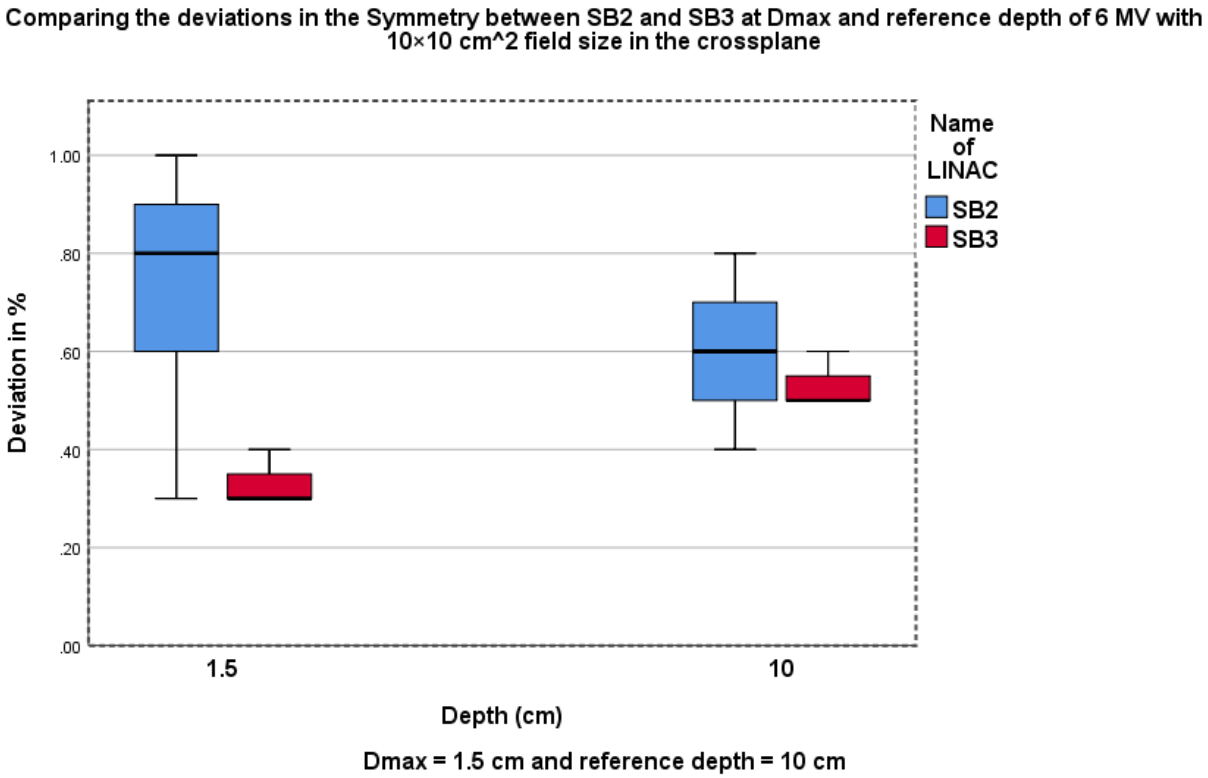

Figure 4. 31: The result of comparing the performance between SB2 and SB3 in terms of symmetry (crossplane) at Dmax and reference depth of 6 MV

In the inplane profile depicted in figure 4.32, the deviation in symmetry of SB2 was greater than in SB3 at D_{max}, the peak deviation in SB2 exceeded the tolerance limit of ±1% by 0.1%. The mean deviations were 0.500% and 0.720% for SB3 and SB2 respectively. At the reference depth, all the deviations were within the acceptable limit. The mean deviation in SB3 was less than SB2 by 0.003%.

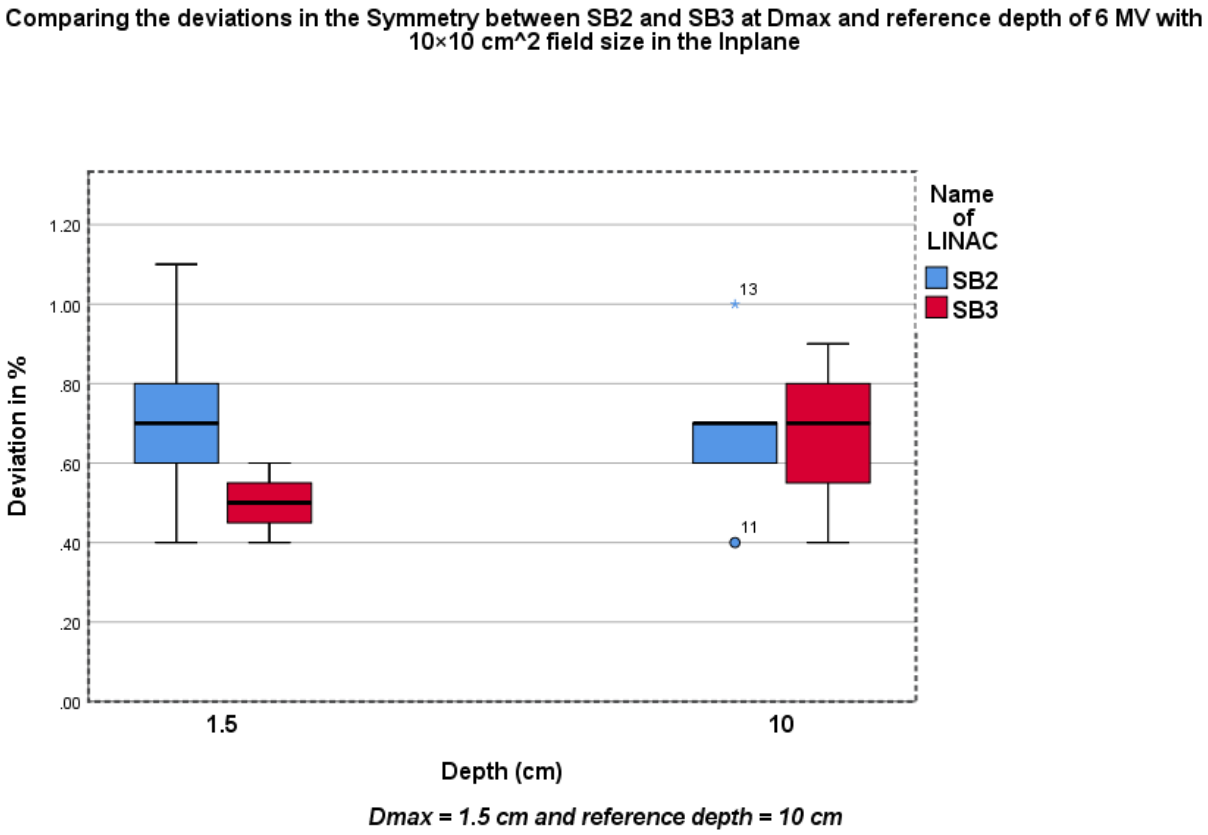

Figure 4. 32: The result of comparing the performance between SB2 and SB3 in terms of symmetry (Inplane) at Dmax and reference depth of 6 MV

Comparing the deviations in the flatness between SB2 and SB3 at D_{max} and at reference depth of 6 MV with field size of 40×40 cm^2 in the crossplane as shown in figure 4.33, at D_{max} both LINACS had deviation within the tolerance limit of ±1%, the mean deviation in the flatness of SB3 was lower than SB2 in the crossplane with values of 0.100% and -0.540% respectively. At the reference, depth the maximum deviation in the flatness of SB2 exceeded the tolerance limit by 0.1% in the figure 4.33**.** The mean deviation in SB2 was greater than the deviation in SB3 by a 0.393%which confirms a more stable performance in SB3.

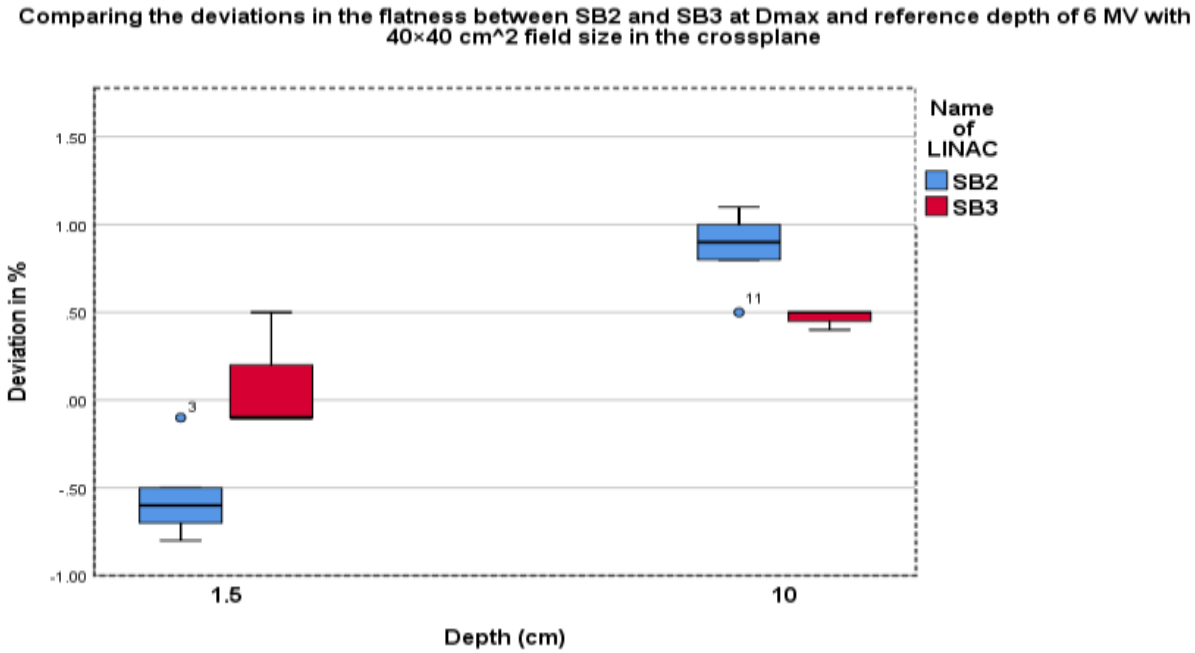

Figure 4. 33: The result of comparing the performance between SB2 and SB3 in terms of flatness (crossplane) at Dmax and reference depth of 6 MV

In the inplane, the deviation in flatness in SB3 was found to be greater than in SB2, although SB2 recorded an outlier which was still in the tolerance limit of ±1% as depicted in figure 4.34. The mean deviation in SB3 (0.267%) was more than twice the mean deviation of SB2 (0.100%) at D_{max}. At the reference depth the SB2 recorded an extreme value which exceeded the tolerance deviation (±1%) by 0.50% in figure 4.34 contributing to a greater mean deviation in SB2 with a value of 0.820% than in SB3 with mean deviation of 0.167%.

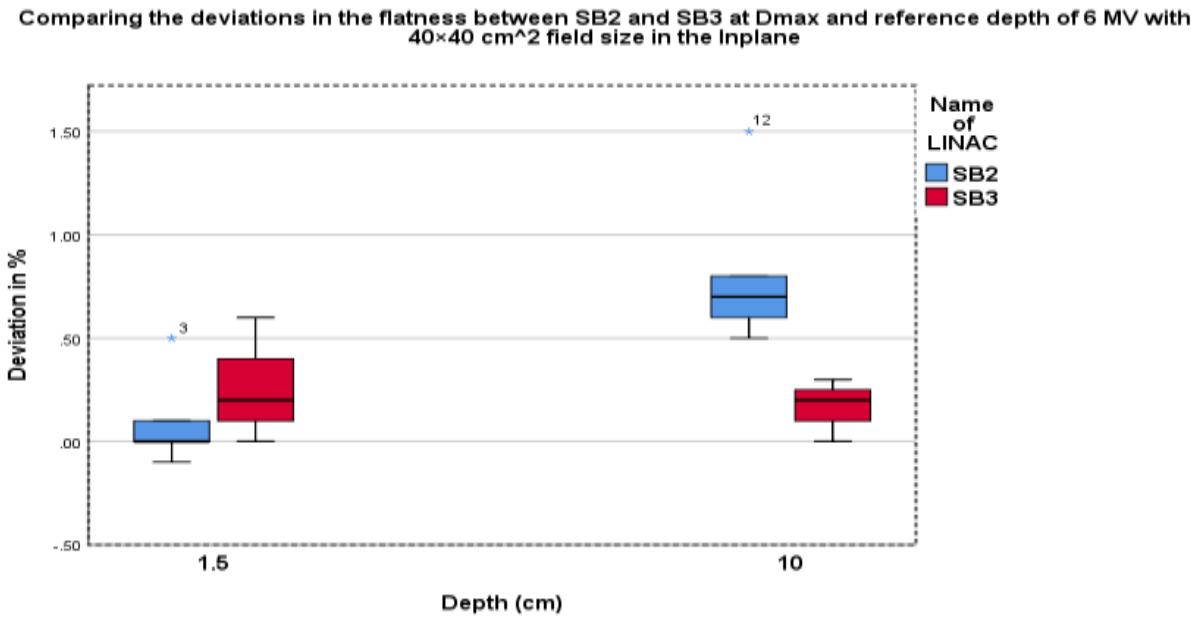

Figure 4. 34: shows the result of comparing the performance between SB2 and SB3 in terms of flatness (Inplane) at Dmax and reference depth of 6 MV

The deviations in the symmetry between SB2 and SB3 at D_{max} and reference depth were also analyzed for 6 mv for 40×40 cm^2 field size in the crossplane as shown in figure 4.35, at D_{max} the maximum deviations were 0.90% and 0.80% for SB3 and SB2 respectively. The mean deviation in SB3 was greater than SB2 by a factor of 0.227. The deviation in SB2 recorded outliers which fell within acceptable deviation of ±1% at the reference depth. The mean deviation in SB3 was higher the mean deviation in SB2 by 0.067% at the reference depth. All the deviations were found in the tolerance limit of ±1%.

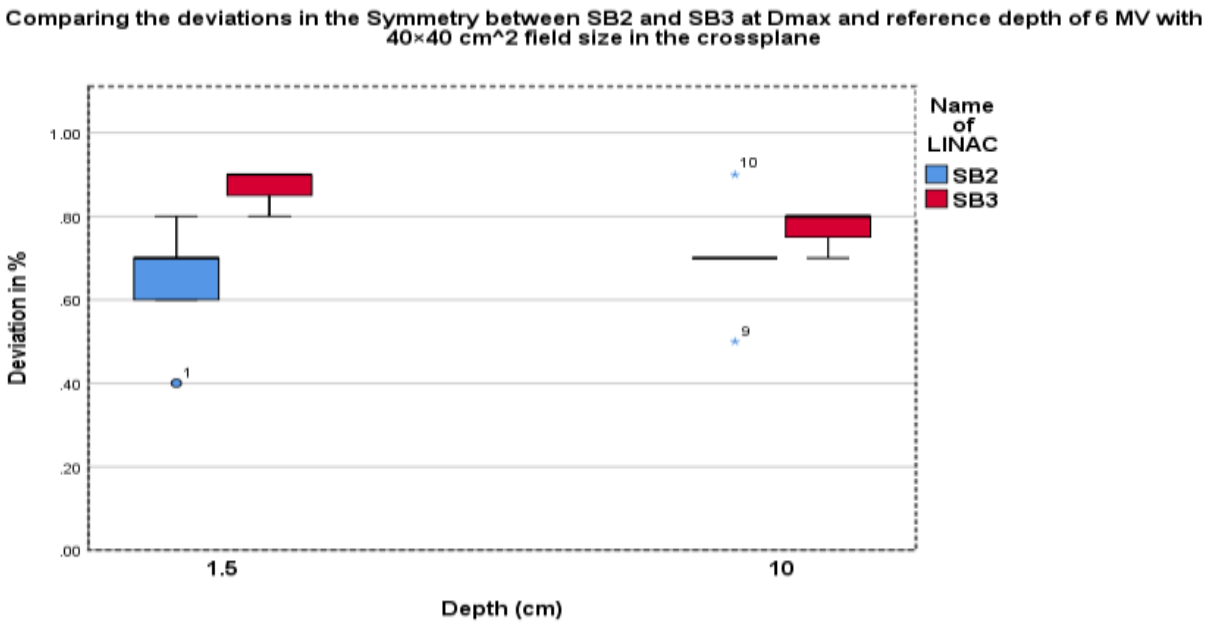

Figure 4. 35: The result of comparing the performance between SB2 and SB3 in terms of symmetry (crossplane) at Dmax and reference depth of 6 MV

In the inplane profile in figure 4.36, the 6 MV of SB2 produced a maximum deviation in the symmetry that exceeded the tolerance limit of ±1% by 0.1%. The mean deviations were 0.833% and 0.780% for SB3 and SB2 respectively at the D_{max}. At the reference depth, the SB2 again exceeded the tolerance limit by 0.1%. The mean deviation in SB2 was greater than SB3 by 0.027%.

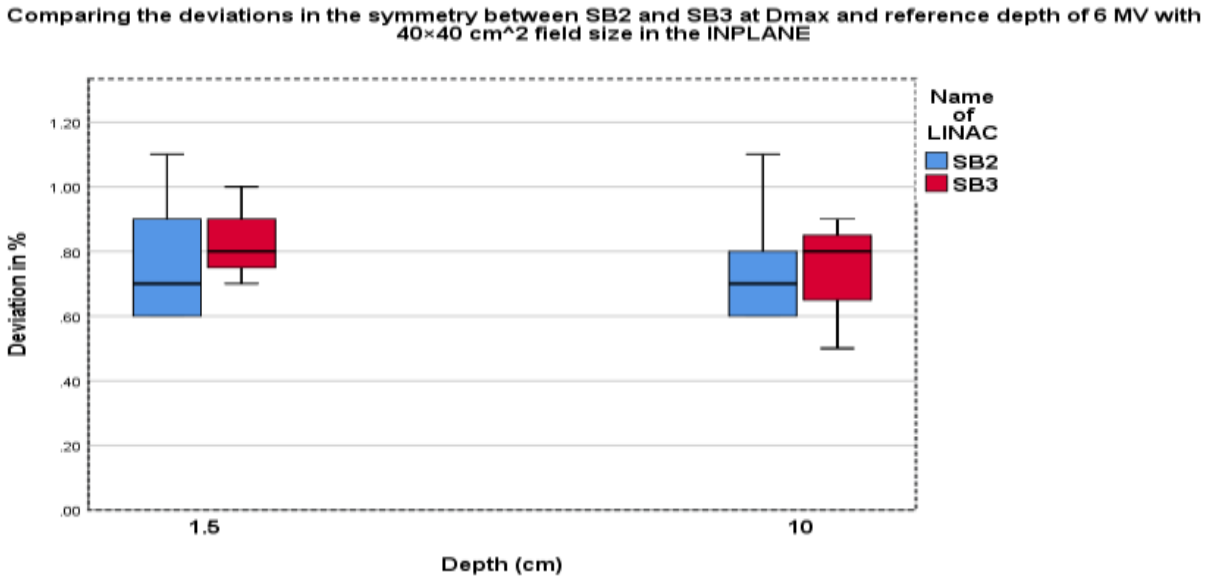

Figure 4. 36: The result of comparing the performance between SB2 and SB3 in terms of symmetry (crossplane) at Dmax and reference depth of 6 MV

The performance of the fieldwidth was also assessed between SB2 and SB3 of 6 MV with field size of 40 × 40 cm^2 in both crossplane and inplane profiles as shown in figure 4.37. In the crossplane profile, the SB2 had a maximum deviation which drifted beyond the tolerance limit (±2 mm) by 0.4 mm. The mean deviations were 1.420 mm and 1.067 mm respectively. In the inplane profile the SB2 had outliers which were all within the tolerance limit of 2 mm. the mean deviations were 0.060 mm and -0.567 mm for SB2 and SB3 respectively.

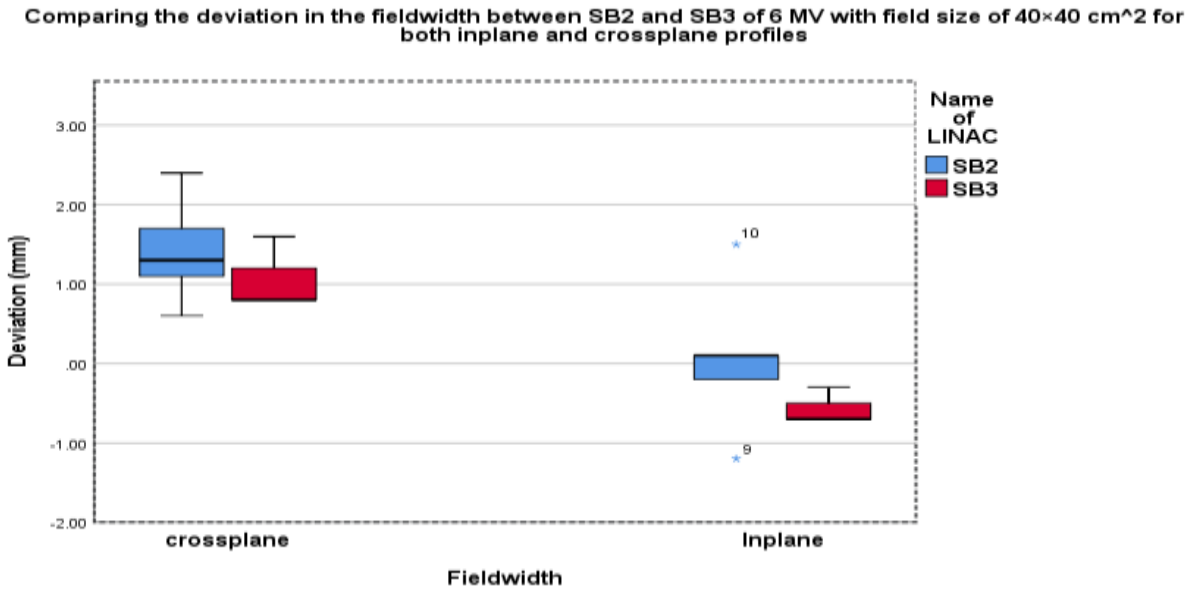

Figure 4. 37: The performance in the fieldwidth between SB2 and SB3

Analyzing the deviations in the flatness between SB2 and SB3 at D_{max} and reference depth of 15 MV with 10 × 10 cm^2 field size in the crossplane as depicted in figure 4.38, at D_{max}, the results indicated that the deviation in the flatness was greater in SB2 than SB3, the mean deviation in SB2 (1.200%) was more than twice the mean deviation in SB3 (0.533%). The SB2 had an outlier of 2.7% which fell outside the tolerance limit of ±1%. At the reference depth, SB2 again recorded an outlier which drifted significantly from the tolerance deviation. The mean deviation of SB2 was larger than SB3 by 0.693%.

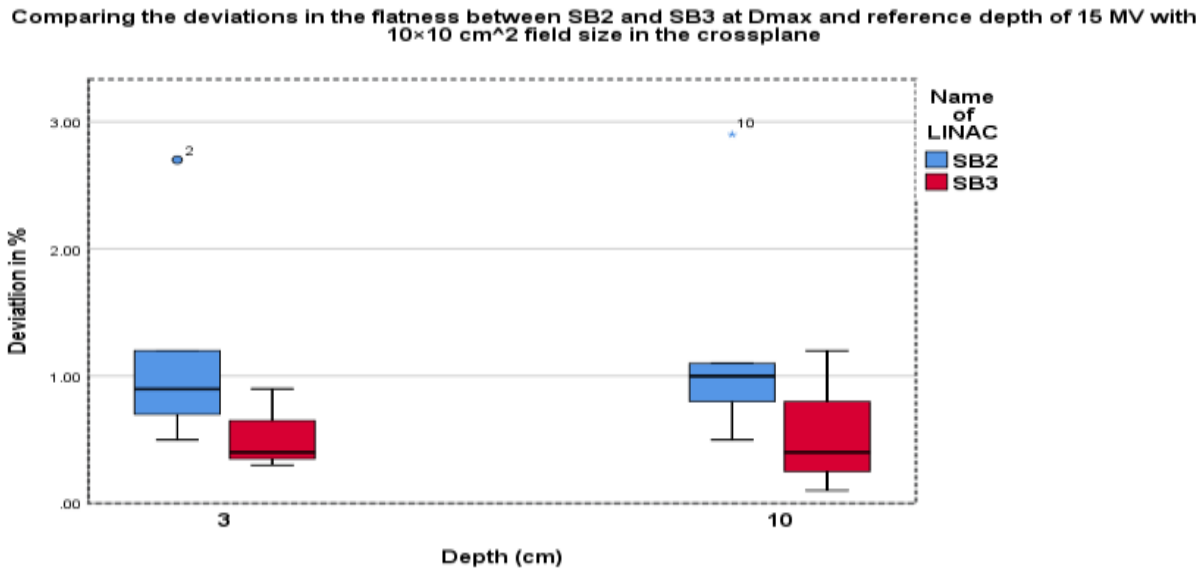

Figure 4. 38: The result of comparing the performance between SB2 and SB3 in terms of flatness (crossplane) at Dmax and reference depth of 15 MV

Comparing the deviation in the flatness in the between SB2 and SB3 at D_{max} and at reference depth of 15 MV with 10 × 10 cm^2 field size in the inplane profile as shown figure 4.39. At D_{max}, the SB2 LINAC had an outlier that exceeded the tolerance limit of ±1% by 1.2% resulting in a greater mean deviation than in SB3, the mean deviation of SB3 LINAC was 0.773% less than SB2. Also at the reference depth, the SB2 recorded maximum deviation of 2.2% drifting significantly beyond the tolerance deviation to a peak value of 2.2%. This increase in the deviation influenced the mean deviation in SB2. The mean deviation of SB2 and SB3 were 0.840% and -0.100% respectively.

Figure 4. 39: The result of comparing the performance between SB2 and SB3 in terms of flatness (Inplane) at Dmax and reference depth of 15 MV

The deviations in the symmetry between SB2 and SB3 at D_{max} and reference depth were also investigated for 15 MV for 10 × 10 cm^2 field size in the crossplane in figure 4.40, at D_{max}, all the deviations were within the tolerance limit of ±1%, the peak deviations of SB2 and SB3 were0.8% and 0.7% respectively. The mean deviation in SB3 was greater than SB2 by 0.02%. At the reference depth, the deviation in the symmetry exceeded the tolerance limit (±1%) by 0.3%. The mean deviations were 0.740% and 0.767% for SB2 and SB3 respectively.

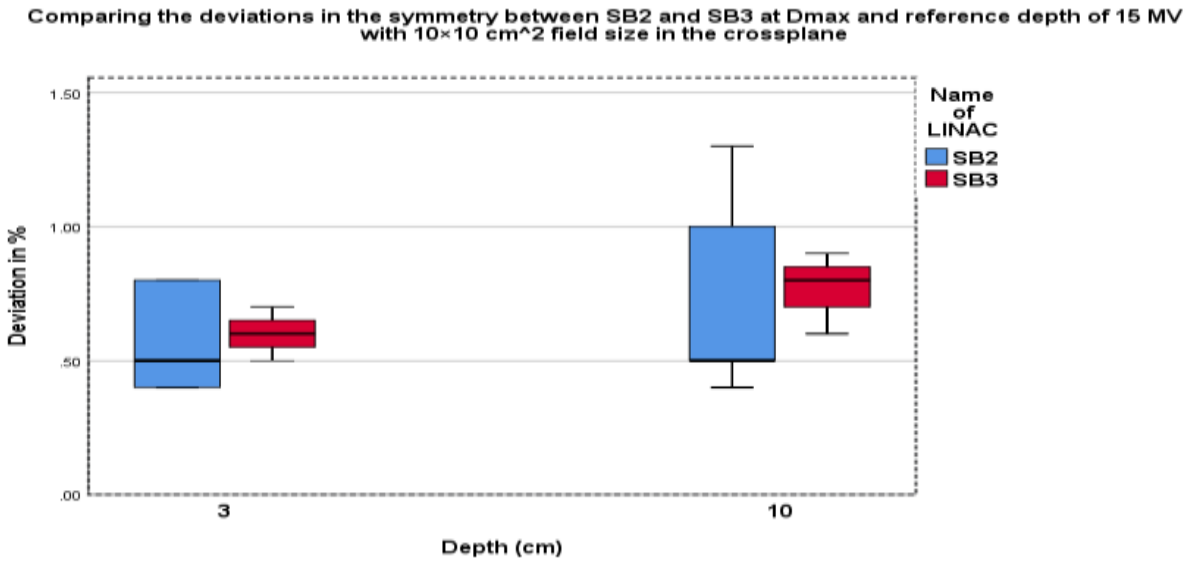

Figure 4. 40: The result of comparing the performance between SB2 and SB3 in terms of symmetry (crossplane) at Dmax and reference depth of 15 MV

In the inplane profile in figure 4.41, the deviation in symmetry of SB2 was greater than in SB3 at D_{max}, the peak deviation in SB2 fell beyond the tolerance limit of ±1% by 0.2%. The mean deviations in SB2 was greater than SB3 by 0.273%. At the reference depth, all the deviations were within the acceptable limit ±1% with maximum deviation. The mean deviation in SB3 was less than SB2 by 0.253%.

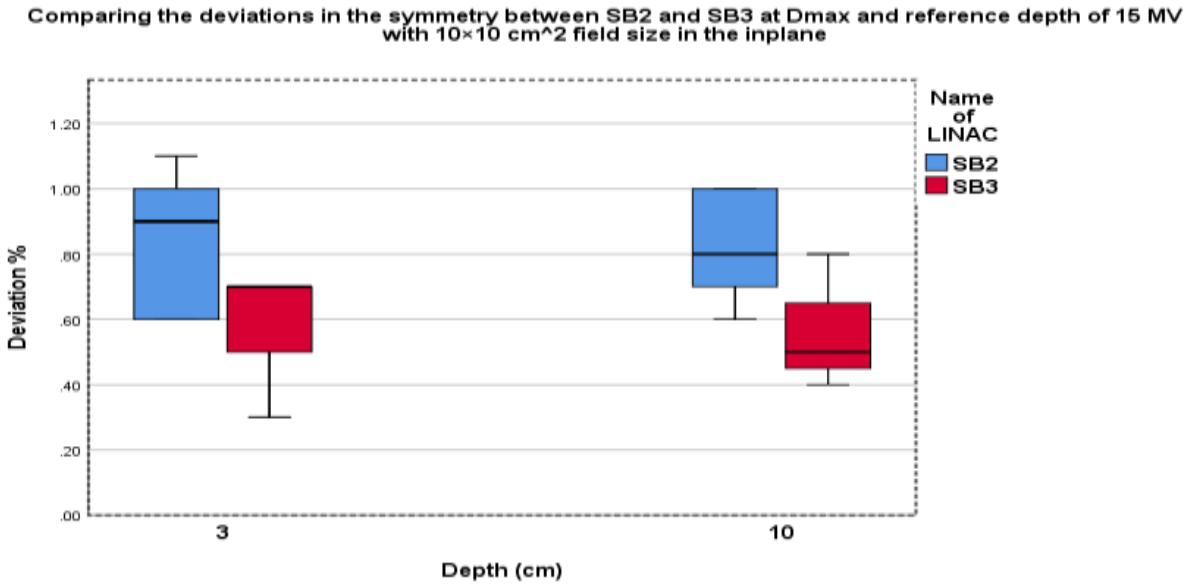

Figure 4. 41: The result of comparing the performance between SB2 and SB3 in terms of symmetry (Inplane) at Dmax and reference depth of 15 MV

The deviations in the flatness between SB2 and SB3 at D_{max} and at reference depth of 15 MV with field size of 40 × 40 cm^2 field size was evaluated in the crossplane as shown in figure 4.42, at D_{max} SB2 and SB3 were all within the tolerance deviation of ±1% with the peak deviation of SB3 equal to the tolerance deviation in the positive direction. The mean deviation of SB2 and SB3 were -0.360% and 0.133% respectively. At the reference depth the peak deviation in the flatness of SB2 exceeded the tolerance limit by 0.3% in the figure 4.42. The mean deviation was higher in SB2 than in SB3 by a 0.573% which proves a more stable performance in SB3.

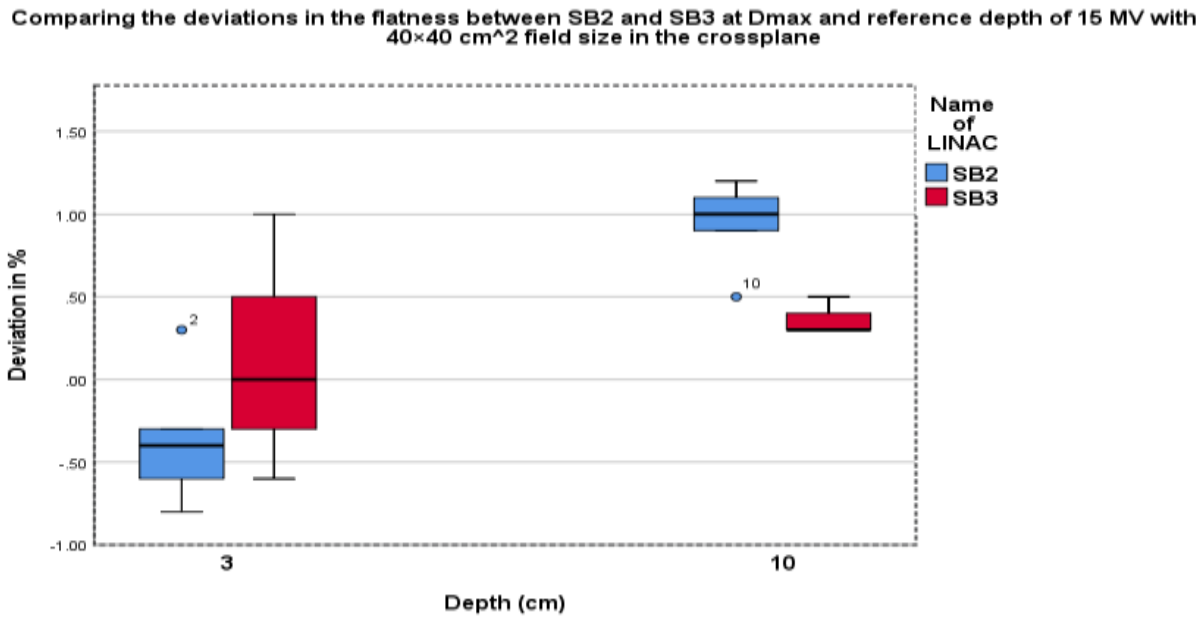

Figure 4. 42: The result of comparing the performance between SB2 and SB3 in terms of flatness (crossplane) at Dmax and reference depth of 15 MV

In the inplane, the deviation in flatness were found in the acceptable limit of ±1%, although SB2 recorded an outlier which was still in the tolerance limit of ±1% as depicted in figure 4.43. The mean deviation in SB2 and SB3 were -0.540% and 0.100% respectively at D_{max}. At the reference depth the minimum deviation in SB2 was 1.0 % which is the same as the tolerance deviation in the positive direction. The mean deviation of SB2 was higher than SB3 with a difference of 1.00%.

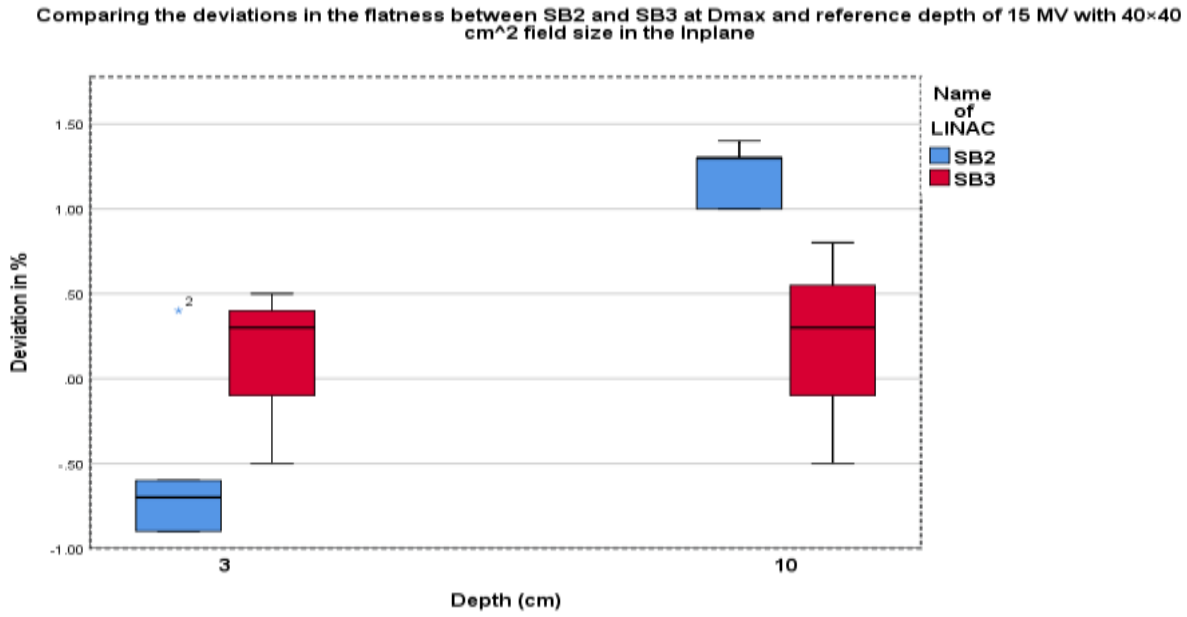

Figure 4. 43: The result of comparing the performance between SB2 and SB3 in terms of flatness (Inplane) at Dmax and reference depth of 15 MV

The deviations in the symmetry between SB2 and SB3 at D_{max} and reference depth were also analyzed for 15 MV for 40 × 40 cm^2 field size were compared in the crossplane as shown in figure 4.44**,** at D_{max} the maximum deviations were the same for both LINACS with a value of 0.80%. The mean deviation in SB3 was greater than SB2 by a factor of 0.007. The mean deviation in SB3 was higher than the mean deviation in SB2 by 0.027% at the reference depth. All the deviations were found in the tolerance limit of ±1%.

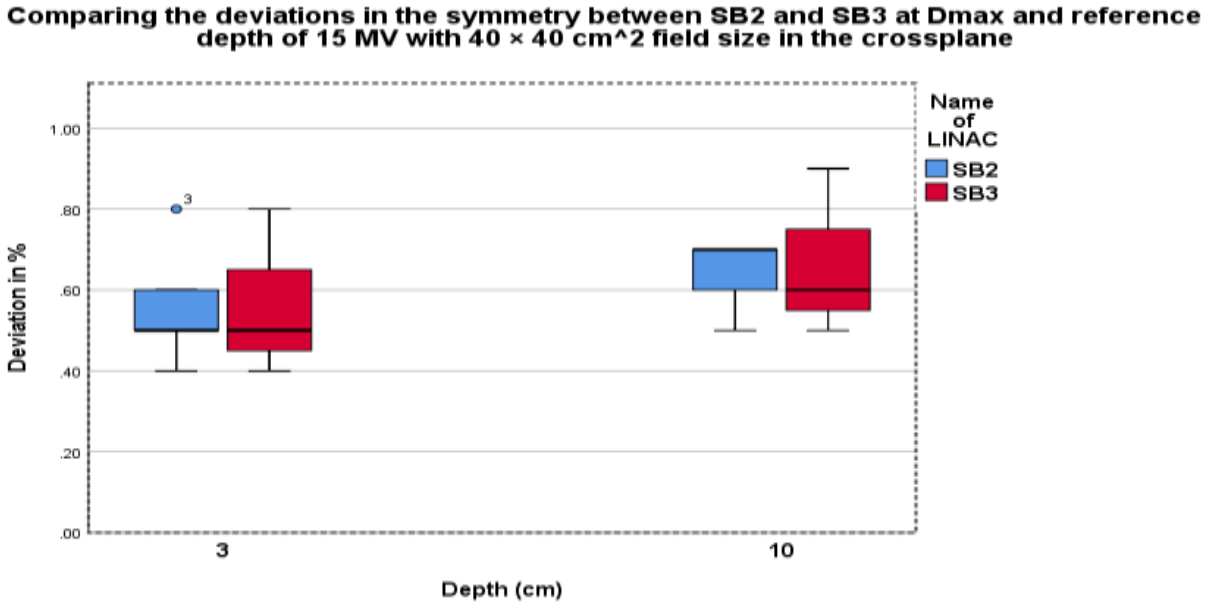

Figure 4. 44: The result of comparing the performance between SB2 and SB3 in terms of Symmetry (crossplane) at Dmax and reference depth of 15 MV

In the inplane profile, 15 MV energy of SB2 produced a maximum deviation which exceeded the tolerance limit of ±1% by 0.4%. The mean deviations were 1.100% and 0.500% for SB2 and SB3 respectively at the D_{max}. At the reference depth, the SB2 had outlier which exceeded the tolerance limit by 0.1% 0.7%. The mean deviation in SB2 was greater than SB3 by 0.607% in figure 4.45.

Acquah & Schiestl, (2014), did a similar study on performance evaluation of an Elekta LINAC, the average deviation of flatness and symmetry of the photon energy were 1.0% and 1.3% respectively in the annual control falling within the tolerance limit of 2%. In the same study the symmetry and flatness of the electron recorded mean deviations of 0.4% and 1.1% in the annual control which also fell within the tolerance limit of 2% for over a year operational period. (Acquah & Schiestl, 2014). Their results were higher than the findings of this study in table 4.3-4.10, this could be due to the difference in the tolerance

limits. Their tolerance deviation was ±2% whiles this study has a tolerance deviation of ±1%.

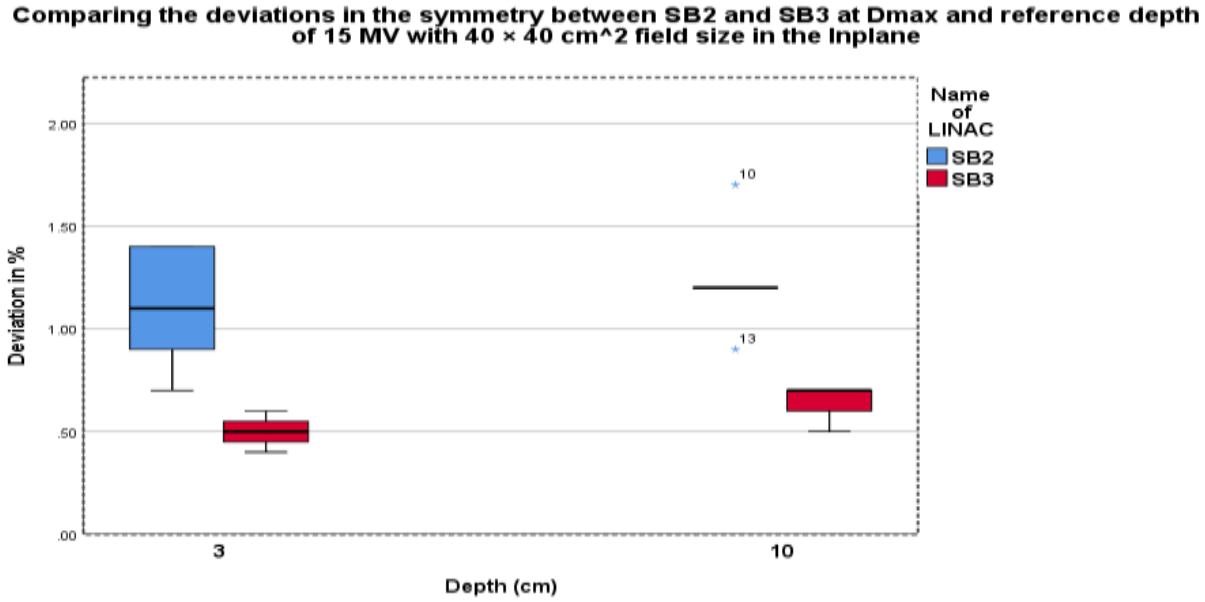

Figure 4. 45: The result of comparing the performance between SB2 and SB3 in terms of Symmetry (Inplane) at Dmax and reference depth of 15 MV

4.11 Comparing the beam profiles of electron energies

The beam profiles of the electron energies were compared among the electron energies in the crossplane for 20 × 20 cm^2 field size as shown in figure 4.46**,** all deviations in the fieldwidth of the energies were within the tolerance limit of ±1mm. E10 and E12 recorded the peak deviation of 0.4 mm in the fieldwidth. The deviation in the symmetry of E8 and E10 had maximum deviations which exceeded beyond the tolerance limit of ±1% by 0.1%. These significant deviation in E8 and E10 contributed to a high mean deviation of 0.760% and 0.780% in E8 and E10 respectively. The highest deviations in E6 and E12 had the same value of 1% which fell exactly on the tolerance deviation of ±1% in the positive direction.

The mean deviations were 0.640% for E6 and 0.680% for E12. The symmetry of E15 was more stable than the rest of the electron energies with a least mean deviation of 0.560%. The flatness of the electron energies performed better with all the deviations falling within the tolerance limit of ±1% over the years. E8 produced the highest mean deviation with a value of 0.460% from Appendix (Table 5.15).

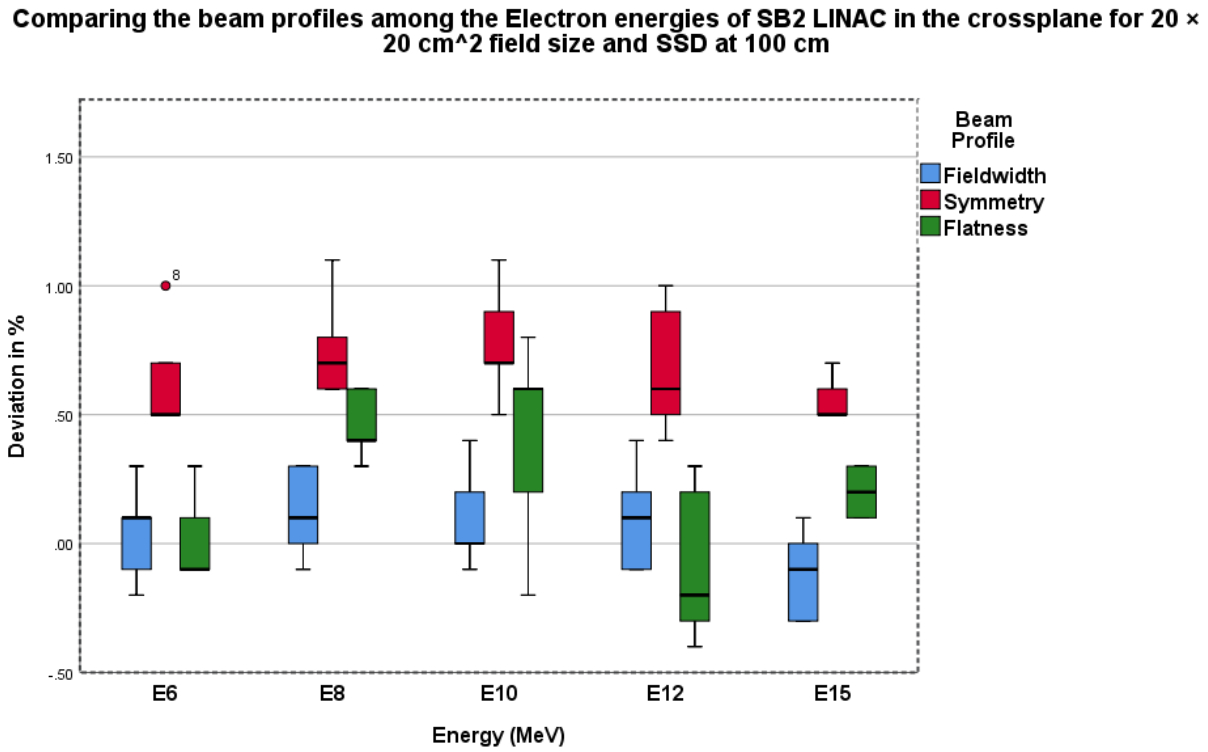

Figure 4. 46: Comparison of the beam profiles among the electron energies in the crossplane.

In the inplane profile, the deviations in the fieldwidth of the electron energies were all within the tolerance limit of ±1 mm as shown in figure 4.47, E6 produced the maximum mean deviation in the fieldwidth with a value of 0.140 mm. E8 recorded the minimum mean deviation of 0.00 mm, and 0.080 mm for E10, E12 and E15. In the symmetry, E8 recorded a maximum deviation exceeding the tolerance limit of ±1% by 0.1%. The

deviations in the symmetry of rest of the electron energies were found in the acceptable limit. The highest and the least mean deviation in the symmetry occurred in E10 and E15 with a values of 0.720% and 0.620% respectively. E8 and E12 had the same mean deviation of 0.640%, and 0.680% for E12**.** The deviations in the flatness lied within the tolerance deviation of 1%. E10 recorded the highest mean deviation of 0.260%. The mean deviations were 0.00%, 0.200%,-0.140%, and -0.080% for E6, E8, E12 and E15 respectively.

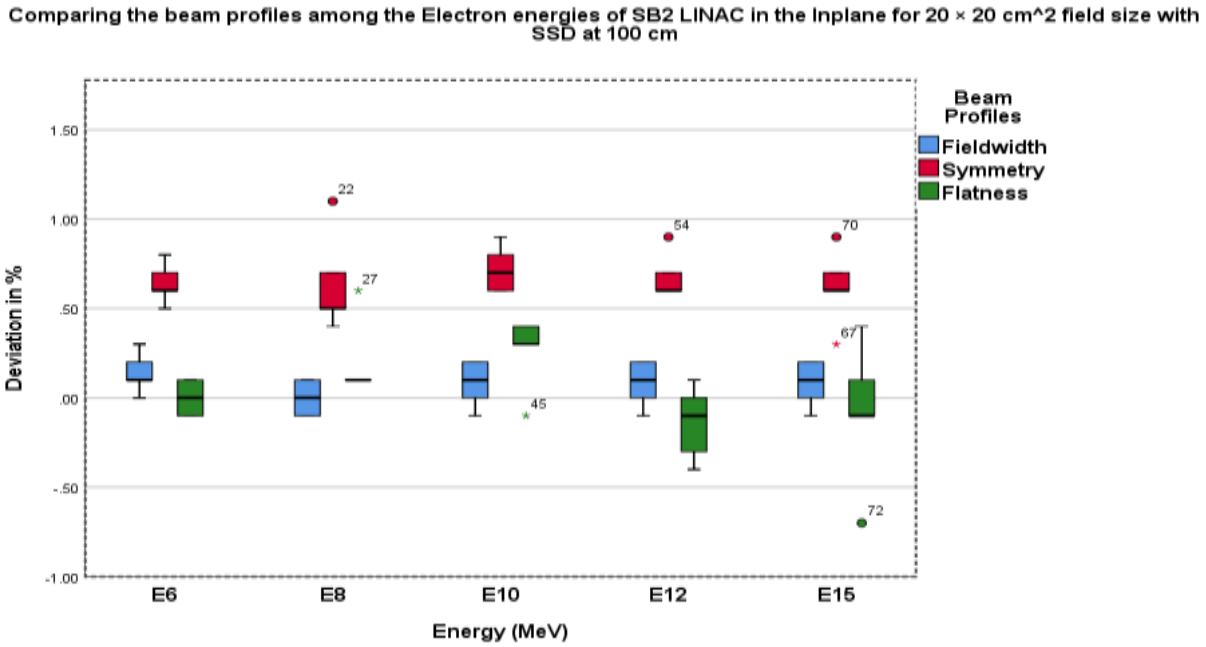

Figure 4. 47: Comparison of the beam profiles among the electron energies in the inplane profile

4.12 Performance of Photon Energies

All the deviations in the tissue phantom ratio (TPR) of 6 MV energy were within the tolerance limit of ±1% when compared with the reference value (0.588). From Figure 4.48, the maximum deviation was 0.3% which occurred in 2015. Three out of the five deviations were within one standard deviation (1δ) from the mean (-0.04) in Figure 4.48

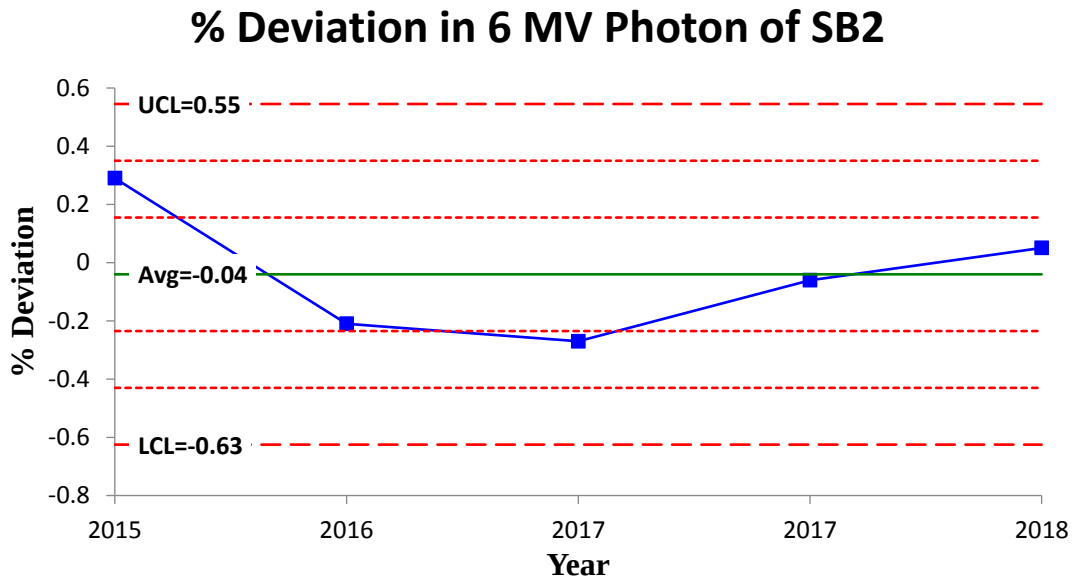

Figure 4. 48: shows the deviations in the Tissue Phantom Ratio (TPR) of 6 MV of SB2 LINAC

The deviations in the tissue phantom ratio of 15 MV fell within the tolerance limit of ±1% when the measurements were compared with reference value (0.652). All the points were within one standard deviation (1δ) from the mean (-0.11) except the maximum deviation (-0.6) in 2016 which lied in two standard deviation away from the mean as shown in figure 4.49.

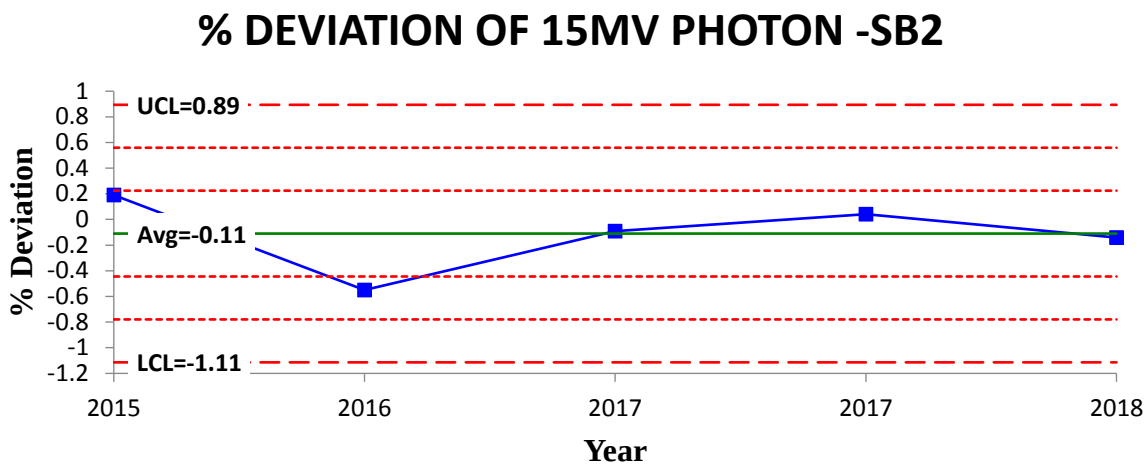

Figure 4. 49: The deviations in the Tissue Phantom Ratio (TPR) of 15 MV of SB2 LINAC

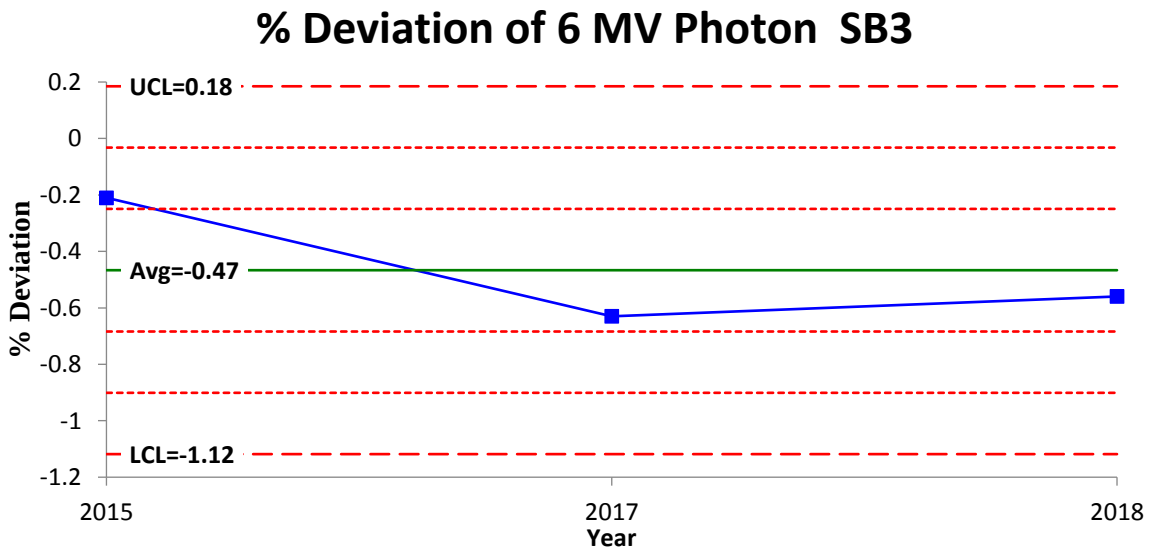

Figure 4. 50: The deviations in the Tissue Phantom Ratio (TPR) of 6 MV of SB3 LINAC

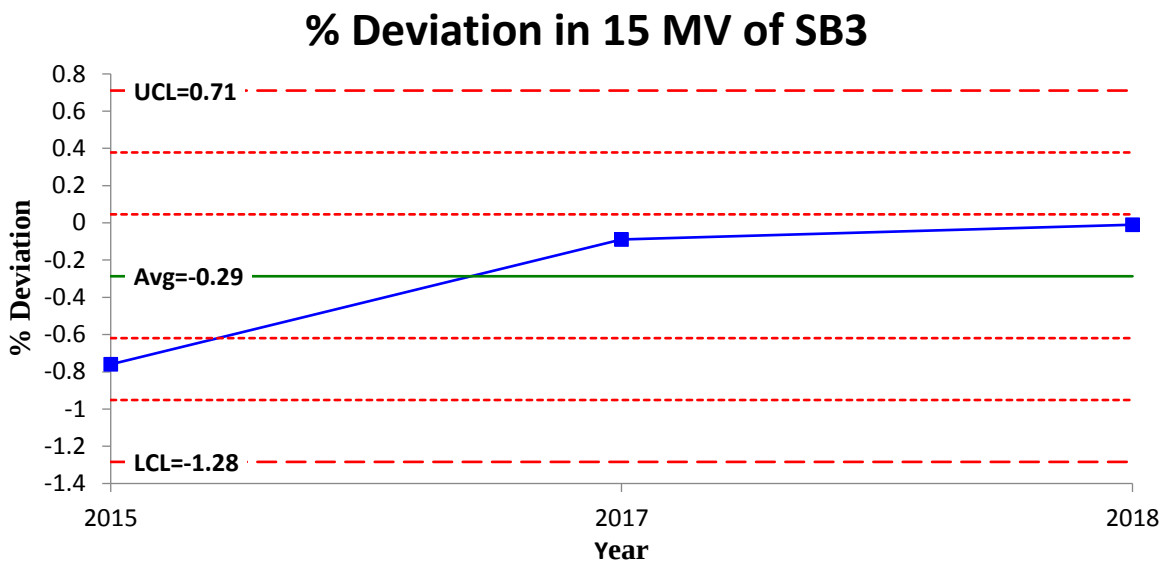

Figure 4. 51: The deviations in the tissue phantom ratio (TPR) of 15 MV of SB3 LINAC

The deviations in both 6 MV and 15 MV of SB3 LINAC were within the tolerance limit of ±1%. The peak deviations in the energies were -0.8% and -0.6% for 15 MV and 6 MV respectively. The mean deviations were 0.29% in Figure 4.51 for 15 MV and -0.47 % for 6 MV as shown in Figure 4.50.

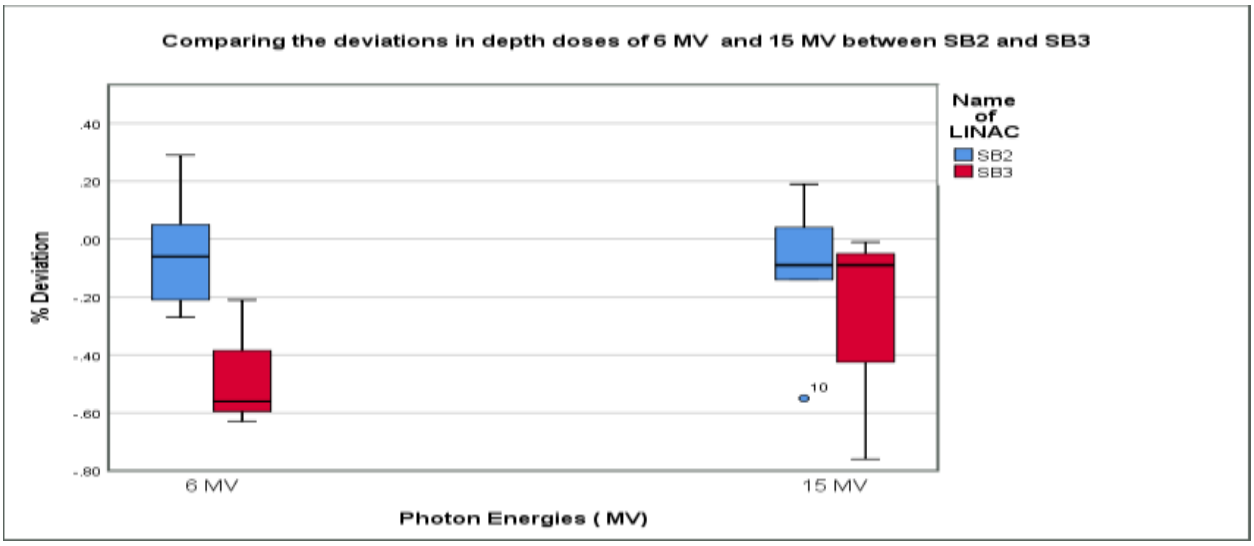

Figure 4. 52: Plot comparing the deviation in depth doses of 6 MV and 15 MV between the LINACS

From Figure 4.52, all the deviations in the depth dose measurements of 6 MV and 15 MV of the two LINACS were found to be stable over the years performing within the tolerance limit of ±1%, for the 6 MV from Figure 4.52, SB2 was more stable over the years than SB3 with mean deviations of -0.040 % and -0.467 % respectively. Also in the 15 MV, SB2 with a mean deviation of -0.110 % was again more stable than SB3 which had a mean deviation of -0.287%**.** Comparing the energies (6 MV AND 15 MV) of SB2, 6 MV was more stable than 15 MV with mean deviations of -0.040 % and -0.110% respectively. 15 MV performed better than 6 MV in SB3. The mean deviations were -0.426% and -0.287% for 6 mv and 15 mv respectively. Also, 15 MV of SB2 was found to be more stable than 15 MV of SB3 with mean deviation of -0.110% for SB2 and -0.27% for SB3. 6 MV of SB2 produced a better performance than 6 MV of SB3 with mean deviation of -0.040% and -0.467% respectively.

4.13 Performance of Electron Energies

The deviations in R_{50} of E6 were all found in the tolerance limit of ±0.5mm except in 2016 that recorded a peak deviation of 1.1mm exceeding the tolerance limit of ±0.5 mm by 0.6 mm. The mean deviation was 0.2 mm in figure 4.53. In figure 4.54, the 8 MeV had a maximum which drifted beyond the tolerance limit of ±0.5 mm by 0.4 mm in 2016, the deviations in R_{50} of the remaining years were within the tolerance limit. The mean deviation was 0.1 mm. The maximum deviation in 10 MeV was -0.5 mm which occurred in 2017. All the deviations were within the tolerance limit as shown in figure 4.55 with a mean value of -0.18 mm. In 2017, 12 MeV recorded a peak deviation of 0.8 that lied outside the tolerance deviation in figure 4.56, the mean deviation was -0.16 mm. all the deviations of the 15 MeV energy were found within the acceptable deviation with a mean value of -0.1 mm as shown in figure 4.57.

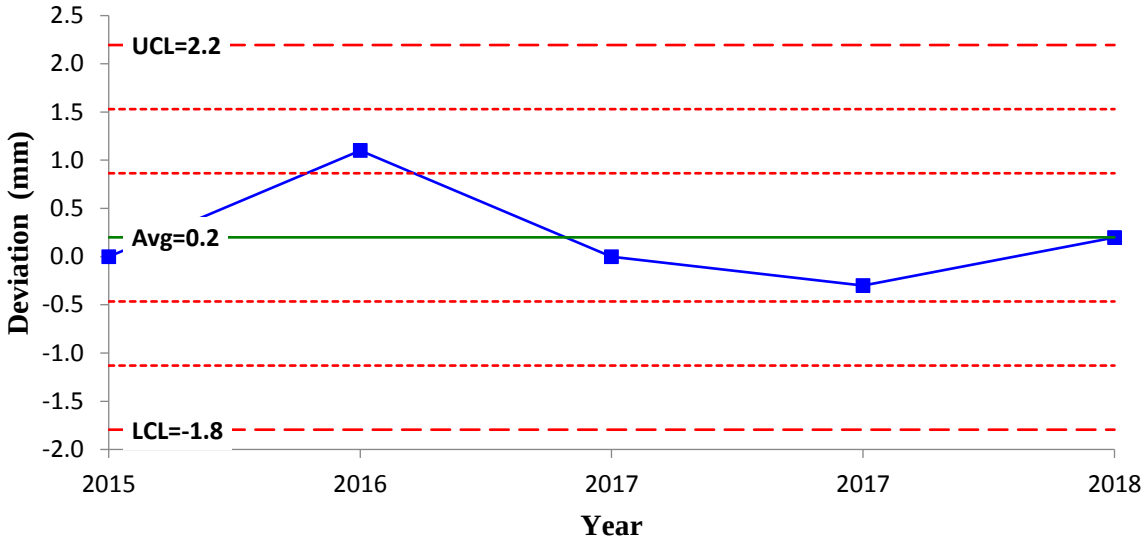

Figure 4. 53 Deviations in R50 of 6 MeV of SB2 LINAC

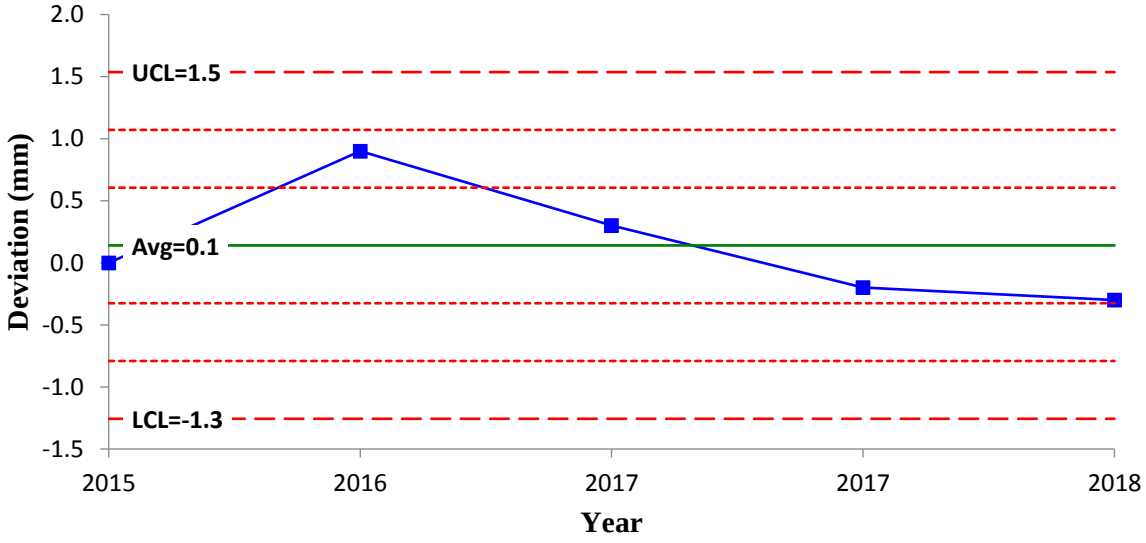

Figure 4. 54: Deviations in R50 of 8 MeV of SB2 LINAC

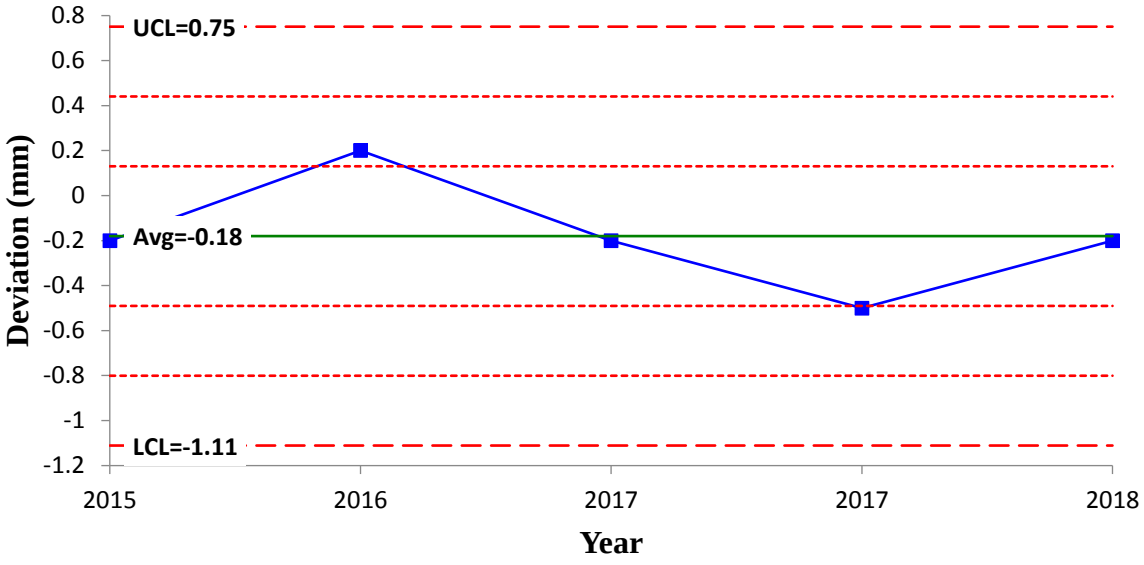

Figure 4. 55: Deviations in R50 of 10 MeV of SB2 LINAC

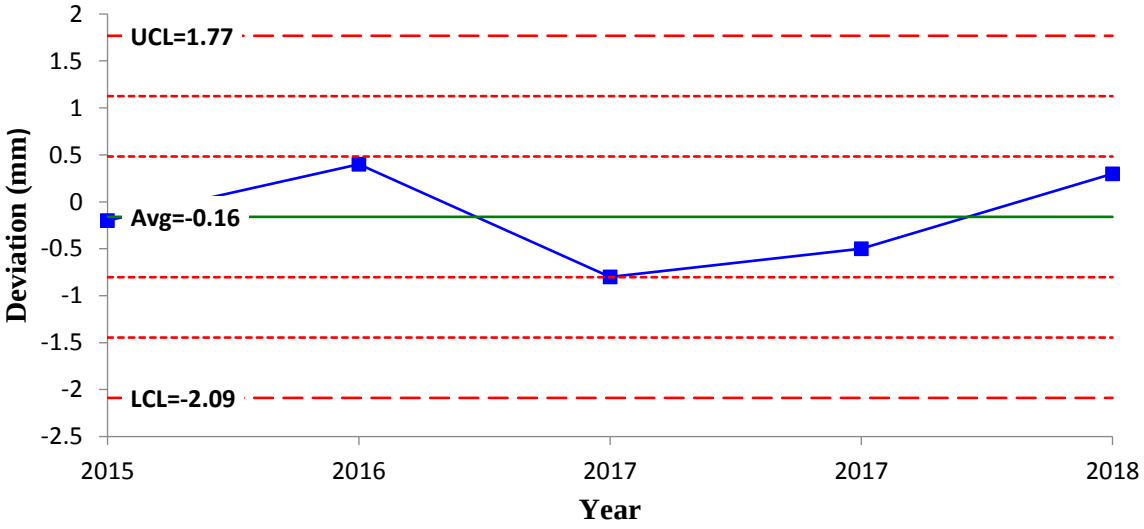

Figure 4. 56: Deviations in R_{50} of 12 MeV of SB2 LINAC

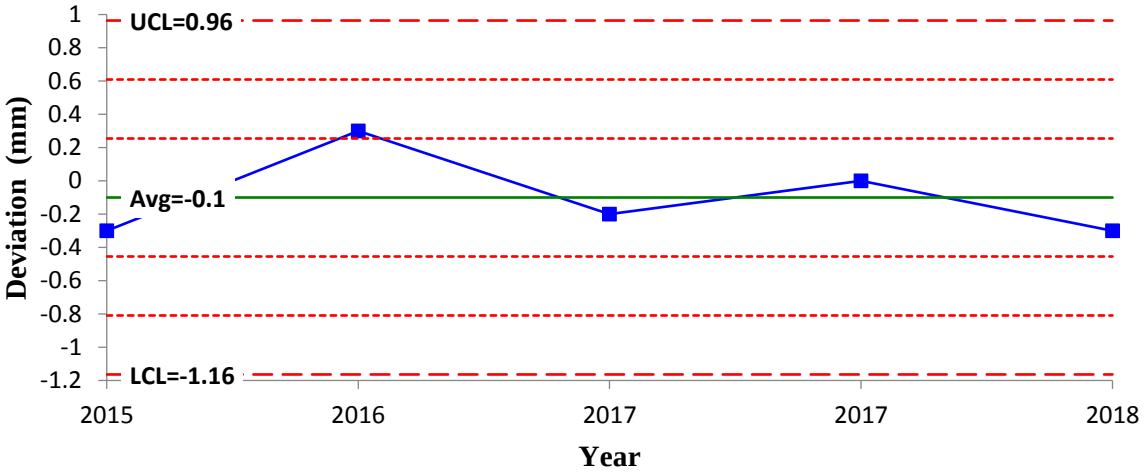

Figure 4. 57: Deviations in R_{50} of 15 MeV of SB2 LINAC

CHAPTER FIVE

CONCLUSION AND RECOMMENDATION

The chapter presents conclusion and recommendations based on the findings of this research.

5.1 Conclusion

The objective of the study was to perform an in depth analysis on the QA/QC data of LINAC machines over five year period and check their performance if they were functioning within the acceptable limits. The performance of the XVI was analyzed and the results showed that all the three directions of the XVI were stable in SB2, SB3 and SB4 LINACS over the years. The same cannot be said about SB6 which recorded mean deviation that drifted beyond the tolerance limit of ±0.1 cm by -0.01 cm, 0.12 cm and 0.1cm in the lateral(x), longitudinal (y) and vertical (z) directions respectively. These significant deviations in the XVI of SB6 were due to a major maintenance on the LINAC in the year 2015. The results also showed that some of the deviations in the first dose calibration measurements in the LINACS were extremely high exceeding the tolerance deviation of ±0.5%, this contributed to a higher mean deviation among the LINACS. The mean deviations were 0.291%,-0.368%, 0.006% and -0.848% for SB2, SB3, SB4, and SB6 respectively of the 6 MV energy. The 15 MV recorded mean deviation of 0.265% for SB2, -0.140% for SB3, -0.131% for SB4 and -0.483% for SB6 in the first calibration measurements. The second reading after adjustment had been made on the machine proved a more stable performance on the LINACS with SB2, SB3, SB4 and SB6 recording mean

deviations of 0.007%, 0.105%, 0.019% and 0.048% respectively of 6 MV photon energy. The mean deviations of the 15 MV were -0.026%, 0.023%, 0.007% and 0.018% for SB2, SB3, SB4 and SB6 respectively. This work again analyzed the quality of the photon beams and the results demonstrated that 6 MV was more stable than 15 MV with mean deviations of -0.040% and -0.110% respectively. In SB3, the study demonstrated that 15 MV performed better than 6 MV with mean deviations of -0.278% and 0.426% respectively. The performance between 15 MV of SB2 and 15 MV of SB3 were also investigated, the result showed that 15 MV of SB2 was found to perform better than 15 MV of SB3 with mean deviations of -0.110% for SB2 and 0.27% for SB3. The 6 MV of SB2 produced a better performance than 6 MV of SB3 with mean deviations of -0.040% and 0.467% respectively. The quality of the electron energies of SB2 were also checked using R_{50} and the result indicated that 15 MeV was the most stable among the electron energies with mean deviation of -0.100 mm and 6 MeV being the least stable with a mean deviation of 0.200%. The 8, 10 and 12 MeV recorded a mean deviation of 0.140, -0.180 and -0.160 mm respectively. The mean deviations in flatness, symmetry and fieldwidth of crossplane and inplane profiles of both electrons and photons were found to be in the tolerance limit of ±1%, ±1% and ±1mm (for 10 x 0 cm^2 and 20 x 20 cm^2 field size and ±2 mm for 40 x 40 cm^2 field size) respectively. The study has shown that all the controls selected for this research were stable and performing within their acceptable limits although there were deviations that were significantly high that needed attention such as the beam profiles of 15 MV of SB2 and the symmetry of the electron energies of SB2.

5.2 Recommendation

It was observed that most of the QA/QC procedures were not performed at their scheduled frequencies and some of the comments indicating the reasons for the drift of the values beyond the tolerance limits were not documented, It is recommended that QA/QC procedures should be done at their respective specified frequencies and there should be documentations on issues relating to the QA/QC procedures. The study should be taken further by considering extensively the daily, weekly, monthly, annual controls and the LINACS that were not covered in this study. The beam profiles of the photon energies and the electron energies should be given attention as some of the deviations exceeded their tolerance limit.

REFERENCES

Acquah, G., & Schiestl, B. (2014). Quality Assurance and Performance Evaluation of an Elekta Linear Accelerator : Results From Over a Year QA Experience in Ghana, *4531*, 354–363.

Akorsah, K. (2016). University of Ghana http://ugspace.ug.edu.gh, (10551334). https://doi.org/10.1038/253004b0

An, I. (2009). CHAPTER 3 ASSESSMENT OF BEAM STABILITY AND QUANTIFICATION OF MLC POSITIONAL ERRORS OF A HIGH ENERGY VARIAN MEDICAL LINEAR, (1994), 40–58.

Chapman, J. (1996). The Novice's Guide To Electron Linear Accelerators, 1–7.

European Commission. (2015). *General guidelines on risk management in external beam radiotherapy*. https://doi.org/10.2833/667305

Ford, E.C., Smith, K., Terezakis, S., Croog, V., Gollamudi, S., Gage, I., Keck, J., DeWeese, T., and Sibley, G. "A streamlined failure mode and effects analysis," Med. Phys. 41, 061709 (6pp.) (2014)

Gao, Q., Zha, H., Chen, H., and Shi, J. "Design and Optimization of the Target in Electron Linear Accelerator", Proceedings, 4th International Particle Accelerator Conference (IPAC 2013), THPWA016, 2013.

Hossain, M., & Rhoades, J. (2016). On beam quality and flatness of radiotherapy megavoltage photon beams. *Australasian Physical & Engineering Sciences in*

Medicine, *39*(1), 135–145. https://doi.org/10.1007/s13246-015-0408-8

Huq, M. S., Fraass, B. A., Dunscombe, P. B., Gibbons Jr., J. P., Ibbott, G. S., Mundt, A. J., Yorke, E. D. (2016). The report of Task Group 100 of the AAPM: Application of risk analysis methods to radiation therapy quality management. *Medical Physics*, *43*(7), 4209. https://doi.org/10.1118/1.4947547

IAEA (1997): Quality Assurance in Radiotherapy. IAEA–TECDOC-1040. International Atomic Energy Agency, Vienna.

IBA (2018): Blue phantom2-efficiency for LINAC commissioning and annual QA. world wide web:http://iba-dosimetry.com. Retrieved on 3rd April, 2018.

Juntong, N., Pharaphan, K., Light, S., & Ratchasima, N. (2016). THE OPTIMIZED X-RAY TARGET OF ELECTRON LINEAR ACCELERA - TOR FOR RADIOTHERAPY, 1–3.

Khan, F. M., & Gibbons, J. P. (2014). *The Physics of Radiation Therapy* (5th Edition), 46-93.

Klein, E. E., Hanley, J., Bayouth, J., Yin, F.-F., Simon, W., Dresser, S., … Holmes, T. (2009). Task Group 142 report: Quality assurance of medical acceleratorsa). *Medical Physics*, *36*(9Part1), 4197–4212. https://doi.org/10.1118/1.3190392

Lee, H., Jeong, S., Jo, Y., & Yoon, M. (2015). Study of quality assurance regulations for linear accelerators in Korea : A comparison study between the current status in Korea and the international guidelines, 1–22.

Mackie, T. R. (2015.). Linac Based Radiosurgery and Stereotactic Radiotherapy, 35-38.

Mayles, P., Nahum, A., & Rosenwald. (2007). *Handbook of Radiotherapy Physics*. (P. Mayles, A. Nahum, & and J. . Rosenwald, Eds.) (1st ed.). CRC Press.

Nordström, F. (2012). *Development and evaluation of new tools for improved patient safety in external beam therapy*, 18-38.

Orton, C. G., & Hendee, W. R. (2012). *Controversies in Medical Physics : a Compendium of Point / Counterpoint Debates Volume 2 Edited by : and* (Vol. 2).

Pichoff, N. (2006). Introduction to RF linear accelerators. *Proceedings*, 105.

Podgorsak, E. B. (2008). *Radiation Oncology Physics: A Handbook for Teachers and Students*. *British journal of cancer* (Vol. 98). https://doi.org/10.1038/sj.bjc.6604224

Suvendu, Kumar Sahoo, R. M. (2016). STUDY ON VARIATION OF QUALITY ASSURANCE DATA OF A LINEAR ACCELERATOR AFTER THIRTEEN YEARS OPERATION FOR CANCER, *3*(2), 177–180.

Tech, V., & Forest, W. (2014). An Interface for Analysis of Medical Linear Accelerator Performance Parameters Using Process Behavior Charts, 23-87.

Tello, V. M. (2016). " Medical Linear Accelerators and how they work ", 3-23.

Thomadsen, B., Williamson, J., Ph, D., Palta, J., & Huq, S. (2013). Quality and Safety in Radiotherapy : Learning the New Approaches in Task Group 100 and Beyond Management Programs. *Medical Physics Monograph*, (36). Retrieved from https://medicalphysics.org/documents/quality_ch4.pdf

Thwaites, D. I., Centre, E. C., Hospital, W. G., Kingdom, U., Mijnheer, B. J., & Mills, J.

A. (2003). Chapter 12 QUALITY ASSURANCE OF EXTERNAL BEAM RADIOTHERAPY. *Quality Assurance*, 407–450.

Uddin, T. (2010). QUALITY CONTROL OF MODERN LINEAR ACCELERATOR : DOSE STABILITY LONG AND SHORT-TERM, *3041*, 6–8.

WHO, Darin, C., Training, R. O., Kimberly, M., Deepa, G., Board, E., … Co-investigator, N. (1988). *Quality Assurance in Radiotherapy*. *World Health Organization 1988*. https://doi.org/10.1007/s13398-014-0173-7.2

APPENDIX

Table 5. 1: Deviations in the tissue phantom ratio of photon energies of SB2 and SB3

Year	SB2		SB3	
	6 MV	15 MV	6 MV	15 MV
	Dev %	Dev %	Dev %	Dev %
2015	0.29	0.19	-0.21	-0.76
2016	-0.21	-0.55	--	--
2017	-0.27	-0.09		
2017	-0.06	0.04	-0.63	-0.09
2018	0.05	-0.14	-0.56	-0.01
Mean	-0.04	-0.11	-0.46	-0.29
Std dev	0.22	0.27	0.22	0.41
Skewness	0.73	-1.07	1.54	-1.66

Table 5. 2 Deviations in the R_{50} of the electron energies

Year	E6	E8	E10	E12	E15
	Dev (mm)	Dev (mm)	Dev (mm)	Dev (mm)	Dev (mm)
2015	0.0	0.0	-0.2	-0.2	-0.3
2016	1.1	0.9	0.2	0.4	0.3
2017	0.0	0.3	-0.2	-0.8	-0.2
2017	-0.3	-0.2	-0.5	-0.5	0.0
2018	0.2	-0.3	-0.2	0.3	-0.3
Mean	0.2	0.1	-0.2	-0.2	-0.1
Std dev	0.5	0.5	0.2	0.5	0.3
Skewness	1.6	1.2	0.6	-0.1	1.2

Table 5. 3: Mean deviation in the three Coordinates (x, y and z) Of the XVIs of the LINACS

Year	SB4			SB6		
	Dev-x(cm)	Dev-y(cm)	Dev-z(cm)	Dev-x(cm)	Dev-y(cm)	Dev-z(cm)
2011	-0.05	0.00	0.03	--	--	--
2012	-0.02	0.01	0.03	--	--	--
2013	-0.05	0.04	0.03	--	--	--
2014	-0.06	0.06	0.05	--	--	--
2015	-0.05	0.05	0.02	-0.11	0.22	0.20
2016	-0.05	0.06	0.03	0.00	0.06	0.03
2017	-0.02	0.03	0.02	-0.05	0.05	0.02
2018	-0.01	0.04	-0.02	-0.06	0.04	-0.02
Mean	-0.04	0.04	0.02	-0.06	0.09	0.06
Std dev	0.02	0.02	0.02	0.05	0.09	0.10
Skewness	0.62	-0.65	-1.55	0.00	1.95	1.70

Table 5. 4: Mean deviation in the three Coordinates (x, y and z) Of the XVIs of the LINACS

Year	SB2			SB3		
	Dev-x(cm)	Dev-y(cm)	Dev-z(cm)	Dev-x(cm)	Dev-y(cm)	Dev-z(cm)
2011	0.02	-0.01	0.06	--	--	--
2012	-0.26	0.00	0.09	--	--	--
2013	0.00	0.00	0.02	--	--	--
2014	0.00	0.02	0.04	0.03	-0.02	0.05
2015	0.01	0.01	0.04	0.01	0.05	0.05
2016	0.00	0.07	0.01	0.01	0.08	0.07
2017	-0.03	0.02	0.01	0.01	0.03	0.01
2018	-0.04	0.01	0.05	-0.02	0.04	0.03
Mean	-0.04	0.02	0.04	0.01	0.036	0.042
Std dev	0.09	0.02	0.03	0.02	0.036	0.023
Skewness	-2.58	1.87	0.68	-0.82	-0.755	-0.405

Table 5. 5: Deviations in the beam profiles of 6 MeV of SB2 LINAC

E6 Deviation						
Year	**Crossplane**		Flatness	**Inplane**		Flatness
	Fieldwidth	**Symmetry**		**Fieldwidth**	**Symmetry**	
	Dev(mm)	Dev (%)	Dev (%)	Dev (%)	Dev (%)	Dev (%)
2015	-0.2	0.5	-0.1	0.0	0.8	0.1
2016	0.3	0.5	-0.1	0.3	0.6	-0.1
2017	0.1	1.0	0.3	0.1	0.6	0.0
2017	0.1	0.7	0.1	0.2	0.7	-0.1
2018	-0.1	0.5	-0.1	0.1	0.5	0.1
Mean	0.0	0.6	0.0	0.1	0.6	0.0
Std dev	0.2	0.2	0.2	0.1	0.1	0.1
Skewness	0.1	1.5	1.3	0.4	0.4	0.0

Table 5. 6: Deviations in the beam profiles of 8 MeV of SB2 LINAC

E8 Deviation						
Year	**Crossplane**		Flatness	**Inplane**		Flatness
	Fieldwidth	**Symmetry**		**Fieldwidth**	**Symmetry**	
	Dev (mm)	Dev (%)	Dev (%)	Dev (%)	Dev (%)	Dev (%)
2015	0.0	0.8	0.6	-0.1	0.7	0.1
2016	0.3	0.6	0.6	0.1	1.1	0.6
2017	0.1	0.6	0.4	-0.1	0.5	0.1
2017	0.3	1.1	0.3	0.1	0.5	0.1
2018	-0.1	0.7	0.4	0.0	0.4	0.1
Mean	0.1	0.8	0.5	0.0	0.6	0.2
Std dev	0.2	0.2	0.1	0.1	0.3	0.2
Skewness	-0.1	1.4	0.2	0.0	1.5	2.2

Table 5. 7: Deviations in the beam profiles of 10 MeV of SB2 LINAC

E10 Deviation						
Year	**Crossplane**		Flatness	**Inplane**		Flatness
	Fieldwidth	**Symmetry**		**Fieldwidth**	**Symmetry**	
	Dev(mm)	Dev (%)	Dev (%)	Dev (%)	Dev (%)	Dev (%)
2015	-0.1	0.7	0.6	-0.1	0.6	0.3
2016	0.4	0.5	0.2	0.2	0.8	0.4
2017	0.0	0.9	0.6	0.1	0.9	0.4
2017	0.2	1.1	0.8	0.2	0.7	0.3
2018	0.0	0.7	-0.2	0.0	0.6	-0.1
Mean	0.1	0.8	0.4	0.1	0.7	0.3
Std dev	0.2	0.2	0.4	0.1	0.1	0.2
Skewness	0.9	0.4	-0.9	-0.5	0.5	-1.9

Table 5. 8: Deviations in the beam profiles of 12 MeV of SB2 LINAC

E12 Deviation						
Year	**Crossplane**		Flatness	**Inplane**		Flatness
	Fieldwidth	**Symmetry**		**Fieldwidth**	**Symmetry**	
	Dev (mm)	Dev (%)	Dev (%)	Dev (%)	Dev (%)	Dev (%)
2015	-0.1	0.5	-0.2	-0.1	0.7	-0.1
2016	0.4	0.6	-0.3	0.2	0.6	-0.3
2017	0.1	0.4	-0.4	0.2	0.6	-0.4
2017	0.2	1.0	0.2	0.1	0.9	0.1
2018	-0.1	0.9	0.3	0.0	0.6	0.0
Mean	0.1	0.7	-0.1	0.1	0.7	-0.1
Std dev	0.2	0.3	0.3	0.1	0.1	0.2
Skewness	0.5	0.4	0.4	-0.5	1.7	-0.2

Table 5. 9: Deviations in the beam profiles of 12 MeV of SB2 LINAC

E15 deviation						
Year	**Crossplane**		Flatness	**Inplane**		Flatness
	Fieldwidth	**Symmetry**		**Fieldwidth**	**Symmetry**	
	Dev (mm)	Dev (%)	Dev (%)	Dev (mm)	Dev (%)	Dev (%)
2015	-0.3	0.5	0.3	-0.1	0.6	-0.1
2016	0.1	0.7	0.1	0.2	0.3	-0.7
2017	-0.1	0.6	0.2	0.1	0.7	-0.1
2017	0.0	0.5	0.3	0.2	0.6	0.4
2018	-0.3	0.5	0.1	0.0	0.9	0.1
Mean	-0.1	0.6	0.2	0.1	0.6	-0.1
Std dev	0.2	0.1	0.1	0.1	0.2	0.4
Skewness	0.1	1.3	0.0	-0.5	-0.4	-0.8

Table 5. 10: One way ANOVA for the x- coordinates of XVIs

	Sum of Squares	df	Mean Square	F	Sig.
Between Groups	19.973	11	1.816	2.493	0.060
Within Groups	9.467	13	0.728		
Total	29.440	24			

Table 5. 11: One way ANOVA for the y- coordinate of XVIs

	Sum of Squares	df	Mean Square	F	Sig.
between Groups	18.940	11	1.722	2.132	0.098
Within Groups	10.500	13	0.808		
Total	29.440	24			

Table 5. 12: One way ANOVA test for z-coordinates of XVIs

	Sum of Squares	df	Mean Square	F	Sig.
Between Groups	19.523	9	2.169	3.281	0.021
Within Groups	9.917	15	0.661		
Total	29.440	24			

Table 5. 13: Deviations in the dose calibration measurement of the LINACS

Year	SB2 LINAC				SB3 LINAC			
	6 MV		15 MV		6 MV		15 MV	
	1st dev	2nd dev	1st dev	2nd dev	1st dev	2nd dev	1st dev	2nd dev
2011	-0.05	0.03	0.16	-0.03	--	--	--	--
2012	-0.05	0.06	0.09	-0.12	--	--	--	--
2013	-0.75	0.01	-0.71	0.03	--	--	--	--
2014	0.58	0.00	1.10	0.03	0.62	0.12	0.80	0.00
2015	1.04	-0.05	0.23	-0.07	0.11	0.22	0.32	0.03
2016	1.26	0.04	1.35	0.04	0.11	0.02	-1.01	0.00
2017	0.00	-0.04	-0.16	-0.06	-2.31	0.06	-0.67	0.06
2018	0.30	--	0.06	--	--	--	--	--
Mean	0.29	0.01	0.27	-0.03	-0.37	0.11	-0.14	0.02
Std Dev	0.65	0.04	0.66	0.06	1.31	0.09	0.84	0.03
Skewness	0.08	-0.33	0.55	-0.34	-1.79	0.83	0.13	0.86

Table 5. 14: Deviations in the dose calibration measurement of the LINACS

Year	SB4 LINAC				SB6 LINAC			
	6 MV		15 MV		6 MV		15 MV	
	1st dev	2nd dev	1st dev	2nd dev	1st dev	2nd dev	1st dev	2nd dev
2011	0.21	-0.10	0.13	0.04	--	--	--	--
2012	-0.40	0.01	-0.85	-0.03	--	--	--	--
2013	-0.04	0.08	-0.59	0.06	--	--	--	--
2014	0.38	0.02	0.33	-0.03	--	--	--	--
2015	0.38	0.11	1.13	-0.01	-1.56	0.06	-0.72	0.00
2016	-0.62	0.01	-1.03	0.00	-1.04	-0.01	-0.26	0.01
2017	0.13	0.00	-0.04	0.02	0.40	0.04	0.28	0.07
2018	--	--	--	--	-1.19	0.10	-1.23	-0.01
Mean	0.01	0.02	-0.13	0.01	-0.85	0.05	-0.48	0.02
Std Dev	0.39	0.07	0.75	0.04	0.86	0.05	0.64	0.04
Skewness	-0.80	-0.53	0.51	0.44	1.61	-0.31	0.06	1.70

Table 5.15: Yearly performance of SB2 LINAC

Procedure	**Tolerance**	**Average Deviation**							
		2011	**2012**	**2013**	**2014**	**2015**	**2016**	**2017**	**2018**
XVI(X-ray volumetric Imaging)	cm	**cm**	**cm**	**cm**	**cm**	**cm**	**cm**	**cm**	**cm**
x(lateral) direction	±0.1	0.02	-0.26	0.00	0.00	0.01	0.00	-0.03	-0.04
y (longitudinal) direction	±0.1	-0.01	0.00	0.00	0.02	0.01	0.07	0.02	0.01
z (vertical) direction	±0.1	0.06	0.09	0.02	0.04	0.04	0.01	0.01	0.05
Dose Calibration									
6 MV	**%**	**%**	**%**	**%**	**%**	**%**	**%**	**%**	**%**
1st Absolute dose calibration measurement	±0.5	-0.05	-0.05	-0.75	0.58	1.04	1.26	0.00	0.30
2nd Absolute dose calibration measurement	±0.5	0.03	0.06	0.01	0.00	-0.05	0.04	-0.04	-
15 MV									
1st Absolute dose calibration measurement	±0.5	0.16	0.09	-0.71	1.10	0.23	1.35	-0.16	0.06
2nd Absolute dose calibration measurement	±0.5	-0.03	-0.12	0.03	0.03	-0.07	0.04	-0.06	-
Beam quality of photon energies									
Tissue Phantom Ratio (TPR) of 6 MV	1	-	-	-	-	0.29	-0.21	-0.17	0.05
Tissue Phantom Ratio (TPR) of 15 MV	1	-	-	-	-	0.19	-0.55	-0.03	-0.14
Beam quality of Electron energies	mm					mm	mm	mm	mm
R50 of 6 MeV	0.5	-	-	-	-	0.00	1.10	-0.15	0.20

R50 of 8 MeV	0.5	-	-	-	-	0.00	0.90	0.05	-0.30
R50 of 10 MeV	0.5	-	-	-	-	-0.20	0.20	-0.35	-0.20
R50 of 12 MeV	0.5	-	-	-	-	-0.20	0.40	-0.65	0.30
R50 of 15MeV	0.5	-	-	-	-	-0.30	0.30	-0.10	-0.30
Beam Profiles(Photons)									
6 MV						%	%	%	%
Flatness(I/P) @ Dmax for 10×10 cm^2	±1%	-	-	-	-	0.2	0.6	0.25	0.7
Flatness(C/P) @ Dmax for 10×10 cm^2	±1%	-	-	-	-	0.5	1.1	0.8	1.1
Flatness(I/P) @ 10 cm for 10×10 cm^2	±1%	-	-	-	-	0.1	1.4	0.2	0.4
Flatness(C/P) @ 10 cm for 10×10 cm^2	±1%	-	-	-	-	0.4	1.7	0.75	0.6
Flatness(I/P) @ Dmax for 40×40 cm^2	±1%	-	-	-	-	0.1	-0.1	0.25	0.0
Flatness(C/P) @ Dmax for 40×40 cm^2	±1%	-	-	-	-	-0.8	-0.7	-0.35	-0.5
Flatness(I/P) @ 10 cm for 40×40 cm^2	±1%	-	-	-	-	0.8	0.6	1.2	0.5
Flatness(C/P) @ 10 cm for 40×40 cm^2	±1%	-	-	-	-	0.9	1.0	0.8	0.8
Symmetry (I/P) @ Dmax for 10×10cm^2	±1%	-	-	-	-	0.7	0.8	0.5	1.1
Symmetry(C/P) @ Dmax for 10×10cm^2	±1%	-	-	-	-	0.6	0.3	0.9	0.9
Symmetry (I/P) @ 10 cm for 10×10cm^2	±1%	-	-	-	-	0.6	0.7	0.55	1.0
Symmetry (C/P) @ 10cm for10×10cm^2	±1%	-	-	-	-	0.6	0.4	0.6	0.8
Symmetry (I/P) @ Dmax for 40×40cm^2	±1%	-	-	-	-	0.1	-0.1	0.25	0.0
Symmetry (C/P) @ Dmax for40×40cm^2	±1%	-	-	-	-	-0.8	-0.7	-0.35	-0.5
Symmetry (I/P) @ 10cm for 40×40cm^2	±1%	-	-	-	-	0.8	0.6	0.8	0.6

Symmetry (C/P) @ 10cm for 40×40cm^2	±1%	-	-	-	-	0.5	0.9	0.7	0.7
Fieldwidth (I/P) for 10×10 cm^2	±1 mm	-	-	-	-	-0.1	1.0	0.3	0.5
Fieldwidth (C/P) for 10×10 cm^2	±1 mm	-	-	-	-	0.5	1.1	0.75	1.0
Fieldwidth (I/P) for 40×40 cm^2	±2 mm	-	-	-	-	-1.2	1.5	0.1	-0.2
Fieldwidth (C/P) for 40×40 cm^2	±2 mm	-	-	-	-	0.6	2.4	1.2	1.7
15 MV									
Flatness(I/P) @ Dmax for 10×10 cm^2	±1%	-	-	-	-	0.8	2.2	0.4	0.5
Flatness(C/P) @ Dmax for 10×10 cm^2	±1%	-	-	-	-	0.7	2.7	1.1	0.5
Flatness(I/P) @ 10 cm for 10×10 cm^2	±1%	-	-	-	-	0.5	2.2	0.4	0.5
Flatness(C/P) @ 10 cm for 10×10 cm^2	±1%	-	-	-	-	0.5	2.9	1.1	0.8
Flatness(I/P) @ Dmax for 40×40 cm^2	±1%	-	-	-	-	-0.6	0.4	-0.9	-0.7
Flatness(C/P) @ Dmax for 40×40 cm^2	±1%	-	-	-	-	-0.4	0.3	-0.6	-0.6
Flatness(I/P) @ 10 cm for 40×40 cm^2	±1%	-	-	-	-	1.0	1.3	1.4	1.0
Flatness(C/P) @ 10 cm for 40×40 cm^2	±1%	-	-	-	-	1.0	0.5	1.1	1.1
Symmetry (I/P) @ Dmax for 10×10 cm2	±1%	-	-	-	-	1.1	0.9	0.8	0.6
Symmetry(C/P) @ Dmax for 10×10 cm^2	±1%	-	-	-	-	0.4	0.8	0.6	0.5
Symmetry (I/P) @ 10 cm for 10×10 cm^2	±1%	-	-	-	-	1.0	1.0	0.7	0.7
Symmetry (C/P) @ 10cm for 10×10 cm^2	±1%	-	-	-	-	0.4	1.3	0.8	0.5
Symmetry (I/P) @ Dmax for 40×40 cm^2	±1%	-	-	-	-	1.4	1.4	1.0	0.7

Symmetry (C/P) @ Dmax for 40×40cm^2	±1%	-	-	-	-	0.5	0.6	0.7	0.4
Symmetry (I/P) @ 10 cm for 40×40 cm^2	±1%	-	-	-	-	1.2	1.7	1.2	0.9
Symmetry (C/P) @ 10cm for 40×40cm^2	±1%	-	-	-	-	0.7	0.7	0.7	0.5
Fieldwidth (I/P) for 10×10 cm^2	±1 mm	-	-	-	-	-0.1	1.1	0.3	0.6
Fieldwidth (C/P) for 10×10 cm^2	±1 mm	-	-	-	-	0.6	1.3	0.7	0.9
Fieldwidth (I/P) for 40×40 cm^2	±2 mm	-	-	-	-	-1.1	1.6	0.2	-0.1
Fieldwidth (C/P) for 40×40 cm^2	±2 mm	-	-	-	-	0.7	2.5	1.2	1.8
Beam Profiles (Electrons)									
6 MeV									
Flatness (I/P)	±1%	-	-	-	-	0.1	-0.1	-0.1	0.1
Symmetry (I/P)	±1%	-	-	-	-	0.8	0.6	0.7	0.5
Fieldwidth (I/P)	±1 mm	-	-	-	-	0.0	0.3	0.2	0.1
Flatness (C/P)	±1%	-	-	-	-	-0.1	-0.1	0.2	-0.1
Symmetry (C/P)	±1%	-	-	-	-	0.5	0.5	0.85	0.5
Fieldwidth (C/P)	±1 mm	-	-	-	-	-0.2	0.3	0.1	-0.1
8 MeV									
Flatness (I/P)	±1%	-	-	-	-	0.1	0.6	0.1	0.1
Symmetry (I/P)	±1%	-	-	-	-	0.7	1.1	0.5	0.4
Fieldwidth (I/P)	±1 mm	-	-	-	-	-0.1	0.1	0.0	0.0
Flatness (C/P)	±1%	-	-	-	-	0.6	0.6	0.35	0.4
Symmetry (C/P)	±1%	-	-	-	-	0.8	0.6	0.85	0.7
Fieldwidth (C/P)	±1 mm	-	-	-	-	0.0	0.3	0.2	-0.1
10 MeV									
Flatness (I/P)	±1%	-	-	-	-	0.3	0.4	0.35	-0.1

Symmetry (I/P)	±1%	-	-	-	-	0.6	0.8	0.8	0.6
Fieldwidth (I/P)	±1 mm	-	-	-	-	-0.1	0.2	0.15	0.0
Flatness (C/P)	±1%	-	-	-	-	0.6	0.2	0.7	-0.2
Symmetry (C/P)	±1%	-	-	-	-	0.7	0.5	1.0	0.7
Fieldwidth (C/P)	±1 mm	-	-	-	-	-0.1	0.4	0.1	0.0
12 MeV									
Flatness (I/P)	±1%	-	-	-	-	-0.1	-0.3	-0.2	0.0
Symmetry (I/P)	±1%	-	-	-	-	0.7	0.6	0.8	0.6
Fieldwidth (I/P)	±1 mm	-	-	-	-	-0.1	0.2	0.2	0
Flatness (C/P)	±1%	-	-	-	-	-0.2	-0.3	-0.1	0.3
Symmetry (C/P)	±1%	-	-	-	-	0.5	0.6	0.7	0.9
Fieldwidth (C/P)	±1 mm	-	-	-	-	-0.1	0.4	0.2	-0.1
15 MeV									
Flatness (I/P)	±1%	-	-	-	-	-0.1	-0.7	0.2	0.1
Symmetry (I/P)	±1%	-	-	-	-	0.6	0.3	0.7	0.9
Fieldwidth (I/P)	±1 mm	-	-	-	-	-0.1	0.2	0.2	0.0
Flatness (C/P)	±1%	-	-	-	-	0.3	0.1	0.3	0.1
Symmetry (C/P)	±1%	-	-	-	-	0.5	0.7	0.6	0.5
Fieldwidth (C/P)	±1 mm	-	-	-	-	-0.3	0.1	-0.1	-0.3

C/P and I/P denote crossplane and inplane profiles respectively.

Table 5.16: Yearly performance of SB3 LINAC

Procedure	Tolerance	Average Deviation				
		2014	2015	2016	2017	2018
XVI(X-ray volumetric Imaging)		**cm**	**cm**	**cm**	**cm**	**cm**
x(lateral) direction	±0.1 cm	0.03	0.01	0.01	0.01	-0.02
y (longitudinal) direction	±0.1 cm	-0.02	0.05	0.08	0.03	0.04
z (vertical) direction	±0.1 cm	0.05	0.05	0.07	0.01	0.03
Dose Calibration						
6 MV		**%**	**%**	**%**	**%**	**%**
1st Absolute dose calibration measurement	±0.5%	0.62	0.11	0.11	-2.31	-
2nd Absolute dose calibration measurement	±0.5%	0.12	0.22	0.02	0.06	-
15 MV						
1st Absolute dose calibration measurement	±0.5%	0.80	0.32	-1.01	-0.67	-
2nd Absolute dose calibration measurement	±0.5%	0.00	0.03	0.00	0.06	-
Beam quality of photon energies						
Tissue Phantom Ratio (TPR) of 6 MV	1%	-	-0.21	-	-0.63	-0.56
Tissue Phantom Ratio (TPR) of 15 MV	1%	-	-0.76	-	-0.09	-0.01
Beam Profiles of 6 MV						
Flatness(I/P) @ Dmax for 10×10 cm^2	±1%	-	0.10	-	0.20	0.20
Flatness(C/P) @ Dmax for 10×10 cm^2	±1%	-	0.20	-	0.20	0.20
Flatness(I/P) @ 10 cm for 10×10 cm^2	±1%	-	0.10	-	0.20	0.20
Flatness(C/P) @ 10 cm for 10×10 cm^2	±1%	-	0.60	-	0.30	0.50
Flatness(I/P) @ Dmax for 40×40 cm^2	±1%	-	0.60	-	0.00	0.20
Flatness(C/P) @ Dmax for 40×40 cm^2	±1%	-	0.50	-	-0.10	-0.10
Flatness(I/P) @ 10 cm for 40×40 cm^2	±1%	-	0.30	-	0.20	0.00
Flatness(C/P) @ 10 cm for 40×40 cm^2	±1%	-	0.40	-	0.50	0.50
Symmetry (I/P) @ Dmax for 10×10 cm^2	±1%	-	0.60	-	0.40	0.50
Symmetry(C/P) @ Dmax for 10×10 cm^2	±1%	-	0.30	-	0.40	0.30
Symmetry (I/P) @ 10 cm for 10×10 cm^2	±1%	-	0.70	-	0.40	0.90
Symmetry (C/P) @ 10 cm for 10×10 cm^2	±1%	-	0.50	-	0.50	0.60
Symmetry (I/P) @ Dmax for 40×40 cm^2	±1%	-	0.80	-	0.70	1.00
Symmetry (C/P) @ Dmax for 40×40 cm^2	±1%	-	0.80	-	0.90	0.90
Symmetry (I/P) @ 10 cm for 40×40 cm^2	±1%	-	0.90	-	0.50	0.80
Symmetry (C/P) @ 10 cm for 40×40 cm^2	±1%	-	0.70	-	0.80	0.80
Fieldwidth (I/P) for 10×10 cm^2	±1 mm	-	0.20	-	0.10	0.10
Fieldwidth (C/P) for 10×10 cm^2	±1 mm	-	0.80	-	0.60	0.60
Fieldwidth (I/P) for 40×40 cm^2	±2 mm	-	-0.30	-	-0.70	-0.70
Fieldwidth (C/P) for 40×40 cm^2	±2 mm	-	1.60	-	0.80	0.80
Beam Profiles of 15 MV						
Flatness(I/P) @ Dmax for 10×10 cm^2	±1%	-	-0.10	-	0.40	-0.10

Flatness(C/P) @ Dmax for 10×10 cm^2	±1%	-	0.30	-	0.90	0.40
Flatness(I/P) @ 10 cm for 10×10 cm^2	±1%	-	-0.20	-	0.40	-0.50
Flatness(C/P) @ 10 cm for 10×10 cm^2	±1%	-	0.40	-	1.20	0.10
Flatness(I/P) @ Dmax for 40×40 cm^2	±1%	-	0.50	-	-0.50	0.30
Flatness(C/P) @ Dmax for 40×40 cm^2	±1%	-	1.00	-	-0.60	0.00
Flatness(I/P) @ 10 cm for 40×40 cm^2	±1%	-	-0.50	-	0.80	0.30
Flatness(C/P) @ 10 cm for 40×40 cm^2	±1%	-	0.50	-	0.30	0.30
Symmetry (I/P) @ Dmax for 10×10 cm^2	±1%	-	0.30	-	0.70	0.70
Symmetry(C/P) @ Dmax for 10×10 cm^2	±1%	-	0.70	-	0.60	0.50
Symmetry (I/P) @ 10 cm for 10×10 cm^2	±1%	-	0.50	-	0.80	0.40
Symmetry (C/P) @ 10 cm for 10×10 cm^2	±1%	-	0.90	-	0.80	0.60
Symmetry (I/P) @ Dmax for 40×40 cm^2	±1%	-	0.40	-	0.50	0.60
Symmetry (C/P) @ Dmax for 40×40 cm^2	±1%	-	0.80	-	0.50	0.40
Symmetry (I/P) @ 10 cm for 40×40 cm^2	±1%	-	0.50	-	0.70	0.70
Symmetry (C/P) @ 10 cm for 40×40 cm^2	±1%	-	0.90	-	0.60	0.50
Fieldwidth (I/P) for 10×10 cm^2	±1 mm	-	0.10	-	0.10	0.00
Fieldwidth (C/P) for 10×10 cm^2	±1 mm	-	0.90	-	0.60	0.00
Fieldwidth (I/P) for 40×40 cm^2	±2 mm	-	-0.20	-	-0.60	0.00
Fieldwidth (C/P) for 40×40 cm^2	±2 mm	-	1.60	-	0.70	0.00